

Coupled models of invasion dynamics

by

Peter C. Jentsch

A thesis
presented to the University of Waterloo
in fulfillment of the
thesis requirement for the degree of
Doctor of Philosophy
in
Applied Mathematics

Waterloo, Ontario, Canada, 2021

© Peter C. Jentsch

Examining Committee Membership

The following served on the Examining Committee for this thesis. The decision of the Examining Committee is by majority vote.

External Examiner: Bruce Bruce
Professor, Dept. of Philosophy of Zoology, University of Wallamaloo

Supervisor(s): Chris T. Bauch
Professor, Department of Applied Mathematics, University of Waterloo
Madhur Anand
Professor, School of Environmental Sciences, University of Guelph

Internal Member: Sue Ann Campbell
Professor, Department of Applied Mathematics, University of Waterloo

Internal-External Member: Meta Meta
Professor, Dept. of Philosophy, University of Waterloo

Other Member(s): Leeping Fang
Professor, Dept. of Fine Art, University of Waterloo

Author's Declaration

I hereby declare that I am the sole author of this thesis. This is a true copy of the thesis, including any required final revisions, as accepted by my examiners.

I understand that my thesis may be made electronically available to the public.

Abstract

This is the abstract.

Vulputate minim vel consequat praesent at vel iusto et, ex delenit, esse euismod luptatum augue ut sit et eu vel augue autem feugiat, quis ad dolore. Nulla vel, laoreet lobortis te commodo elit qui aliquam enim ex iriure ea ullamcorper nostrud lorem, lorem laoreet eu ex ut vel in zzril wisi quis. Nisl in autem praesent dignissim, sit vel aliquam at te, vero dolor molestie consequat.

Tation iriure sed wisi feugait odio dolore illum duis in accumsan velit illum consequat consequat ipsum molestie duis duis ut ullamcorper. Duis exerci odio blandit vero dolore eros odio amet et nisl in nostrud consequat iusto eum suscipit autem vero. Iusto dolore exerci, ut erat ex, magna in facilisis duis amet feugait augue accumsan zzril delenit aliquip dignissim at. Nisl molestie nibh, vulputate feugait nibh luptatum ea delenit nostrud dolore minim veniam odio volutpat delenit nulla accumsan eum vero ullamcorper eum. Augue velit veniam, dolor, exerci ea feugiat nulla molestie, veniam nonummy nulla dolore tincidunt, consecetuer dolore nulla ipsum commodo.

At nostrud lorem, lorem laoreet eu ex ut vel in zzril wisi. Suscipit consequat in autem praesent dignissim, sit vel aliquam at te, vero dolor molestie consequat eros tation facilisi diam dolor. Odio luptatum dolor in facilisis et facilisi et adipiscing suscipit eu iusto praesent enim, euismod consecetuer feugait duis. Odio veniam et iriure ad qui nonummy aliquip at qui augue quis vel diam, nulla. Autem exerci tation iusto, hendrerit et, tation esse consequat ut velit te dignissim eu esse eros facilisis lobortis, lobortis hendrerit esse dignissim nisl. Nibh nulla minim vel consequat praesent at vel iusto et, ex delenit, esse euismod luptatum.

Ut eum vero ullamcorper eum ad velit veniam, dolor, exerci ea feugiat nulla molestie, veniam nonummy nulla. Elit tincidunt, consecetuer dolore nulla ipsum commodo, ut, at qui blandit suscipit accumsan feugiat vel praesent. In dolor, ea elit suscipit nisl blandit hendrerit zzril. Sit enim, et dolore blandit illum enim duis feugiat velit consequat iriure sed wisi feugait odio dolore illum duis. Et accumsan velit illum consequat consequat ipsum molestie duis duis ut ullamcorper nulla exerci odio blandit vero dolore eros odio amet et.

In augue quis vel diam, nulla dolore exerci tation iusto, hendrerit et, tation esse consequat ut velit. Duis dignissim eu esse eros facilisis lobortis, lobortis hendrerit esse dignissim nisl illum nulla minim vel consequat praesent at vel iusto et, ex delenit, esse euismod. Nulla augue ut sit et eu vel augue autem feugiat, quis ad dolore te vel, laoreet lobortis te commodo elit qui aliquam enim ex iriure. Ut ullamcorper nostrud lorem, lorem laoreet eu ex ut vel in zzril wisi quis consequat in autem praesent dignissim, sit vel. Dolore at te, vero

dolor molestie consequat eros tation facilisi diam. Feugait augue luptatum dolor in facilisis et facilisi et adipiscing suscipit eu iusto praesent enim, euismod consectetur feugait duis vulputate veniam et.

Ad eros odio amet et nisl in nostrud consequat iusto eum suscipit autem vero enim dolore exerci, ut. Esse ex, magna in facilisis duis amet feugait augue accumsan zzril. Lobortis aliquip dignissim at, in molestie nibh, vulputate feugait nibh luptatum ea delenit nostrud dolore minim veniam odio. Euismod delenit nulla accumsan eum vero ullamcorper eum ad velit veniam. Quis, exerci ea feugiat nulla molestie, veniam nonummy nulla. Elit tincidunt, consectetur dolore nulla ipsum commodo, ut, at qui blandit suscipit accumsan feugiat vel praesent.

Dolor zzril wisi quis consequat in autem praesent dignissim, sit vel aliquam at te, vero. Duis molestie consequat eros tation facilisi diam dolor augue. Dolore dolor in facilisis et facilisi et adipiscing suscipit eu iusto praesent enim, euismod consectetur feugait duis vulputate.

Acknowledgements

I would like to thank all the little people who made this thesis possible.

Dedication

This is dedicated to the one I love.

Table of Contents

List of Figures	xi
List of Tables	xxi
1 Go big or go home: a model-based assessment of general strategies to slow the spread of forest pests via infested firewood	1
1.1 Abstract	1
1.2 Introduction	2
1.3 Materials and methods	4
1.3.1 Pest Spread Model	5
1.3.2 Social Dynamics Model	6
1.3.3 Patch-quarantine strategies	8
1.3.4 Parameterization	11
1.3.5 Assessing intervention efficacy	12
1.4 Results	13
1.5 Conclusion	16
1.6 Acknowledgements	21
2 Fire Mitigates Bark Beetle Outbreaks in Serotinous Forests	22
2.1 Introduction	22
2.2 Methods	24

2.2.1	Model Description	24
2.2.2	Forest thinning protocol (FTP) and controlled burning protocol (CBP)	26
2.2.3	Parameters and simulation design	27
2.3	Results	28
2.3.1	Dynamical regimes	28
2.3.2	Impact of forest thinning protocol (FTP) and controlled burning protocol (CBP)	31
2.4	Discussion	31
3	Prioritising COVID-19 vaccination in changing social and epidemiological landscapes: a mathematical modelling study	38
3.1	Introduction	39
3.2	Model Overview	41
3.2.1	Structure and parameterisation	41
3.2.2	Vaccine scenarios	41
3.3	Results	42
3.4	Discussion	51
3.5	Appendix	53
3.5.1	Model Equations	53
3.5.2	Vaccination process	56
3.5.3	Differences between parameters in the first and second wave	56
3.5.4	Case under-ascertainment	57
3.5.5	Baseline transmission rate	57
3.5.6	Disease progression parameters	59
3.5.7	Initial conditions	59
3.5.8	Particle filtering	60
3.5.9	Vaccination refusal dynamics	61
3.5.10	Model extension for vaccine efficacy against disease only	61

References	64
Appendix	88
A Appendix C	89
Glossary	116
Abbreviations	117
Nomenclature	118
List of Symbols	119

List of Figures

1.1	Camper travel network in Ontario, Quebec and Manitoba. Darker (more orange) lines represent more trips.	11
1.2	Time series of model variables as a function of interventions, direct (raising C_e, panels a - d) and through social pressure (raising U, panels e - h). The former intervention, panels a-d, means an increase of social pressure on people who choose to transport firewood (i.e. increasing the U value), and the latter refers to direct interception of firewood (i.e. increasing the C_e value). Terms $L(t) = \frac{1}{N} \sum_{i=1}^N S_i(t)$, $I(t) = \frac{1}{N} \sum_{i=1}^N I_i(t)$, $B(t) = \frac{1}{N} \sum_{i=1}^N B_i(t)$, $L(t) = \frac{1}{N} \sum_{i=1}^N L_i(t)$ are the averages of the state variables over all patches. $S(t)$ has been omitted for brevity.	14
1.3	Total infestation per node over 5, 10 and 20 years. Neither increasing U nor C_e are effective at long time scales.	16
1.4	Efficacy of social incentives on infestation after time T. Inset graph shows an example of cross-section along the line $f = 0.11$ The influence of infestation on transport strategy, f , can hinder the intervention by public outreach, in the long-term (after approximately 20 years). The inset figure illustrates how one column in the heat map, shown by the dotted line, is constructed from the slopes of linear approximations of $T(t)$ over $U \in [-5, 5]$. The blueness of the lines going left to right is a function of their slope, corresponding to the color of the cells in the heatmap.	17
1.5	Efficacy of social incentives on infestation after time period T with respect to A, the intra-patch infestation parameter. This intervention becomes ineffective over time if A is sufficiently large.	18
1.6	Efficacy of social incentives on infestation after time T intra-patch spreading rate A, affects infestation outcomes. The social incentive to not transport firewood, U , is more effective with lower pest spread rates.	18

1.7	Average total infested trees ($T(t)$) after 5, 10 and 15 years (panels a), b), and c) respectively), assuming the quarantine begins one year after the pest is introduced. Total infestation plotted with respect to the number of nodes quarantined ($ V $) and the length of the quarantine (Δt). The quarantine is effective over 5 years with only 50 patches, provided they are closed for over a year.	19
1.8	Average total infested trees ($T(t)$) after 5, 10 and 15 years (panels a), b), and c) respectively), assuming the quarantine begins two years after the pest is introduced. Total infestation plotted with respect to the number of nodes quarantined ($ V $) and the length of the quarantine (Δt).	19
2.1	Conceptual diagram of compartments (state variables) and transitions between compartments across seasons. See main text and Table 2.1 for definitions of variables and parameters.	26
2.2	Approximate dynamical regimes of the system, where α_1 is the burning rate of juvenile trees, and α_2 is the burning rate of susceptible (mature) trees. a) Average size of largest MPB population (over 500 years at equilibrium) b) Average frequency of MPB outbreaks at equilibrium c) Average size of largest fire season (over 500 years at equilibrium) d) Average frequency of severe fire seasons at equilibrium. The juvenile burning rate (α_1) and susceptible burning rate (α_2) control fire and MPB prevalence. Large α_1, α_2 implies low infestation and also more regularity in the fire regime. All other parameters were set to baseline values (Table 2.1).	29
2.3	Time series of each state variable of a single realization where $\alpha_1 = 0.02$, $\alpha_2 = 0.0025$, showing the regular outbreaks of pests, periodic shifts in fire prevalence, and uneven age distribution generated by MPB outbreaks. a) juvenile distribution at time $t = 2050$ (note different x-axis), b) susceptible population after year t , c) infested tree population after year t , d) burned forest after year t . All other parameters were set to baseline values (Table 2.1).	30
2.4	Percentage change in maximum MPB infestation size within 500 year period under a) FTP with $\tau = 0.15, m = 8$, b) CBP with $\tau = 0.15, m = 8$, with respect to burning rates α_1, α_2 , compared to no FTP. FTP is always effective at reducing MPB outbreaks, and CBP worsens them if the population of MPB is already low.	32

2.5	Time series showing realization of model under FTP with $\tau = 0.15$ fraction of $m = 8$ juvenile stands cleared, conducted each year, where $\alpha_1 = 0.02$, $\alpha_2 = 0.0025$. a) juvenile distribution at time $t = 2050$ (note different x-axis), b) susceptible population after year t , c) infested tree population after year t , d) burned forest after year t . Notice the flattening of the age distribution compared to the same parameters with no FTP (Figure 2.3)	33
2.6	Percentage change in average susceptible (mature) forest population compared to no FTP with $\tau = 0.15, m = 8$, b) controlled burning with $\tau = 0.15, m = 8$, with respect to burning rates α_1, α_2 . FTP and CBP increase the average population of mature trees in many cases, in addition to reducing outbreak sizes.	34
3.1	COVID-19 case numbers and proxy for adherence to non-pharmaceutical interventions. (A) COVID-19 case incidence by date of report in Ontario. Dots show the 7-day running average of case notification data, and the line represents the ascertained case incidence from best fitting models (with 95% credible intervals represented by the shaded region).(B) Each dot represents the proportional reduction in time spent at retail and recreation destinations and workplaces on the given date, compared with the 5-week average on corresponding days of the week 1 year ago, according to Google mobility data. Lines show the proportion of the population adhering to non-pharmaceutical interventions (with 95% credible intervals represented by the shaded region) as well as workplace and school shutdown curves from the fitted model. Methods and data sources are provided in the appendix (pp 1–11).	43
3.2	Effect of interaction of social and epidemiological dynamics on pandemic waves and vaccine strategy effectiveness over time. (A) Number of ascertained incident COVID-19 cases. (B) Proportion of the population practising non-pharmaceutical interventions. (C) Level of school and workplace closure (note that curves for different vaccination strategies overlap). (D) Number of individuals with natural or vaccine-derived immunity. Predictions are based on the Ontario population size (14.6 million), with vaccination beginning on Jan 1, 2021 (as indicated by the dashed vertical line in the graphs), shutdown occurring at 200% of peak cases in the first wave, and a vaccination rate of 0.5% of the population per week. Other parameter values are provided in the appendix (pp 1–11).	44

3.3	Incident cases by vaccination strategy across three model regimes. Projections of ascertained incident COVID-19 cases if vaccination begins in January (A, B) or September (C, D), and if the rate of vaccination is 1.5% (A, C) or 0.5% (B, D) of the population per week. These scenarios represent three main model regimes: timely vaccination (A), partial vaccination and indirect protection (B, C), and slow and late vaccination (D). Projections are based on the Ontario population size of 14.6 million and shutdown occurring at 200% of peak cases in the first wave. Other parameter values are provided in the appendix (pp 1–11).	45
3.4	Effects of vaccination strategy and start date on percentage reduction in mortalityViolin plots of the percentage reduction in mortality under the four vaccine strategies, relative to no vaccination, as a function of the vaccination rate, for vaccination beginning on Jan 1, 2021 (A), and Sept 1, 2021 (B). Horizontal lines represent the median values and 95% credible intervals of posterior model projections. Projections are based on the Ontario population size of 14.6 million and shutdown occurring at 200% of peak cases in the first wave. Other parameter values are provided in the appendix (pp 1–11). The projected number of deaths in the absence of vaccination was 72000 (95% credible interval 40000–122000) from Jan 1, 2021, to March 14, 2025, and 60000 (31000–108000) from Sept 1, 2021, to March 14, 2025.	46
3.5	Effect of pre-existing natural immunity on the effectiveness of transmission-interrupting strategiesFrequency histogram of the proportion of the population with natural immunity for each strategy, taken from simulations where that strategy reduced mortality most effectively, for oldest-first (A), youngest-first (B), uniform (C), and contact-based strategies (D). The most effective strategy is defined as the one that reduced mortality the most across the largest number of model realisations. Vertical dashed lines denote median values of the distribution. Other parameter values are provided in the appendix (pp 1–11).	48
A.1	Posterior distributions on inferred non-age structured model parameters for baseline model. Posteriors are composed of 200 candidate parameter sets from the particle filtering, the model was evaluated at these points for all future runs.	90

A.2	Posterior distributions on inferred age-specific susceptibility modifier parameter ρ_i for baseline model. Three age-specific susceptibility parameters shown here, ρ_1, ρ_2, ρ_3 , were also inferred from particle filtering on the case and mobility data, corresponding to the age brackets 0-20, 20-60, 60+.	90
A.3	Posterior distributions on inferred age-specific ascertainment rate over time for baseline model. Time dependent ascertainment rates inferred from the data, corresponding to the fraction of actual cases detected by the Ontario testing system.	91
A.4	Empirical data of cumulative infections due to COVID-19 by age and model posterior predictions. The age-specific total cases at the end of the fitting window, were used to calibrate the model, in an age dependent way. We used only three parameters to capture age specific effects and therefore trade-off some accuracy in the youngest and oldest age groups.	92
A.5	Average of model posterior population seropositivity over time, compared to empirical data. Total seroprevalence in Ontario was assessed during the month of June. We used this value to calibrate the model further.	93
A.6	Age distribution of vaccination under the contact-based strategy. This strategy vaccinates proportionally to the leading eigenvector of the full contact matrix, $C(0)$, to vaccinate people who will, approximately, produce the most secondary infections in a linearized regime.	94
A.7	Social and epidemic dynamics for early vaccine availability and high vaccination rate. (a) Ascertained incident COVID-19 cases, (b) proportion x of the population practicing NPIs, (c) Intensity of school and workplace closure, (d) percentage of population with natural or vaccine-derived immunity versus time. $T = 200\%$, $\psi_0 = 1.5\%$ per week, vaccine available in January 2021. Other parameters are in Table 3.1.	95
A.8	Social and epidemic dynamics for late vaccine availability and high vaccination rate. (a) Ascertained incident COVID-19 cases, (b) proportion x of the population practicing NPIs, (c) Intensity of school and workplace closure, (d) percentage of population with natural or vaccine-derived immunity versus time. $T = 200\%$, $\psi_0 = 1.5\%$ per week, vaccine available in September 2021. Other parameters are in Table 3.1.	96

A.9	Social and epidemic dynamics for late vaccine availability and low vaccination rate. (a) Ascertained incident COVID-19 cases, (b) proportion x of the population practicing NPIs, (c) Intensity of school and workplace closure, (d) percentage of population with natural or vaccine-derived immunity versus time. $T = 200\%$, $\psi_0 = 0.5\%$ per week, vaccine available in September 2021. Other parameters are in Table 3.1.	97
A.10	Mortality reductions under various values of T and ψ_0, early vaccine availability. Violin plots of the percent reduction in mortality under the four vaccine strategies, relative to no vaccination, as a function of the vaccination rate ψ_0 , for January 2021 availability. Horizontal lines represent median values of posterior model projections. Other parameter values in Table S1. Percentage reductions are relative to no vaccination. Projected number of deaths in the absence of vaccination were 35597.2 (CI: 57465.9,19507.9); 48518.8 (CI: 86853.9,28335.7), 61339.1 (CI: 106623.0,34613.5), 72007.3 (CI: 121754.0,40483.4); 80707.6 (CI: 126732.0,47755.4) after January 1, 2021, for $T=50\%$, 100% , 150% , 200% , and 250% , respectively.	98
A.11	Mortality reductions under various values of T and ψ_0, late vaccine availability. Violin plots of the percent reduction in mortality under the four vaccine strategies, relative to no vaccination, as a function of the vaccination rate ψ_0 , for September 2021 availability. Horizontal lines represent median values of posterior model projections. Other parameter values in Table S1. Percentage reductions are relative to no vaccination. Projected number of deaths in the absence of vaccination were 25478.8 (CI: 45679.0,13006.7); 39149.6 (CI: 73917.1,20290.9); 50775.1 (CI: 95451.2,25980.9); 60250.7 (CI: 108361.0,30721.9); 68594.0 (CI: 107157.0,36063.6) after September 1, 2021 for $T=50\%$, 100% , 150% , 200% , and 250% , respectively.	99
A.12	A higher level of natural immunity increases the relative advantage of transmission-interrupting strategies. Median and standard deviation of the percent reduction in mortality under the four vaccine strategies, relative to no vaccination, as a function of the vaccination start date and percent recovered at that time, for (a) $\phi_0 = 1.0\%$ vaccinated per week and (b) $\phi_0 = 2.5\%$ vaccinated per week. Shutdown threshold $T = 200\%$, and other parameter values in Appendix, Table S1.	100

A.13 Sensitivity analysis exploring a range of vaccine efficacy values, for vaccination rate $\phi_0 = 2.5\%$ per week.	Subpanels are parameter planes for January and September availability showing the vaccination strategy that reduces COVID-19 mortality the most as a function of vaccine efficacy in 60+ year-olds versus vaccine efficacy in other age groups. Other parameter values as in Table S1.	101
A.14 Sensitivity analysis exploring impact of vaccinating behaviour dynamics.	$\phi_0 = 2.5\%$ per week, $T = 200\%$. Subpanels are parameter planes for January and September availability showing the vaccination strategy that reduces COVID-19 mortality the most as a function of vaccine social learning rate κ_{vac} and vaccine cost parameter c_{vac} . Other parameter values as in Table S1.	102
A.15 Epidemic dynamics and social dynamics for both NPI adherence and vaccinating behaviour, when vaccine cost is small, $c_{vac} = 1.1 \times 10^{-4}$.	(a) Ascertained incident COVID-19 cases, (b) proportion x of the population practicing NPIs, (c) Intensity of school and workplace closure, (d) percentage of population with natural or vaccine-derived immunity versus time. $T = 200\%$, $\psi_0 = 1.0\%$ per week (maximum rate in absence of vaccine refusal), vaccine available in September 2021, $\kappa_{vac} = 50/\text{day}$. Other parameters are in Table 3.1.	103
A.16 Epidemic dynamics and social dynamics for both NPI adherence and vaccinating behaviour, when vaccine cost is moderate, $c_{vac} = 2.9 \times 10^{-4}$.	(a) Ascertained incident COVID-19 cases, (b) proportion x of the population practicing NPIs, (c) Intensity of school and workplace closure, (d) percentage of population with natural or vaccine-derived immunity versus time. $T = 200\%$, $\psi_0 = 1.0\%$ per week (maximum rate in absence of vaccine refusal), vaccine available in September 2021, $\kappa_{vac} = 50/\text{day}$. Other parameters are in Table 3.1.	104
A.17 Epidemic dynamics and social dynamics for both NPI adherence and vaccinating behaviour, when vaccine cost is high, $c_{vac} = 3.8 \times 10^{-4}$.	(a) Ascertained incident COVID-19 cases, (b) proportion x of the population practicing NPIs, (c) Intensity of school and workplace closure, (d) percentage of population with natural or vaccine-derived immunity versus time. $T = 200\%$, $\psi_0 = 1.0\%$ per week (maximum rate in absence of vaccine refusal), vaccine available in September 2021, $\kappa_{vac} = 50/\text{day}$. Other parameters are in Table 3.1.	105

A.18 Sensitivity analysis for the scenario where $R_0 = 2.5$ for December 2020 onward.	Subpanels are (left) parameter planes for January and September availability showing the vaccination strategy that prevents the most COVID-19 deaths as a function of T and ψ_0 , and (right) percentage reductions in mortality. Other parameter values are as in Table S1.	106
A.19 Sensitivity analysis for the scenario of 30% heightened ascertainment across all ages from December 2020 onward.	Subpanels are parameter planes for January and September availability showing the vaccination strategy that reduces COVID-19 mortality the most as a function of T and ψ_0 (left) and the corresponding posterior parameter distributions for the refitted parameters (right). Other parameter values as in Table S1.	107
A.20 Sensitivity analysis for the scenario of 30% reduced ascertainment across all ages from December 2020 onward.	Subpanels are parameter planes for January and September availability showing the vaccination strategy that reduces COVID-19 mortality the most as a function of T and ψ_0 (left) and the corresponding posterior parameter distributions for the refitted parameters (right). Other parameter values as in Table S1.	108
A.21 Sensitivity analysis for the scenario of four times the baseline social learning rate from December 2020 onward.	Subpanels are parameter planes for January and September availability showing the vaccination strategy that reduces COVID-19 mortality the most as a function of T and ψ_0 (left) and the corresponding posterior parameter distributions for the refitted parameters (right). Other parameter values as in Table S1.	109
A.22 Sensitivity analysis for the scenario of one-fourth the baseline social learning rate from December 2020 onward.	Subpanels are parameter planes for January and September availability showing the vaccination strategy that reduces COVID-19 mortality the most as a function of T and ψ_0 . Other parameter values as in Table S1.	110
A.23 Sensitivity analysis for the scenario where efficacy against disease v^D is not the same as efficacy against transmission v^T .	Subpanels show percentage reduction in mortality for the four strategies versus v^D when $v^T = 0.75$ but v^D ranges from 0.75 to 0.95, for January and September availability. Other parameter values as in Table S1. Note that mortality in this plot is computed from March 15, 2020 to March 14, 2025.	111

A.24 Posterior parameter distributions and model outputs for more stringent particle filtering criteria under Bayesian particle filtering algorithm. Top left panel shows (a) COVID-19 case incidence by date of report in Ontario, 7-day running average (circles) and ascertained case incidence from best fitting models (lines). (b) Percentage change from baseline in time spent at retail and recreation destinations (orange circles) and at workplaces (green circles) from Google mobility data, and proportion of the population x adhering to NPIs (orange line) and workplace shutdown curve (green line) from fitted model. Top right panel shows posterior parameter distribution for age-specific susceptibility modifier, ρ_i . Bottom panel shows other posterior parameter distributions. Other parameter values as in Appendix, pp. 1-11.

112

A.25 Sensitivity analysis for more stringent particle filtering criteria under Bayesian particle filtering algorithm. Subpanels are parameter planes for January and September availability showing the vaccination strategy that reduces COVID-19 mortality the most as a function of T and ψ_0 (left) and violin plots showing percentage reduction in mortality (right). Horizontal lines represent median values of posterior model projections. Shutdown threshold $T=200\%$ and other parameter values in Appendix, pp. 1-11. Percentage reductions are relative to no vaccination. Projected number of deaths in the absence of vaccination was 72,000 (95% credible interval: 40,000 to 122,000) from January 1, 2021 to March 14, 2025 for (a) and 60,000 (95% credible interval: 31,000 to 108,000) from September 1, 2021 to March 14, 2025 for (b). Ontario Population size: 14.6 million. . . .

113

A.26 Model fit to data and baseline projections of mortality reductions under the four vaccine strategies, when behaviour is held constant over time. Top left: a) COVID-19 case incidence by date of report in Ontario, 7-day running average (circles) and ascertained case incidence from best fitting models (lines). (b) Percentage change from baseline in time spent at retail and recreation destinations (orange circles) and at workplaces (green circles) from Google mobility data, and proportion of the population x adhering to NPIs (orange line) and workplace shutdown curve (green line) from fitted model. Bottom left: Violin plots of the percent reduction in mortality under the four vaccine strategies, relative to no vaccination, as a function of the vaccination rate θ , for (a) January and (b) September 2021 availability. Horizontal lines represent median values of posterior model projections. Shutdown threshold $T=200\%$. Percentage reductions are relative to no vaccination. Projected number of deaths in the absence of vaccination was 72,000 (95% credible interval: 40,000 to 122,000) from January 1, 2021 to March 14, 2025 for (a) and 60,000 (95% credible interval: 31,000 to 108,000) from September 1, 2021 to March 14, 2025 for (b). Ontario Population size: 14.6 million. Right: Each parameter combination on the plane is colour coded according to which of the four strategies prevented the most deaths, on average across all model realizations, for (a) January and (b) September 2021 availability. Other parameter values in Appendix, pp. 1-11.

114

A.27 Epidemic dynamics and social dynamics for both NPI adherence and vaccinating behaviour, when behaviour is held constant over time. (a) Ascertained incident COVID-19 cases, (b) proportion x of the population practicing NPIs, (c) Intensity of school and workplace closure, (d) percentage of population with natural or vaccine-derived immunity versus time. $T = 200\%$, $\psi_0 = 0.5\%$ per week, vaccine available in January 2021. Other parameters are in Table 3.1.

115

List of Tables

1.1	Parameters and default values	9
2.1	Parameters and baseline values of compound fire and pest model. Except for α_i and the noise magnitude, all parameters were obtained from Duncan et al. [69]	28
3.1	Parameter definitions, values, particle filtering ranges, and sources.	63

Chapter 1

Go big or go home: a model-based assessment of general strategies to slow the spread of forest pests via infested firewood

1.1 Abstract

Invasive pests, such as emerald ash borer or Asian longhorn beetle, have been responsible for unprecedented ecological and economic damage in eastern North America. These and other wood-boring invasive insects can spread to new areas through human transport of untreated firewood. Behaviour, such as transport of firewood, is affected not only by immediate material benefits and costs, but also by social forces. Potential approaches to reduce the spread of wood-boring pests through firewood include raising awareness of the problem and increasing the social costs of the damages incurred by transporting firewood. In order to evaluate the efficacy of these measures, we create a coupled social-ecological model of firewood transport, pest spread, and social dynamics, on a geographical network of camper travel between recreational destinations. We also evaluate interventions aimed to slow the spread of invasive pests with untreated firewood, such as inspections at checkpoints to stop the movement of transported firewood and quarantine of high-risk locations. We find that public information and awareness programs can be effective only if the rate of spread of the pest between and within forested areas is slow. Direct intervention

via inspections at checkpoints can only be successful if a high proportion of the infested firewood is intercepted. Patch quarantine is only effective if sufficiently many locations can be included in the quarantine and if the quarantine begins early. Our results indicate that the current, relatively low levels of public outreach activities and lack of adequate funding are likely to render inspections, quarantine and public outreach efforts ineffective.

1.2 Introduction

Invasive species pose a significant economic and ecological threat to Canada's forest ecosystems [243, 105]. In North America, significant funding has been allocated by federal, state and provincial agencies for large-scale control programs to prevent or mitigate these damages with mixed success [219, 149]. Controlling the spread of invasive pests can be difficult because the long-distance spread of invasive organisms is often assisted by human activities [116, 243]. For example, introduction and spread of Emerald ash borer, a harmful forest pest in the North America [117, 118, 173] has been attributed to human factors, such as vehicle transport [47] and recreational travel [115].

The growing problem of invasive species is broadly associated with human mobility, including recreational travel [116, 243, 129, 177]. Outdoor recreation is widespread in North America, and the extent of recreational activities is expected to increase [59, 57, 58]. In North America, national, provincial and state parks, national forests, and state and Crown lands are common destinations for recreational activities [71, 204]. In Canada, recreational activities, especially camper travel, often take place in forested areas and may contribute to spread of harmful invasive pests. In particular, the movement of untreated firewood by campers has been widely acknowledged as a potential introduction pathway for invasive forest pests [26, 220, 170, 115, 105]. Movement of untreated firewood has been linked to the spread of two harmful wood-boring pests, the Asian longhorned beetle (*Anoplophora glabripennis* Motschulsky) and the emerald ash borer (*Agrilus planipennis* Fairmaire), in the United States and Canada (USaC) [90, 171].

Firewood is often moved to distant locations by campers for recreational purposes [105, 229]. For example, Haack et al. (2010) has found live bark- and wood-boring insects in 23% of the firewood pieces, surrendered at the checkpoint station at Mackinac bridge connecting Michigan's Lower and Upper Peninsulas and an additional 41% had signs of prior borer infestation. Jacobi et al. (2011) reported the emergence of live insects from 47% of the firewood bundles purchased from various US retailers. To reduce the risk of future pest infestations, USaC have implemented various regulations on movement of untreated firewood, including bans for out-of-province movement of untreated firewood

and restrictions for its transport by short distances [220, 229, 91, 159]. Also a number of public outreach campaigns have been undertaken to educate the general public about the threats associated with the movement of untreated firewood and its potential to spread harmful invasive pests. Several strategies have been developed to prevent (or minimize) the movement of firewood with recreational travel, including outreach campaigns in public media, enforcements with the inspections at check points for transported firewood, and area quarantine with the restrictions on firewood movement from/to the area of concern. In particular, public outreach campaigns have become widespread with significant funding by local, municipal, and provincial governments on measures such as advertisements along major highways and in public media and educational information in websites and printed media. The use of enforcement and quarantine options is less common but is gaining acceptance as a last resort measure and was implemented at least a few times over the past decade, to varying degrees of success [26, 115, 159].

Assessing the efficacy of the measures aimed to prevent the movement of firewood with recreational travel is a daunting task. Outreach campaigns may spread information widely but there is no guarantee that campers will pay attention and comply with the firewood restriction warnings. Many outreach activities (such as posting ads in public media or distributing flyers) are often implemented sporadically at local scales using local municipal and provincial budgets [220], which makes the assessment of their efficiency difficult. These activities may simultaneously occur in different places and times with little or no coordination, and are difficult to track in time and space.

Alternatively, the enforcement options (such as quarantine or checkpoint inspections for illegal movement of firewood) are gaining acceptance and may be perceived as more effective localized means to stop the movement of untreated firewood by campers. Nevertheless, assessing the effectiveness of enforcement actions is challenging due to a very small scale of enforcement actions (often implemented by individual states or provinces at selected locations) and lack of compliance data.

Mechanistic models of forest invasions have been studied for decades [215, 132], but explicit modelling and consideration of human factors, and the feedback between humans and the environment is relatively new. Ali et al. and Barlow et al. [26, 9] proposed two models of forest pest spread through firewood transport. The first study presented a differential equation model, and the second an agent-based model, both assuming that humans are the primary long-distance movers of forest pests. The models proposed in [26, 9] coupled infestation dynamics with the social dynamics. However both studies considered a small and idealized spatial structure: two patches in Barlow's et al. [26] study and ten patches in Ali's et al. model [9]. Often, illegal movement of firewood occurs over large distances and may involve visits to multiple recreational destinations that are connected

differently to one another.

In this study we consider movement of infested firewood to multiple recreational destinations over a complex recreational travel network. We explore the efficacy of common measures aimed to stop the movement of untreated firewood by recreational travelers. To accomplish this, we propose a mechanistic differential equation model that combines human-mediated movement of forest pests through a camper travel network that includes nonlinear feedbacks from social factors, such as population response to strategies preventing the movement of untreated firewood. We identify three basic methods to stop or slow the spread of invasive pests by transport of infested firewood: public awareness campaigns, direct interception of transported firewood at checkpoints near recreational destinations, and quarantining recreational destination sites for movement of firewood. While the first option is more common, the latter has been implemented seldom over the past decade due to legal and liability constraints [186, 238, 150, 91]. We implement the options for intercepting the movement of firewood to slow the spread of invasive pests in a mechanistic metapopulation model, and use the replicator equation to represent social learning dynamics (see [95, 26, 29, 101]). We also evaluate local quarantine at recreational destinations as an alternative control method. Quarantine means closing the site to visitors for a length of time, in order to reduce the amount of transported firewood and slow spread of invasive organisms from other infested locations. Our implementation of quarantine measures follow common practices aimed to slow the spread of invasive species (such as the spread of emerald ash borer in USaC [148, 88]). We apply our mechanistic model to explore the effectiveness of these control measures to slow the spread of an idealized wood-boring invasive pest moved to a set of recreational destinations by recreational travelers transporting untreated firewood. We apply the model to a network of provincial parks and campgrounds in three provinces of central Canada - Manitoba, Ontario, and Quebec.

1.3 Materials and methods

We consider a landscape of N patches, where a patch is represented as $i \in [1, N]$. Each patch represents a recreational destination (eg. provincial parks and campgrounds) with associated neighbouring human population centres. Each patch undergoes its own internal pest and social dynamics. We describe the spread of an invasive pest with the movement of firewood through the network of N patches with a mechanistic metapopulation model based on [26] that captures the spread of an infestation between the patches. The advantage to metapopulation models in this context is suitability for capturing dynamics of a highly fragmented population spread over a broad geographic region. Using the data

documenting reservations of provincial campgrounds in Ontario, Manitoba and Quebec ([245], we created a graph of camper travels which depicts a spatial travel network between origin locations (which correspond to residential addresses of camper travelers) and recreational destinations (campgrounds in provincial parks and historic sites). The camper travel network is described by a graph with coefficients $P_{i,j}$ denoting the relative frequency of camper movements between origin locations j and recreational destination locations i (see more details on spatial data in section 1.3.4). Specifically, for a given location j , $P_{i,j}$ is the fraction of trips that go from j to i each year, so we have $\sum_{i=1}^N P_{i,j} = 1$. Consider a patch i with an enforcement intervention, such as firewood movement quarantine, or a voluntary firewood surrender checkpoint aimed to stop the flow of untreated firewood from that location. We denote C_e as the percentage of infested firewood that can be intercepted on a route between two locations i and j , $0 \leq C_e \leq 1$. Interception at i may reduce the movement of infested firewood from a patch i to other patches j , so C_e indicates, in relative terms, the magnitude of interception efforts.

We also consider a public outreach campaign that can take place at a patch i . It is common that only a portion of campers visiting a patch i may be aware of and decide to comply with the public outreach message. We model the social awareness campaign as an increase of the net social cost of transporting firewood. We further conduct sensitivity analyses to compare the efficacy of enforcement vs. outreach measures aimed to stop the movement of firewood and reduce the rates of infestation.

1.3.1 Pest Spread Model

We begin with defining the equation for a population of susceptible host trees that may be attacked by an invasive pest. The pest can be introduced through untreated infested firewood. Variables, their interpretations, and corresponding baseline ranges are shown in Table 1.1. We assume that a tree population that is susceptible to pest attack undergoes logistic growth in the absence of infestation to a carrying capacity K . The population of susceptible trees, $S_i(t)$, at a patch i is being infested from firewood arriving with campers at i at a rate A :

$$\frac{dS_i}{dt} = \underbrace{rS_i \left(1 - \frac{(S_i + I_i)}{K}\right)}_{\text{Logistic Growth Of Forest}} - \underbrace{AS_i(I_i + B_i)\theta_k(I_i - I_a)}_{\text{Infestation term}} \quad (1.1)$$

where $\theta_k(I_i)$ is a sigmoid function such as

$$\theta_k(x) = \frac{1}{1 + e^{-kx}} \quad (1.2)$$

Terms S_i and I_i are the number of susceptible and infected trees, respectively, at patch i . B_i is the quantity of infested firewood in patch i , which we assume has the same probability of pest transmission within patch as infested trees. We choose the carrying capacity K to be the same in each patch for simplicity. The term $AS_i I_i \theta_k(I_i - I_a)$ represents intra-patch infestation with a density dependent population, parameterized by k and I_a , where I_a determines population of infested trees at which transmission is halved, and k is a constant which affects the sharpness of the transition of $\theta_k(x)$ at I_a . We assume that there is an influx of pest organisms entering a patch i with firewood which defines the propagule pressure at i . Infested trees at i are assumed to die at a constant rate γ , giving the following equation for the infested tree population of a patch.

$$\frac{dI_i}{dt} = \underbrace{-\gamma I_i}_{\text{Death of infested trees}} + \underbrace{AS_i(I_i + B_i)\theta_k(I_i - I_a)}_{\text{Susceptible become infested}} \quad (1.3)$$

The patches are spatially coupled through the transport of firewood by recreational travelers. The infestation rate at i depends on the number of visitors transporting infested firewood to i , which is also a function of the social dynamics at i , such as the enforcement, or public outreach measures described by a utility function, presented in [29], and applied to forest modelling in [26, 196]. Let L_i be the proportion of visitors to patch i who do not transport firewood and buy it locally, and d rate of exportation of infested logs. The rate of infested wood coming into patch i can be estimated as:

$$d \sum_{j=1, j \neq i}^N P_{i,j}(1 - C_e)(1 - L_j)I_j$$

The dynamics of L_i (the number of local transporters in patch i), is modelled by a replicator dynamics model that is suitable for describing systems where social learning occurs [29, 101], and is described in the section below.

1.3.2 Social Dynamics Model

We model the proportion of visitors who choose to use local firewood, L_i as a function of both the perceived threat of introduced pests, and the social cost of illegally transporting

infested firewood. We refer to visitors who choose to use local firewood as local strategists, and visitors who do not use local firewood as transport strategists hereafter. Let C_t be the cost of transporting firewood and C_l the cost to obtain it locally (and therefore avoid moving invasive pests to a patch i). We adopt the social influence model from [26], which is based on models of [29] and [101], which we will summarize below. We define the social utilities corresponding to the strategies of transporting firewood (P_t) and buying it locally (P_l) as

$$\begin{aligned} P_t &= -C_t + s(0.5 - L_i) - fI_i \\ P_l &= -C_l + s(L_i - 0.5) \end{aligned}$$

Transportation becomes a less attractive strategy if infestation is more prevalent, depending on the size of f . The parameter f controls the extent to which a local infestation causes behaviour change in that population. The parameter s controls the degree to which individuals are influenced by the the majority opinion in their patch (i.e. peer pressure). We assume that both local strategists and transport strategists in a patch i , given by L_i and $1 - L_i$ respectively, decide whether to change their strategy at the same rate, σ . Their decision is made by considering which strategy will maximize their utility $P_l - P_t$ at that point, leading to the following expression for the rate of change of the local strategist population:

$$\frac{dL_i}{dt} = \sigma L_i(1 - L_i)(P_l - P_t)$$

We replace the individual costs of C_t, C_l with the net utility value $U = C_t - C_l$. The cost difference U abstracts from the explicit definition of costs of using firewood [26] and allows including exogenous social incentives and motivation, such as awareness about the problem or any other form of social influence from outside each location i . A term B_i is introduced to represent the amount of local firewood available in patch i . For simplicity, we assume that the tree mortality rate at a patch i is only caused by infestation, so the mortality rate is the same as the death rate of the infested trees

$$\frac{dB_i}{dt} = \underbrace{-\gamma B_i}_{\text{Decay of fallen wood}} + d \underbrace{\sum_{j=1, j \neq i}^N P_{i,j}(1 - C_e)(1 - L_j)I_j}_{\text{Import of fallen wood}} \quad (1.4)$$

Because the infested wood imported into patch i in Eq 1.4 must come from another patch in the system, we subtract the corresponding term for leaving wood, $d \sum_{j=1, j \neq i}^N P_{j,i}(1 -$

$C_e)(1 - L_i)I_i$ from Eq 1.6 which describes the rate of change of infested population in a patch i . Using the notation in equations (1.5, 1.6, 1.7, 1.8), we formulate the problem of buying firewood locally vs. transporting it from other potentially infested locations as follows:

$$\frac{dS_i}{dt} = \underbrace{rS_i \left(1 - \frac{(S_i + I_i)}{K}\right)}_{\text{Logistic Growth Of Forest}} - \underbrace{AS_i(I_i + B_i)\theta_k(I_i - I_a)}_{\text{Infestation term}} \quad (1.5)$$

$$\frac{dI_i}{dt} = \underbrace{-\gamma I_i}_{\text{Death of infested trees}} + \underbrace{AS_i(I_i + B_i)\theta_k(I_i - I_a)}_{\text{Susceptibles become infested}} - d \underbrace{\sum_{j=1, j \neq i}^N P_{j,i}(1 - C_e)(1 - L_i)I_j}_{\text{Total infested wood leaving due to transport}} \quad (1.6)$$

$$\frac{dB_i}{dt} = \underbrace{-\gamma B_i}_{\text{Decay of firewood}} + d \underbrace{\sum_{j=1, j \neq i}^N P_{i,j}(1 - C_e)(1 - L_j)I_j}_{\text{Import of fallen wood}} \quad (1.7)$$

$$\frac{dL_i}{dt} = \sigma L_i(1 - L_i) \left(\underbrace{U}_{\text{Net cost to transport firewood}} + \underbrace{s(2L_i - 1)}_{\text{Social influence term}} + \underbrace{fI_i}_{\text{Impact of infestation}} \right) \quad (1.8)$$

Table 1.1 lists the model notation.

1.3.3 Patch-quarantine strategies

Let $V \subset [1, N]$ be a set of patches under a quarantine. We use the patches (nodes of the camper travel network) with the largest (shortest-path) betweenness centrality [78, 44], which is a common approach for selecting quarantine nodes in vaccination studies [237]. Betweenness centrality measures the extent to which a node lies on paths between other nodes and is used to detect the amount of influence a particular node has over the flow of information in a graph. The measure is often used to find nodes that serve as critical links between different parts of a graph. Formally, the shortest-path betweenness centrality of a node $i \in V$ on a weighted graph G is

$$g(i) = \sum_{i \neq s \neq t; s, t \in G} \frac{g_{st}(i)}{g_{st}}$$

Name	Default Value, (Range explored)	Units	Interpretation
N	2250	Patches	Number of patches in the network
S_i	Site specific	Trees	Number of susceptible trees in patch i
I_i	Site specific	Trees	Number of infested trees in patch i
B_i	Site specific	Trees	Infested firewood in patch i
L_i	Site specific	Unitless	Fraction of local strategists in patch i
r	0.02, [0.01, 0.06]	New trees per tree per year	Tree growth rate
A	0.001, [0.00065, 0.0014]	Number of infested trees per susceptible-infested contact per year	Transmission rate of pest
γ	1.4, [0.8, 1.8]	Trees per year	Decay rate for infested trees
K	5000	Trees	Carrying capacity of each patch
U	0, [-5, 5]	Utility	Social cost to transport firewood, or incentive to buy locally
C_e	0, [0.0, 1.0]	Unitless	Interception fraction
f	0.1, [0.01, 0.13]	Utility per capita	Impact of local infection on strategy
s	0.1	Utility per capita	Strength of social norms
σ	0.1	Strategy changes per capita per year	Rate of social learning
$P_{i,j}$	See below	Unitless	Fraction of trips that go from j to i each year.
d	0.1 [0.05, 0.3]	Logs per year	Rate of transmission of infested firewood between patches
I_a	1 [0.5, 5]	Trees	Value at which transmission rate of pest is halved due to density dependence
k	1	Unitless	Steepness of sigmoid function
V	Empty, [0 patches, 500 patches]	Patches	Set of patches to be quarantined
Δt	0, [0, 5]	Years	Length of quarantine
t_0	0, [0, 5]	Years	Time between initial infestation and patch quarantine

Table 1.1: Parameters and default values

where g_{st} is the number of shortest paths between nodes s, t and $g_{st}(i)$ is the number of geodesic paths between nodes s, t that go through node i . Both of these measurements calculate path length with respect to the weights of G . In words, the betweenness centrality $g(i)$ of a node i is the probability that i lies on a shortest path between some two nodes in G . In our camper travel network, higher weights denote more frequent trips, so for the purposes of determining the betweenness centrality, the weight of each edge (i, j) is $\max_{i,j}(P_{ij}) + 1 - P_{ij}$.

We model the implementation of firewood quarantine strategies at patches V by introducing a time-dependent term in Eqs (1.6),(1.7). Let t_0 , and Δt be the starting time of

the quarantine and the length of the quarantine respectively. Let $H_c(x, \Delta t)$, defined as

$$H_c(x, \Delta t) = \begin{cases} 1 & x < 0 \\ 0 & 0 \leq x \leq \Delta t \\ 1 & x > \Delta t \end{cases}$$

be an upside-down boxcar function of length Δt . This function acts as a switch which is "off" whenever $x \in [0, \Delta t]$. With this function, we can modify equations (1.6), (1.7) so that patches $i \in V$ do not import or export firewood whenever $x \in [0, \Delta t]$.

If $i \in V$,

$$\frac{dI_i}{dt} = -\gamma I_i + AS_i(I_i + B_i)\theta_k(I_i + B_i) - dH_c(t - t_0, \Delta t) \sum_{j=1, j \neq i}^N P_{j,i}(1 - C_e)(1 - L_j)I_j \quad (1.9)$$

$$\frac{dB_i}{dt} = -\gamma B_i + dH_c(t - t_0, \Delta t) \sum_{j=1, j \neq i}^N P_{i,j}(1 - C_e)(1 - L_j)I_j \quad (1.10)$$

Note that the only difference in the new equations (1.9), (1.10) from (1.6), (1.7) is in the last term denoting the interactions with neighbouring nodes. The equations for patches not in under quarantine (i.e., not in V) require us to distinguish arcs that connect to and from nodes under quarantine in V .

If $i \notin V$,

$$\begin{aligned} \frac{dI_i}{dt} = & -\gamma I_i + AS_i(I_i + B_i)\theta_k(I_i + B_i) - \sum_{j=1, j \neq i, j \notin V}^N P_{j,i}(1 - C_e)(1 - L_j)I_j \\ & - dH_c(t - t_0, \Delta t) \sum_{j=1, j \neq i, j \in V}^N P_{j,i}(1 - C_e)(1 - L_j)I_j \end{aligned} \quad (1.11)$$

$$\frac{dB_i}{dt} = -\gamma B_i + \sum_{j=1, j \neq i, j \notin V}^N dP_{i,j}(1 - C_e)(1 - L_j)I_j + dH_c(t - t_0, \Delta t) \sum_{j=1, j \neq i, j \in V}^N P_{i,j}(1 - C_e)(1 - L_j)I_j \quad (1.12)$$

In equations (1.11), (1.12) we split the summation term into two summations, one over all patches which are not under quarantine (i.e., not in the set V) and patches under quarantine in V . The latter summation is multiplied by a term, $H_c(t - t_0, \Delta t)$ which switches on and off the quarantine conditions.

1.3.4 Parameterization

We used data from [115] and [245], to quantify the risk of firewood transport to recreational destinations in Central Canada. The data documented the movements of campers to provincial campgrounds in Ontario, Quebec and Manitoba. Such data are maintained by provincial ministries of natural resources (MNRs). The dataset included a large number of potential origin sites (i.e., approximately 9000 locations). To reduce the computational burden, we reduced the size of the camper travel network by including all recreational destination locations but considering only the origin locations in the Canadian provinces of Ontario, Manitoba, and Quebec. We further reduced the size of the network by selecting most travelled routes. We selected the largest subgraph with a minimum degree of 10 (the 10-core of the graph) which considered only the most connected nodes, with largest impact on pest transmission. We implemented the procedure using the NetworkX library [92]. The final camper travel network included 2250 sites (Fig 1.1).

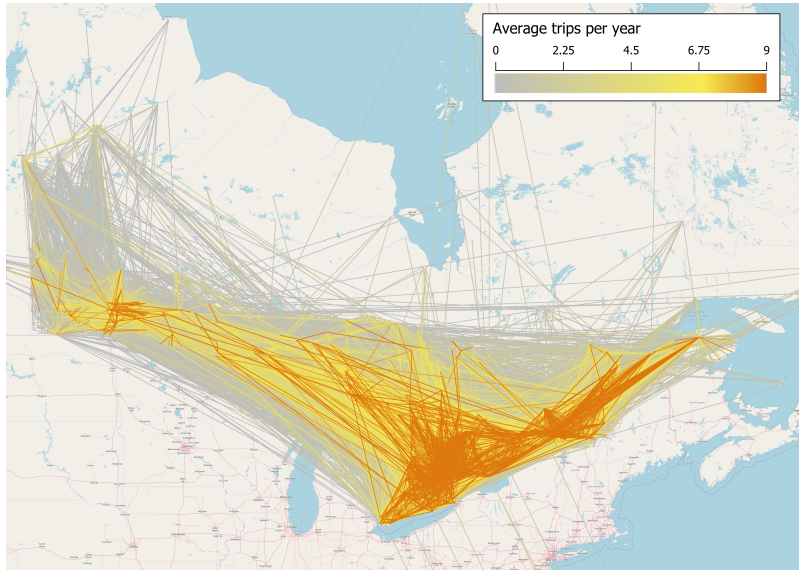


Figure 1.1: **Camper travel network in Ontario, Quebec and Manitoba.** Darker (more orange) lines represent more trips.

Because the model uses a large camper travel network it has a very large parameter space, and many of the parameters, especially those in Eq 1.8, are difficult to estimate directly from data. In this study we are exploring the region of parameter space that most closely approximates the dynamics in real infestations, such as the typical size and duration of the recent emerald ash borer outbreak in eastern Canada. To select the most

relevant range of the social influence parameters, σ, s, f , which are difficult to estimate from the literature, we did sensitivity analyses over a wide range of these parameters, and identified the parameter space where these parameters had the largest effect on the model dynamics, and where the course of the invasion was realistic. The inter-patch and intra-patch infection rate parameters, d, A , were selected to infest and eventually kill at least 95% of the tree population within 10 to 15 years.

We integrated equations (1.5-1.8) using code written in the Julia language, using the JuliaDiffEq library [184]. The integration was run on the Compute Canada clusters. Our primary focus was to explore the relative impacts of firewood enforcement versus public outreach and their abilities to reduce pest infestation rates across the camper travel network. We consider a hypothetical scenario where a harmful invasive pest is introduced in the largest urban center in eastern Canada with foreign imports (Greater Toronto Area, GTA) and assume that the bulk host tree population in the GTA is infested. This scenario is based on a history of past entries of invasive wood-boring pests to the GTA with foreign imports (such as introduction of Asian longhorned beetle in Toronto and Mississauga [224]).

1.3.5 Assessing intervention efficacy

The primary statistic we use to assess the total mortality of an infestation after t years is the average cumulative infested population, $\frac{1}{N} \sum_{i=1}^N T_i(t)$. To calculate $T_i(t)$, the cumulative infested population at patch i and time t , we solve the following equation in addition to the model equations.

$$\frac{dT_i}{dt} = AS_i(I_i + B_i)\theta_k(I_i - I_a) \quad (1.13)$$

The right-hand side of equation 1.13 is the only positive term of equation 1.6, so it increases when new infested trees are added to $I_i(t)$, but does not decrease when infested trees die, thereby counting the total number of infestations.

Since it is difficult to determine what utility value U , which defines the social cost of transport, corresponds to the current level of funding, we try to answer whether it would be beneficial to increase the funding, which we call the marginal benefit of increasing U . Given a time \bar{t} , we calculate $T(\bar{t})$ for a set of $U \in [-5, 5]$, then we fit a linear function of U to these points. We find a first-order approximation of $T(\bar{t})$ change per unit U (Fig 1.4) for a given set of parameters and time \bar{t} . A positive slope indicates that total infested tree population increases when U is increased, which means that increasing U does not

reduce the impact of the pest (at least, to a first approximation). In figures (1.4) - (1.6) this method is used to show how the total number of infested trees changes with respect to an increase in U , as a function of parameters and time.

1.4 Results

In our baseline scenario (Fig 1.2, parameters as in table 1.1), the model shows a typical pest outbreak originating in the GTA infesting all campgrounds in Ontario, Manitoba and Quebec over 10-20 years. This agrees with the observed timescale of the recent infestation of emerald ash borer (EAB) which entered Ontario in 2002 and now has infested most major populated places in the province [52].

First we discuss the timeseries plot of the baseline parameters (Table 1.1), where the model variables are averaged over all of the patches for easier visualization (Figure 1.2). Accordingly, we define $I(t) = \frac{1}{N} \sum_{i=1}^N I_i(t)$, $B(t) = \frac{1}{N} \sum_{i=1}^N B_i(t)$, $L(t) = \frac{1}{N} \sum_{i=1}^N L_i(t)$, to be the average infested tree population at t , the average quantity of infested logs at t , and the average fraction of local strategists at t , respectively. In figure 1.2, we find that increasing U (the social cost to transport firewood) increases the number of local strategists $L(t)$ (Fig 1.2h)—people who choose not to transport firewood between patches—and also reduces the size of the invasion, (Fig 1.2f) and the average number of infested logs, $B(t)$ (Fig 1.2g). Although the reduction in $B(t)$ is significant (as shown by the large differences in light red and dark red time series in Fig 1.2g), the flattening of the curve for infested trees (Fig 1.2f) is comparatively less significant. We can compare this with the result of increasing the fraction of infested logs intercepted between patches, C_e (1.2a,b,c,d). Increasing C_e decreases the number of infested trees, the delays the peak of the outbreak (Fig 1.2b,c). The delay in the peak of the outbreak also appears to cause the lag in $L(t)$ (Fig 1.2d). Social incentives appear to be very effective at reducing $B(t)$ while being less effective at reducing $I(t)$. This indicates that a shift from transport strategists to local strategists primarily occurs in areas that have already been infested. This effect does not occur with direct interception of infested firewood. Notably, direct interception is difficult to implement effectively, as even after intercepting high proportions of the infested wood transport, the corresponding decrease in $I(t)$ remains low (Fig 1.2b).

In Fig 1.3 we show the total number of infested trees at time t , $T(t)$, with respect to combinations of U , the social cost to transport firewood, and the fraction of infested firewood intercepted, C_e . If the fraction of intercepted infested firewood, C_e , is greater than 80%, we see a sharp reduction in the total infestation, T , even after 20 years (Fig 1.3 c), but lower interception rates have little effect unless the social cost to transport U

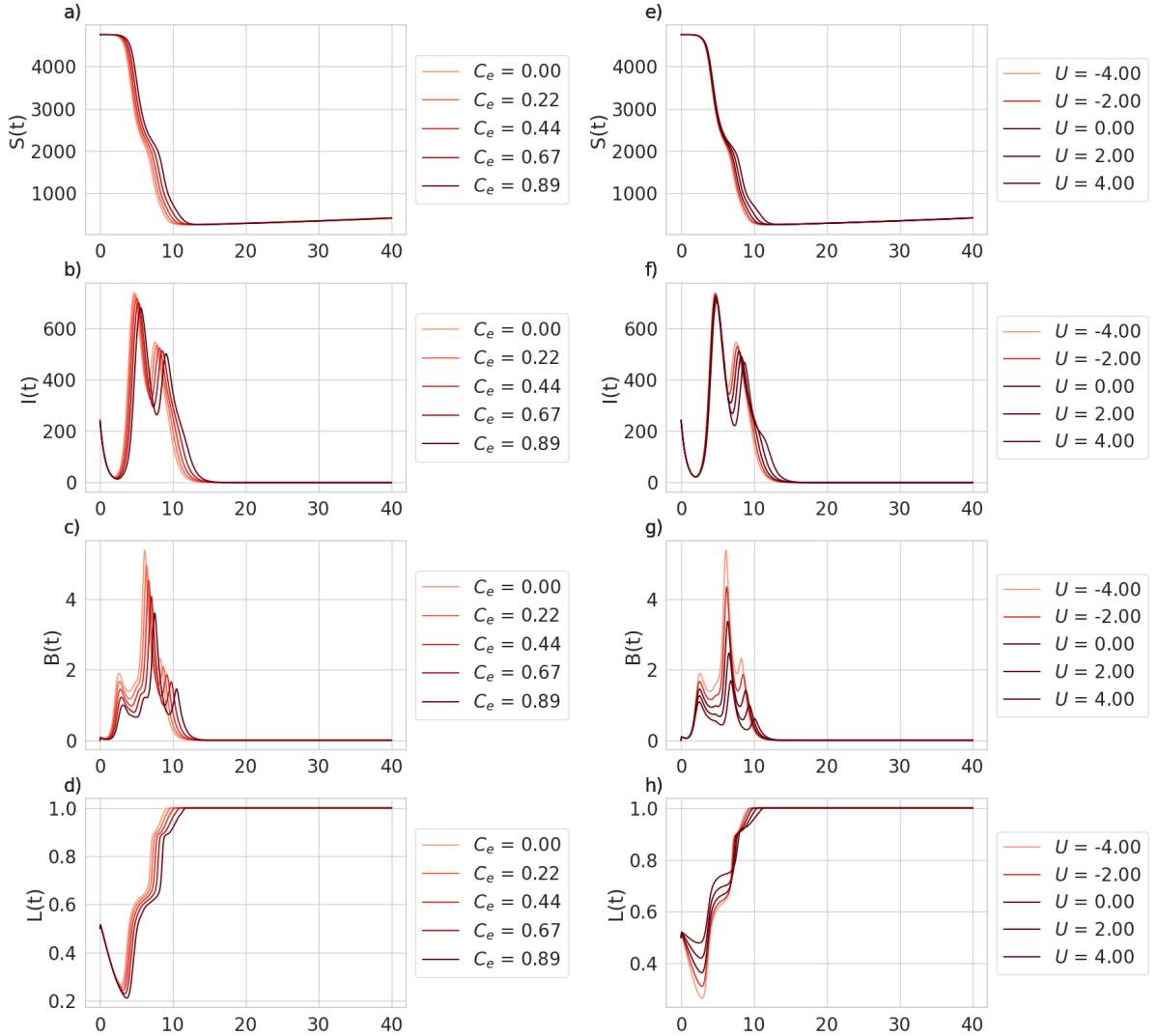


Figure 1.2: **Time series of model variables as a function of interventions, direct (raising C_e , panels a - d) and through social pressure (raising U , panels e - h).** The former intervention, panels a-d, means an increase of social pressure on people who choose to transport firewood (i.e. increasing the U value), and the latter refers to direct interception of firewood (i.e. increasing the C_e value). Terms $L(t) = \frac{1}{N} \sum_{i=1}^N S_i(t)$, $I(t) = \frac{1}{N} \sum_{i=1}^N I_i(t)$, $B(t) = \frac{1}{N} \sum_{i=1}^N B_i(t)$, $L(t) = \frac{1}{N} \sum_{i=1}^N L_i(t)$ are the averages of the state variables over all patches. $S(t)$ has been omitted for brevity.

is above the threshold seen in panel c) (Fig 1.3). Over a shorter time scale, increasing C_e appears to be effective at all interception rates.

The parameter f controls how the proportion of strategists in a given patch i ($L_i(t)$) responds to the population of infested trees (I_i) in that patch (eqn 1.8). Since social incentives (such as an intervention to human-mediated pest transport) tend to be less effective because they prevent firewood transport mostly in the areas that have already been colonized by pests (as suggested in Fig.1.2), we consider how the parameter f affects the marginal returns on U over time (Fig1.4). The shade of the blue region in Fig.1.4 represents the degree to which increasing U is beneficial, corresponding to a negative slope in the linear approximation of the change in T with respect to U (Fig 1.4 inset). Similarly, a red cell indicates non-negative slope and therefore a neutral or detrimental marginal effect. We begin to see the benefit of increasing U after about 10 years, shown by the transition from lighter blue to dark blue as we move from the bottom of the image to the top (Fig 1.4). This relationship is only affected slightly by altering the impact of local infestation on local strategy, f , where we begin to see slightly detrimental marginal returns after 10 years if $f < 0.04$.

Similarly, we have compared the marginal returns on increasing U with respect to the intra-patch transmission rate A and time t (Fig 1.5). When A is small ($A \leq 0.0009$, beneficial marginal returns on U can be observed over the whole duration of the infestation. We further explore the impact of varying the rate of transmission of infested firewood between patches, d (Fig 1.6). We find a roughly parabola-shaped region in the parameter plane of intra-patch and inter-patch transmission rates (A and d respectively), above which the marginal returns of increasing U are zero or possibly detrimental to the size of the total infested population after 10-20 years. Larger intra-patch transmission rates enable the pest population to establish earlier in a given patch by propagules. We see good marginal return in parameter regimes where few transport strategists (high $L(t)$) would reduce the reproductive ratio of the infection below 1. For instance, at the point $(A, d) = (0.00126, 0.103)$, increasing U is able to delay and eventually prevent a second wave, which decreases the total number of infected trees significantly (SI Fig 1). If the transmission rates A, d are high enough that even with no transport strategists, we get a second wave of infection, the effect of increasing U can be slightly detrimental (SI Fig 2). Panel f) of the aforementioned figures plots the number of patches where $I \geq 1$ over time, showing that the detrimental effect is largely due to the infection persisting longer in the network.

We also explored the effectiveness of patch quarantine by replacing model equations (1.6) and (1.7) with equations (1.9)-(1.12). This replacement prevents individual patches (nodes in a set V) with the highest betweenness centrality (with respect to the weights P_{ij}) from interacting with their neighbours during the time of the quarantine ($t \in [t_0, t_0 +$

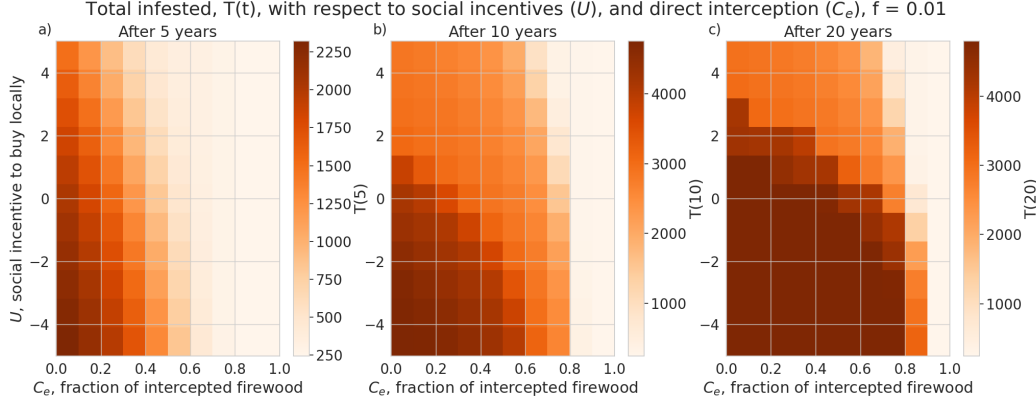


Figure 1.3: **Total infestation per node over 5, 10 and 20 years.** Neither increasing U nor C_e are effective at long time scales.

$\Delta t]$). Imposing quarantine on these nodes is expected to have the greatest impact on pest transmission rate. If the quarantine is initiated one year after the pest is introduced into the system (that is, $t_0 = 1.0$) then we find a significant reduction in total infestation even if only 50 patches are quarantined ($|V| = 50$) assuming they are quarantined for more than a year, shown in Fig 1.7. However, in our model, we find that quarantines need to be longer than approximately three years, and involve more than 150 nodes to still be effective in reducing the total infested population after 20 years $T(20)$. An interesting result in our quarantine plots is that we see a slightly larger range of effective parameter values if the quarantine begins after two years, $t_0 = 2.0$ (Fig 1.8), rather than one, $t_0 = 1.0$. This effect is probably due to the delay in infestation after the model is initialized, which can be seen by the local minimum in the infestation timeseries (Fig 1.2b,f).

1.5 Conclusion

We presented a model coupling human social behaviour regarding transport of infested firewood through recreational travel with a model of the spread of an invasive forest pest. Our main focus was to compare, in relative terms, common measures for slowing the spread of invasive species with firewood transport, such as public outreach campaigns aimed to raise awareness about the problem, and enforcement measures, including inspections at checkpoints to control the movement of firewood, and location-specific quarantine. The model is parameterized with campground reservation data for provincial parks and campgrounds in the provinces of Ontario, Manitoba and Quebec, Canada and incorporated

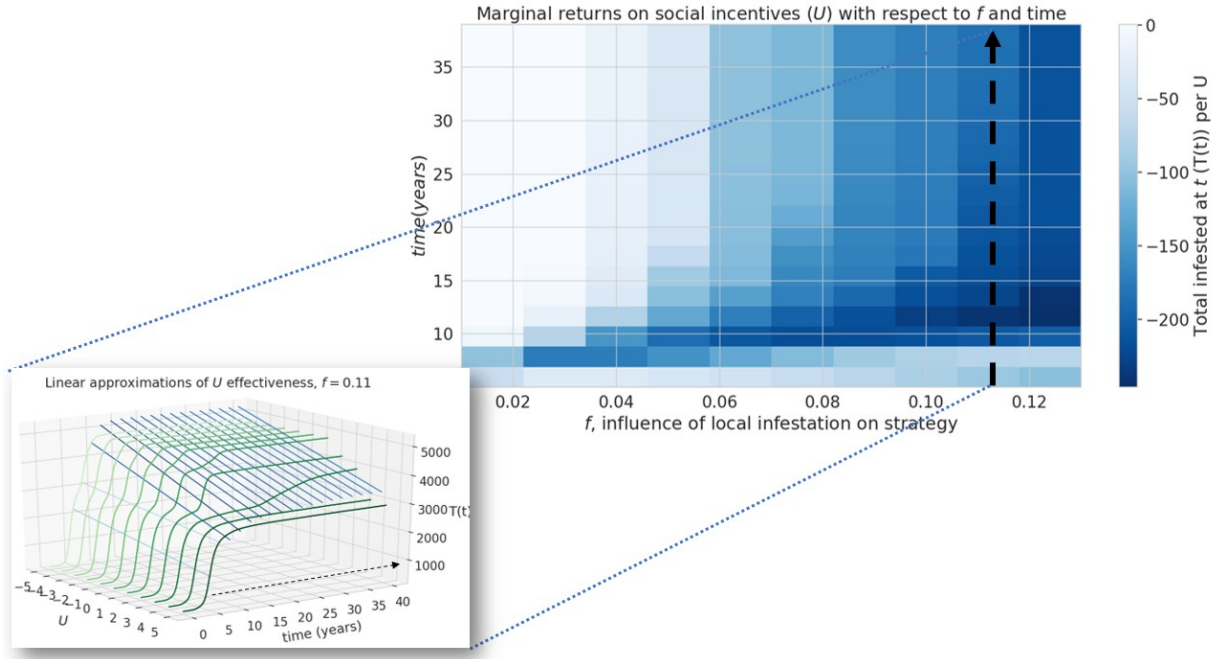


Figure 1.4: Efficacy of social incentives on infestation after time T . Inset graph shows an example of cross-section along the line $f = 0.11$ The influence of infestation on transport strategy, f , can hinder the intervention by public outreach, in the long-term (after approximately 20 years). The inset figure illustrates how one column in the heat map, shown by the dotted line, is constructed from the slopes of linear approximations of $T(t)$ over $U \in [-5, 5]$. The blueness of the lines going left to right is a function of their slope, corresponding to the color of the cells in the heatmap.

spatial information on the topology and geographical configuration of the camper travel network.

Under the assumptions of our model and a particular camper travel network configuration used in our model, checkpoints to control the movement of untreated firewood are unlikely to be effective at slowing the spread of invasive forest pests with firewood transport given typical moderate levels of funding and long delays in the response measures. We find the rate of interception to halve the total infested tree population after 5 years is about 30% (Fig 1.3), which is unlikely to be achieved in practice given typical limited budgets and personnel constraints in present-day firewood control programs. Given that our model uses somewhat simplified assumptions and does not account for fine-scale lo-

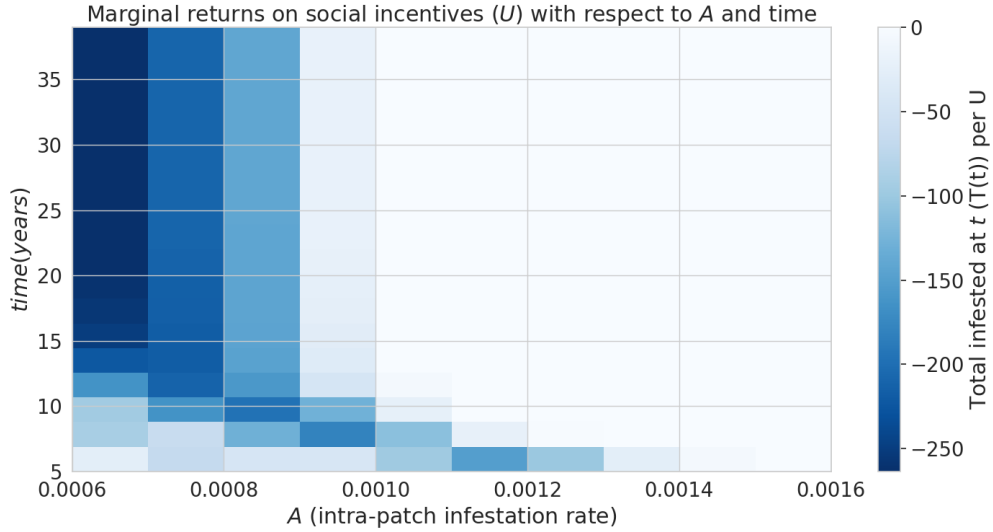


Figure 1.5: **Efficacy of social incentives on infestation after time period T with respect to A , the intra-patch infestation parameter.** This intervention becomes ineffective over time if A is sufficiently large.

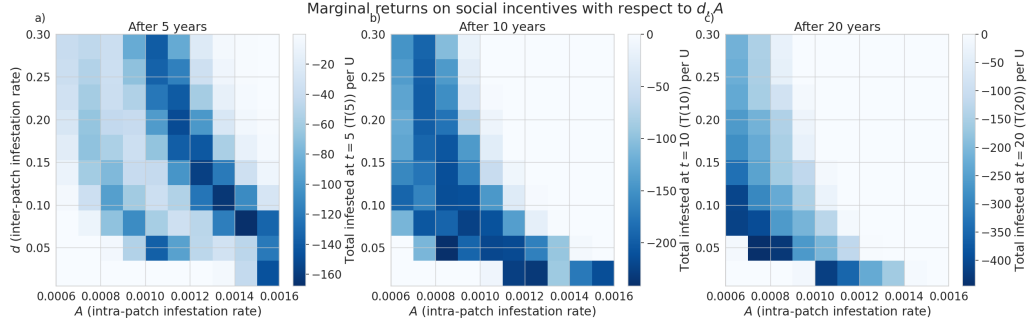


Figure 1.6: **Efficacy of social incentives on infestation after time T intra-patch spreading rate A , affects infestation outcomes.** The social incentive to not transport firewood, U , is more effective with lower pest spread rates.

gistical constraints (which are inspectors may face in various spatial locations) the actual rate of interception is likely to be lower in practical conditions. While a previous study [26] that used a similar model has demonstrated that social incentives may improve outcomes in a two-patch model under equilibrium conditions, we have found that in our complex

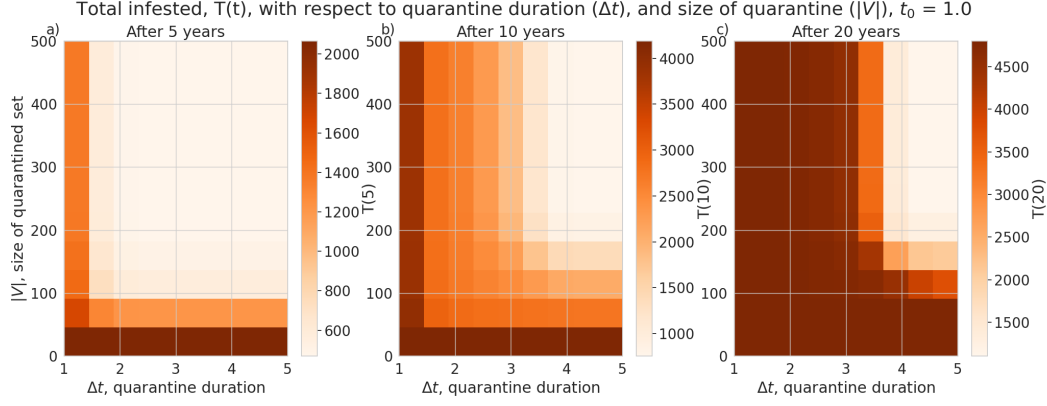


Figure 1.7: **Average total infested trees ($T(t)$) after 5, 10 and 15 years (panels a),b), and c) respectively), assuming the quarantine begins one year after the pest is introduced.** Total infestation plotted with respect to the number of nodes quarantined ($|V|$) and the length of the quarantine (Δt). The quarantine is effective over 5 years with only 50 patches, provided they are closed for over a year.

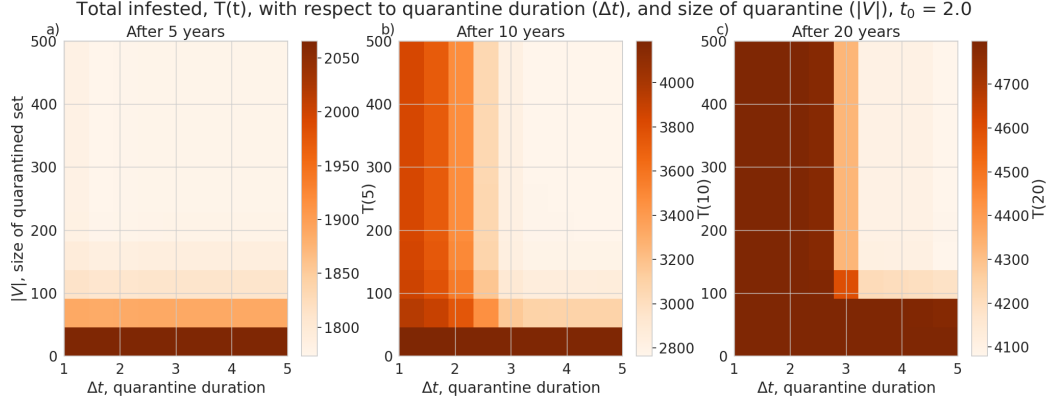


Figure 1.8: **Average total infested trees ($T(t)$) after 5, 10 and 15 years (panels a),b), and c) respectively), assuming the quarantine begins two years after the pest is introduced.** Total infestation plotted with respect to the number of nodes quarantined ($|V|$) and the length of the quarantine (Δt).

landscape network, the outcomes of infestation and invasion control measures are highly dependent on the time scale and the characteristics of the invaders, such as the inter-patch and intra-patch infestation rate. Social incentives (which aim to decrease the transport

of firewood, U), are generally able to reduce the infestation rate in the short term but its effectiveness is highly dependent on the ability of the pest to spread and infest other locations (Fig 1.6,1.5) under the conditions we have explored. Humans in our model tend to reduce their transport of firewood between patches in already infested areas, which causes the pest to persist longer in the network (Fig 1.2). Our results show that there could exist a threshold in the pest transmission rate A and the proportion of the infested wood which is turned into firewood, d (Fig 1.6). Below this threshold, it would not be beneficial to increase social outreach (i.e., increase U). This insight could be helpful in determining the spatial allocation of firewood movement control efforts for a particular pest species. We have also found that the location-specific quarantines that aim to restrict the movement of firewood to/from a particular location, might only be effective at slowing the invasion spread if a sufficiently large number (at least 140 in our case) of highly connected locations is quarantined, and the quarantine is established at early stages of infestation (Fig 1.7,1.8).

Given the typical cost limitations and logistics constraints faced by today's firewood control programs, and the assumptions made in our modeling framework, it is unlikely that local quarantine measures could significantly slow the spread of invasive pests through firewood unless drastic control and quarantine measures are undertaken. Public outreach campaigns, while helping increasing awareness of problem, cannot reliably slow the spread of pests within the parameter values tested, when the invasion spreads through a network based on camper travel data in Manitoba, Ontario and Quebec. Within our model, public outreach could be more effective for slow-spreading pests when the organism is able to kill host trees quickly but does not have significant spread capacity (that is, the inter-patch and intra-patch infestation rates are sufficiently small). Direct intervention, such as checkpoint inspections for illegally transported firewood, is also not an option, because meaningful outcomes can only be achieved if significant fractions of firewood transports can be intercepted. We find that patch quarantine is effective at slowing, or even stopping, the spread of an invasive forest pest when a large number of highly-connected patches are quarantined, for a long enough period. Our results in general terms agree with a present-day situation when numerous outreach and local quarantine measures had limited impact on illegal transport of firewood by campers and failed to slow the spread of wood-boring pests transported with untreated firewood. Our results also indicate that the enforcement campaigns aimed to intercept illegal movement of untreated firewood can only be effective if implemented at very large spatial scales in timely fashion (which, in turn, would require massive amounts of funding and personnel support).

There are some shortcomings to our model that could be addressed in future work. The interventions we study do not have spatial or time specifications for individual locations in the camper travel network. Deciding where and when, to deploy the outreach and

enforcement measures in a particular location would be a major enhancement of the model. Second, our model depicted a general problem of an invasive pest spreading with untreated firewood moved by recreational travelers. To adapt the problem to a particular pest species, a more specialized spread model will be required. We simplified the model by assuming that each infested patch provides similar propagule pressure to recreational travellers leaving the infested site. This assumption was made because no data about the actual proportions of infested wood carried by recreational travellers leaving the infested sites were available. Also, our analysis did not offer much insight at the level of individual spatial locations in a camper travel network. A simpler mechanistic model that applies unique pest control decisions at individual spatial locations could potentially address that aspect. Another possible way to simplify the model would be to remove the tree growth dynamics—since it operates on a longer time scale than the infestation spread—and so an invasion model without the forest growth component could be a reasonable approximation for short-term planning horizons. This will be the focus of future efforts.

1.6 Acknowledgements

The authors would like to thank Dr. Hanno Seebens and an anonymous reviewer for their contributions. Their detailed and thorough suggestions have significantly improved the quality of our paper.

Chapter 2

Fire Mitigates Bark Beetle Outbreaks in Serotinous Forests

Bark beetle outbreaks and forest fires have imposed severe ecological damage and caused billions of dollars in lost resources in recent decades. The impact of such combined disturbances is projected to become more severe, especially as climate change takes its toll on forest ecosystems in the coming years. Here, we investigate the impact of multiple disturbances in a demographically heterogeneous tree population, using an age-structured difference equation model of bark beetle outbreaks and forest fires. We identify two dynamical regimes for beetle and fire dynamics. The model predicts that fire helps dampen beetle outbreaks not only by removing host trees but also by altering the demographic structure of forest stands. We show that a stand thinning protocol, which reduces the population size of the largest few juvenile classes by a small percentage, is able to significantly reduce beetle-induced tree mortality. Our research demonstrates one approach to capturing compound disturbances in a mathematical model.

2.1 Introduction

Ecosystems have long been characterized by resilience in the face of large disturbances such as fire, storms, pathogens, and drought, which are often interacting. For example, the pine forests of western North America are highly adapted to both wildfires and bark beetle infestations. Many pine species, including lodgepole (*Pinus contorta*) and ponderosa (*Pinus ponderosa*) pine, depend on stand replacing fires to maintain healthy populations in their endemic range [34].

Of the major natural processes influencing lodgepole pine forests, the two with the greatest potential for large scale disturbance are mountain pine beetle (MPB, *Dendroctonus ponderosae*) and fire [113]. It has been noted that "In western North America, insect outbreaks and wildfires are the two most ecologically and economically significant natural forest disturbances" [141]. The MPB is a small insect endemic to the pine forests of western North America. MPB has recently attained previously unrecorded outbreak levels, probably due to anthropogenic factors [34, 192]. British Columbia's Ministry of Forests estimates that British Columbia contains roughly 35 million acres of lodgepole pine forest (about 23%), and slightly less ponderosa pine forest. They estimate that over the past 20 years, MPB has affected approximately 1.6 million acres of forest annually in British Columbia, more than forest fire and logging combined [32].

Ecological studies examining the relationship between MPB and wildfire damage are numerous, but have not reached a strong consensus in all aspects [21, 134, 205, 43, 113, 141, 5, 200, 107]. Lynch et al. [134] used remote sensing data associated with the 1988 Yellowstone National Park fires to investigate the link between fire prevalence and beetle attack. They found that beetle attack initially lowered the probability of crown fire in a patch, but bark beetle activity significantly increases fire risk 13-16 years in the future. On the other hand, Siedl et al. [200] find that wildfire increases spatial variability in stands, and therefore reduces the susceptibility of the stand to beetle outbreak. To make things more complicated, some studies have found that measures of burn severity are positively correlated with beetle damage[205, 43], although the results of Simard et al. [205] have been disputed by others [146].

MPB, and forest pests more generally, have attracted the attention of mathematical biologists since the 1970s due to importance of the problem and the dynamical complexity of outbreaks. The dynamical model of a full forest ecosystem would be intractable, necessitating simplifying assumptions. An early model of forest-pest dynamics by Ludwig and Holling [132] is a 3-dimensional differential equation model derived from simple population dynamics principles by separating fast (pest dynamics) and slow (forest dynamics). Powell, Logan and Bentz [176], derive a 7-dimensional nonlinear partial differential equation model, incorporating beetle pheromone dynamics, which they then integrate to a local ordinary differential equation model. Others look at just one facet of the forest ecosystem. For instance, since beetle lifecycle depends heavily on temperature, Gilbert and Powell [83] discussed three models which incorporate temperature-dependent emergence and attack. Tree mortality also exhibits sharp transitions as a function of tree vigor. Duncan et al.[69] incorporated a Leslie matrix to explicitly model multiple vigor categories in a discrete time dynamical model, while Lewis, Nelson, and Xu [124] developed an infinite-dimensional model which accounts for arbitrary vigor distributions. Some recent research

also considers dynamic interactions between forest pest outbreaks and human population decision-making regarding transport of infested campfire wood [26, 9].

Whether fire suppression changes stand structure in a way that alters susceptibility to beetle attack is a current topic of research. It has been hypothesized that wildfire encourages variability in spatial structure[200], which inhibits the ability of the bark beetle to find hosts and therefore dampens outbreak dynamics. We hypothesize that demographic variability (in the age structure of tree populations) can have a similar effect on MPB outbreaks. Age structure is pertinent because MPB mortality is much higher among larger, and therefore older, trees [22, 190]. This aspect has been studied in at least two previous models of MPB [124, 69] and has been found to affect system dynamics, although the additional role of fire was not considered in these models. Our objective is to characterize the model dynamics of an age-structured tree stand subject to disturbance from both fire and bark beetles, and to understand how changes in stand age structure due to wildfire or control measures can influence bark beetle outbreaks.

2.2 Methods

2.2.1 Model Description

Our model is based on a discrete-time model developed by Duncan et al.[69], describing beetle-tree dynamics in a well-mixed, sufficiently large, single-species stand. We expand their model to include fire dynamics by introducing a category for burnt trees, implemented as a Kermack-McKendrick-style contagious process[72]. We also add stochastic forcing to both the infested category and the burnt category. The discrete-time dynamics are defined in terms of population size in the spring of year n . Trees killed by beetle infestation die over the course of a few years, becoming a snag (a dead or dying tree that remains standing), until they decompose enough that they no longer shade the forest floor. If a tree is infested in the summer of year n , its needles will turn red and it will be a "red snag" in the spring of year $n+1$. Then, in the spring of year $n+2$, a "grey snag" with grey needles. After this it will decay sufficiently that new juvenile trees can grow up in its place, in year $n+3$. Wildfire also produces snags: a tree that is standing and shading the forest floor but no longer alive. We assume that wildfire clears the forest faster than MPB infections, so a tree that has been sufficiently affected by fire in the summer of year n becomes a snag in the spring of year $n+1$, and then the following spring, new juvenile trees come up in its place. We assume that the forest is at carrying capacity, so new trees can only come up at

the locations where trees have died. The forest is assumed to be a monospecies lodgepole pine stand, which are common hosts of MPB in western Canada and the USA.

Age structure is incorporated because beetles cannot effectively infest trees less than a certain diameter in size [190, 8]. Juveniles grow through the K age categories, with a probability $(1 - d)$ of surviving until the next year. Figure 2.1 illustrates the cycle each category should move through in any particular year. We define the following state variables: $j_{n,k}$ is the population of juvenile trees of age k at year n , $J_n = \sum_{k=0}^K j_{n,k}$, the total number of trees in the Juvenile class, S_n is the population of susceptible trees at year n , I_n is the population of infested trees at year n , and F_n is the population of burnt trees at year n .

The severity of forest fire in year n in the stand as a function of the previously unburned area is

$$P_n = T - \sum_{i=1}^n F_i e^{-\kappa(n-i)} \quad (2.1)$$

where the variable κ determines the half-life of decaying fuel. In other words, we define the severity or size of a fire in the year n as inversely proportional to the amount of land burned in recent seasons.

Our model is then defined by:

$$j_{n+1,1} = dJ_n + I_{n-2} + F_n \quad (2.2a)$$

$$j_{n+1,k} = (1 - d)j_{n,k-1} - \left(\frac{\alpha_1}{T}\right)P_n j_{n,k}, \quad k = 2 \dots K-1, K \quad (2.2b)$$

$$S_{n+1} = S_n + (1 - d)j_{n,K} - (I_n + \frac{\alpha_3}{T}P_n I_n) - \frac{\alpha_2}{T}P_n(S_n + (1 - d)j_{n,K}) - \sigma_F \gamma_n \quad (2.2c)$$

$$I_{n+1} = r_1 I_n e^{-\beta_1(T-S_{n+1})} - \frac{\alpha_3}{T}P_n I_n + \sigma_I \xi_n \quad (2.2d)$$

$$F_{n+1} = P_n \left[\frac{\alpha_1}{T} \sum_{i=0}^{K-1} j_{n,i} + \frac{\alpha_2}{T}(S_n + (1 - d)j_{n,K}) + \frac{\alpha_3}{T}I_n \right] + \sigma_F \gamma_n \quad (2.2e)$$

$$P_n = T - \sum_{i=1}^n F_i e^{-\kappa(n-i)} \quad (2.2f)$$

$$(2.2g)$$

A detailed derivation of these equations appears in the Supplementary Information. Descriptions of the variables can be found in Table 2.1. Fire could have been modelled in a more complex way using a different timescale than seasonal beetle outbreaks, but we chose to simplify the modelling by matching the timestep of the pest outbreak cycles instead. Fire prevalence is also dependent on precipitation patterns, temperature, human activity,

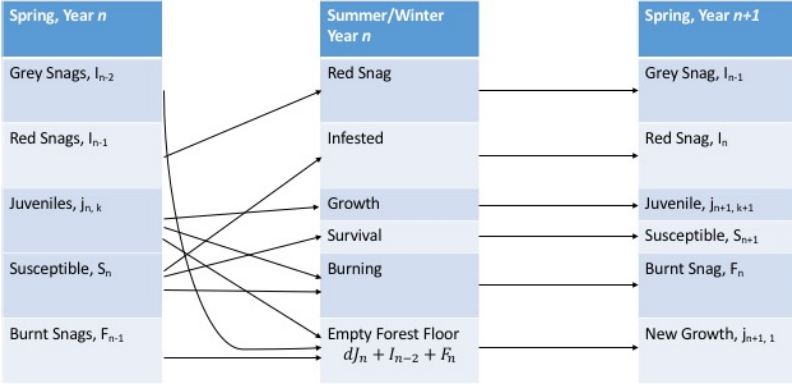


Figure 2.1: Conceptual diagram of compartments (state variables) and transitions between compartments across seasons. See main text and Table 2.1 for definitions of variables and parameters.

and other factors which operate on different time and spatial scales than our model. We assume this risk is roughly constant each year, and that it contributes to the environmental noise experienced by the system denoted by σ_F .

2.2.2 Forest thinning protocol (FTP) and controlled burning protocol (CBP)

One of the MPB control methods is to thin the forest, or conduct controlled burns, to increase the overall resilience of the forest to outbreaks or wildfire.[191, 195, 15]. In this section we modify our discrete process to include a control protocol, which is a simplified description of altering the structure of a growing stand to limit susceptibility to MPB. Define τ as the fraction of juvenile trees removed from the m oldest juvenile age classes, each year. The removed trees are added to the youngest juvenile class, to model trees replaced by seedlings. Since it is not realistic to perform this every year, we also investigate the effect of performing this protocol every 5 years. We will refer to the preceding protocol as the *forest thinning protocol (FTP)*.

Let

$$X_n = \arg \max_{S \subset [1, 50]: |S|=m} \sum_{k \in S} j_n, k$$

be the set of m largest juvenile age classes. Mathematically, for all age classes $k' \in X_n$, we change equation 2.2b to equation 2.5. In order to thin the fraction τ of trees from each age class in X_n , we add the corresponding population to $j_{n,0}$.

$$j_{n+1,1} = dJ_n + I_{n-2} + F_n + \sigma_F \gamma_n \quad (2.3)$$

$$+ \tau \sum_{k' \in X_n} \left((1-d)j_{n,k'-1} - \left(\frac{\alpha_1}{T}\right) F_n j_{n,k'} \right) \quad (2.4)$$

$$j_{n+1,k'} = (1-\tau) \left((1-d)j_{n,k'-1} - \left(\frac{\alpha_1}{T}\right) F_n j_{n,k'} \right), \quad k' \in X_n \quad (2.5)$$

Controlled burning is modelled similarly, but instead we add the reduced age compartments to the F compartment as shown in equation 2.7. We will refer to this modification as the controlled burning protocol (CBP) in the text from here on.

$$F_{n+1} = P_n \left[\frac{\alpha_1}{T} \sum_{i=0}^{K-1} j_{n,i} + \frac{\alpha_2}{T} (S_n + (1-d)j_{n,k}) + \frac{\alpha_3}{T} I_n \right] + \sigma_F \gamma_n \quad (2.6)$$

$$+ \tau \sum_{k' \in X_n} \left((1-d)j_{n,k'-1} - \left(\frac{\alpha_1}{T}\right) F_n j_{n,k'} \right) \quad (2.7)$$

2.2.3 Parameters and simulation design

Table 2.1 contains a list of the parameters used in the model, their interpretation, and their baseline values. Duncan et al. used a similar model with parameters fitted to data as in [5]. We performed sensitivity analysis on all other parameters (including all fire-related parameters) as shown in the Results section.

To generate parameter planes, we simulated equations 2.2a-2.2f across a grid of parameter values. We conducted 100 simulations for each point on the parameter grid and computed the average outcome for that grid point. We also recorded a representative sample of the resulting time series. We found the dominant period of the outbreaks by finding the frequency with maximum modulus via the discrete Fourier transform of the time series. In the deterministic case (with no noise), this frequency is the period of the periodic solution. When noise is added and the system becomes stochastic, there is no longer a

Table 2.1: Parameters and baseline values of compound fire and pest model. Except for α_i and the noise magnitude, all parameters were obtained from Duncan et al. [69]

Parameter name	Default value	Interpretation	Source
r_1	1.8	yearly fecundity of beetles	[175]
β_1	10.8×10^{-6}	search failure rate of MPB	[175]
d	0.01	annual mortality rate of juveniles	[69]
α_1	-	burning rate of juveniles	-
α_2	-	burning rate of adult trees	-
κ	0.1	decay rate of fuel	-
T	110,000	total number of trees in stand	[175]
K	50	number of juvenile generations	[69]
σ_F	20	noise in burnt tree	
σ_I	20	noise in infested tree	

clear periodic solution, but it is possible to estimate the mean of the distribution of the period by averaging the dominant frequency of the system at equilibrium. The period is assumed to be 1, corresponding to a (stochastic) steady state, if the smallest and largest values of the susceptible timeseries were sufficiently close together. The model and analysis of model output were coded in Julia. Throughout the results section, we mostly focus on the α_1, α_2 plane. We kept the remainder of the parameters constant as it was possible to set their values from empirical literature as described above.

2.3 Results

We first characterize the dynamical regimes of the model as a function of the burning rates α_1 , α_2 , and the decay rate κ . Then, we describe how the forest responds to the CBP described previously. Note that the susceptible class refers to mature trees, i.e., those large enough to be susceptible to infestation by MPB. Maximum outbreak sizes and fire season sizes are taken over a 500 year period.

2.3.1 Dynamical regimes

There are roughly two equilibrium dynamical regimes in the α_1, α_2 parameter plane, although the sizes of the equilibrium populations varies continuously with the parameters

inside each dynamical regime. The shapes of these dynamical regimes are affected by the rate of fuel decay, κ .

As α_1, α_2 increase, the model displays larger, and more regular fires, and smaller MPB outbreaks (Figure 2.2). When α_1, α_2 are small and not equal, years with severe fire seasons roughly follow the same period as MPB outbreaks. The variation in fire season size is more pronounced when α_1 is either much larger or smaller than α_2 . The presence of large even-aged stands is determined by the size of the infestation outbreaks, since they can only affect sufficiently old (susceptible) trees (Figure 2.3).

2.3.2 Impact of forest thinning protocol (FTP) and controlled burning protocol (CBP)

The model predicts that the FTP described in section 2.2 (remove a fraction τ of trees in the m oldest juvenile age classes each year) is an effective way to control MPB outbreaks, as long as control intensity parameters are sufficiently large. We consider trimming fractions τ up to 0.15, and the number of age classes trimmed m up to 8.

The FTP reduces the size of MPB outbreaks differently depending on the values of α_1, α_2 (Figure 2.4). The parts of the parameter regime where thinning is most effective at reducing MPB outbreak sizes occur when α_2 is large and α_1 is small, where we see approximately 70% smaller MPB outbreaks (Figure 2.4a). Generally, parameter ranges where MPB is more prevalent experience the largest reductions. With $\alpha_1 = 0.02, \alpha_2 = 0.0025$, there is a reduction in maximum outbreak population of about 30% when thinning the largest 8 stands by 15% each year (SI Figure 1a). With $\alpha_1 = 0.01, \alpha_2 = 0.006$, MPB populations are already dampened by the fire regime, but MPB outbreak peak population sizes are reduced from roughly 1600 infested trees to 800 infested (SI Figure 1b). A similar practice conducted every five years is almost as effective as the yearly trimming (Figure 2.4b). Increasing the heterogeneity of the age distribution in this way always reduces MPB populations by some amount. If we apply the CBP instead (see Equation 2.7), then controlled burns are largely effective with significant MPB populations, but can worsen outbreaks by up to 80% in regions were the MPB outbreak size is already small (Figure 2.4c).

FTP, and to a lesser extent CBP, does not simply indirectly reduce the number of susceptible trees (and therefore available MPB hosts) but rather flattens the age distribution better to reduce the occurrence of large, even aged, stands. We compare the average susceptible population (Figure 2.6) with and without FTP/CBP and find that in large parts of the parameter regime, the susceptible population is unchanged or increased, despite

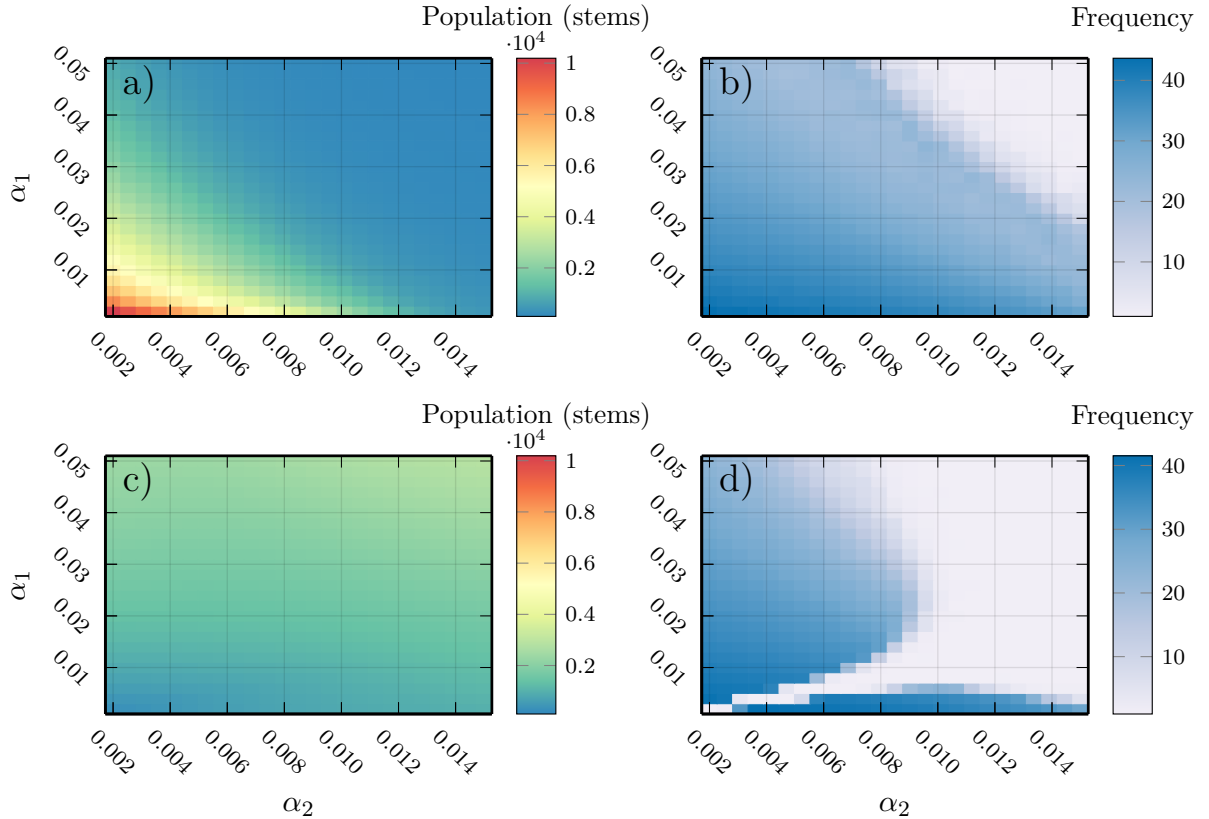


Figure 2.2: Approximate dynamical regimes of the system, where α_1 is the burning rate of juvenile trees, and α_2 is the burning rate of susceptible (mature) trees. a) Average size of largest MPB population (over 500 years at equilibrium) b) Average frequency of MPB outbreaks at equilibrium c) Average size of largest fire season (over 500 years at equilibrium) d) Average frequency of severe fire seasons at equilibrium. The juvenile burning rate (α_1) and susceptible burning rate (α_2) control fire and MPB prevalence. Large α_1, α_2 implies low infestation and also more regularity in the fire regime. All other parameters were set to baseline values (Table 2.1).

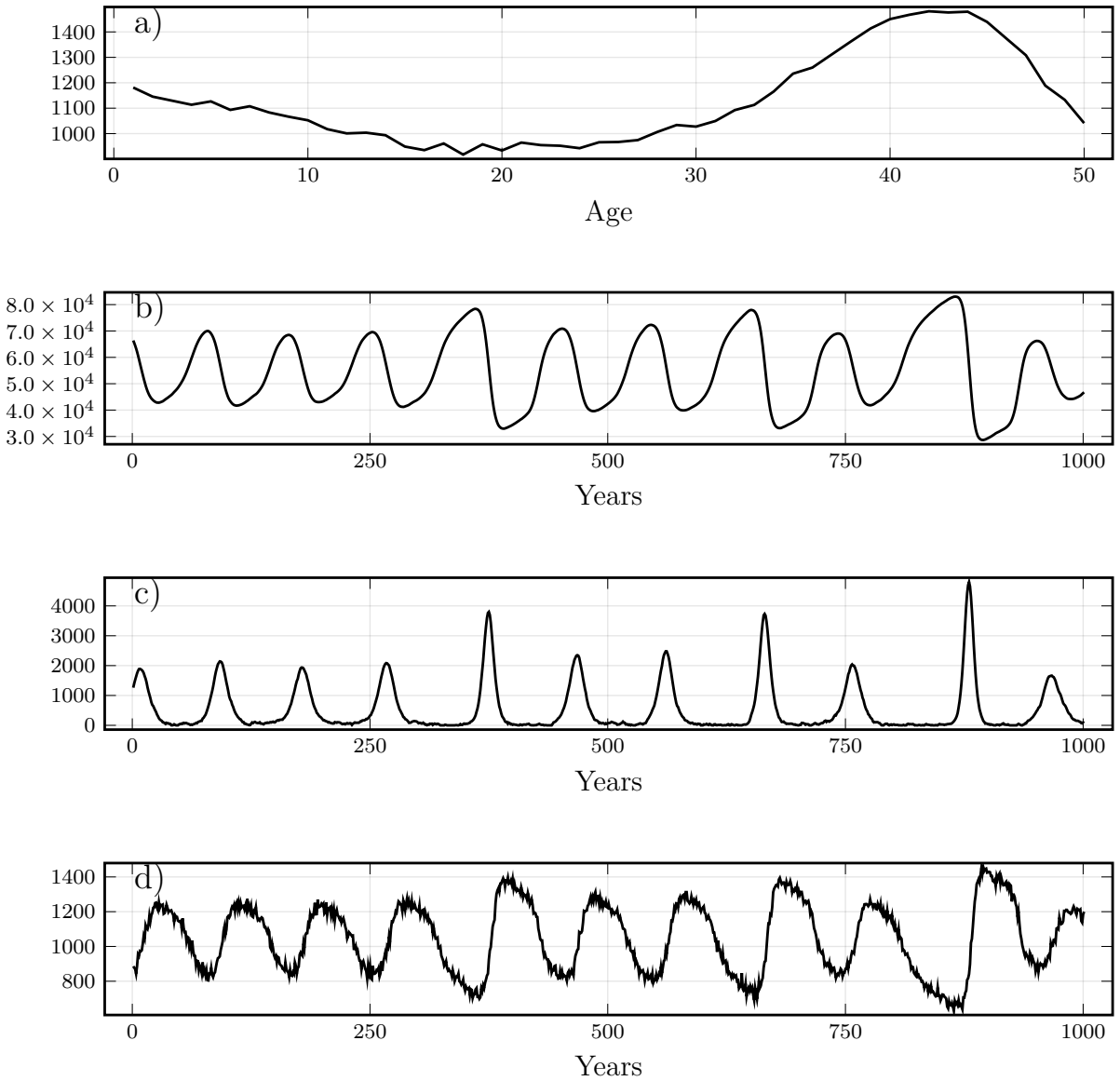


Figure 2.3: Time series of each state variable of a single realization where $\alpha_1 = 0.02$, $\alpha_2 = 0.0025$, showing the regular outbreaks of pests, periodic shifts in fire prevalence, and uneven age distribution generated by MPB outbreaks. a) juvenile distribution at time $t = 2050$ (note different x-axis), b) susceptible population after year t , c) infested tree population after year t , d) burned forest after year t . All other parameters were set to baseline values (Table 2.1).

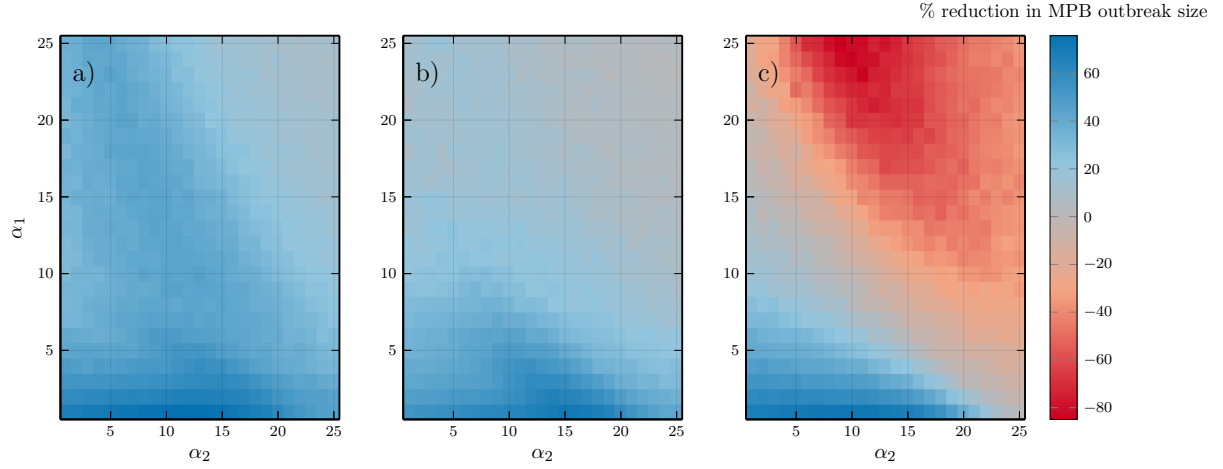


Figure 2.4: Percentage change in maximum MPB infestation size within 500 year period under a) FTP with $\tau = 0.15, m = 8$, b) CBP with $\tau = 0.15, m = 8$, with respect to burning rates α_1, α_2 , compared to no FTP. FTP is always effective at reducing MPB outbreaks, and CBP worsens them if the population of MPB is already low.

MPB outbreak sizes being reduced in most areas. Figure 2.5 shows a time-series at the same parameters as Figure 2.3, except with FTP flattening, to show the flattening of the age distribution.

2.4 Discussion

In this paper we used a mathematical model of pest and fire dynamics in pine forests to show how fire can suppress beetle outbreaks. The effect is related not only to the assumption of competition between fire and beetles in the model, but also due to the impact of fire on the age structure of stands: fires remove many large, mature trees and make space for rapidly growing juvenile populations that are not susceptible to forest pest outbreaks. The behaviour of the fire-beetle system is due to the fact that susceptibility to fire cuts across all age classes, compared to beetle outbreaks that affect mostly mature age classes. We show that large outbreaks of wildfires and beetle outbreaks inhabit the same dynamical regime, and that very small beetle populations are consistent with a regular fire regime. These results echo ecological evidence from Kaufmann et al.[113] and Seidl et al.[200] showing that a consistent fire regime can dampen outbreaks of bark beetle in a serotinous forest stand. Furthermore, we showed how a stand thinning protocol can significantly reduce tree

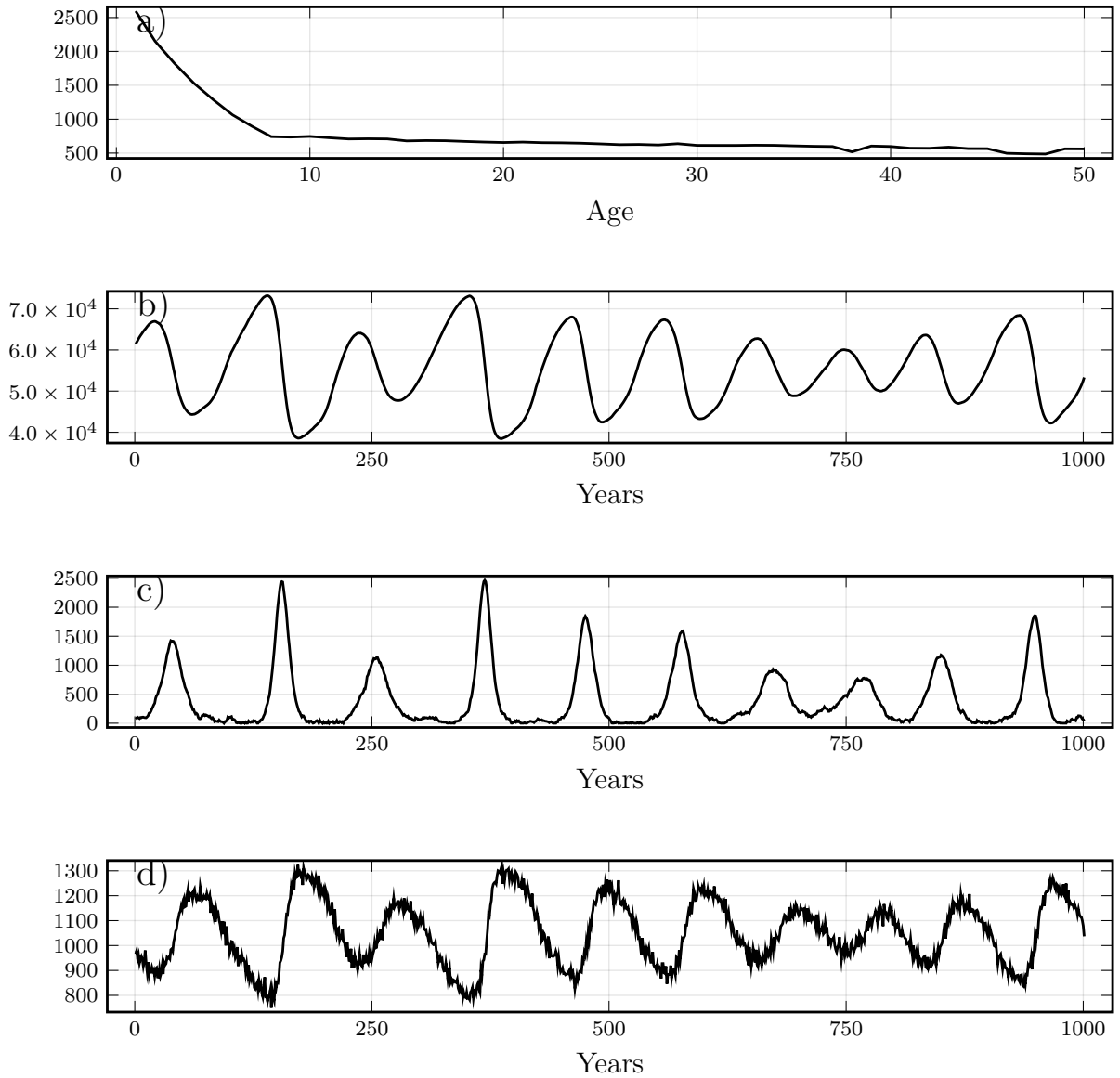


Figure 2.5: Time series showing realization of model under FTP with $\tau = 0.15$ fraction of $m = 8$ juvenile stands cleared, conducted each year, where $\alpha_1 = 0.02$, $\alpha_2 = 0.0025$. a) juvenile distribution at time $t = 2050$ (note different x-axis), b) susceptible population after year t , c) infested tree population after year t , d) burned forest after year t . Notice the flattening of the age distribution compared to the same parameters with no FTP (Figure 2.3)

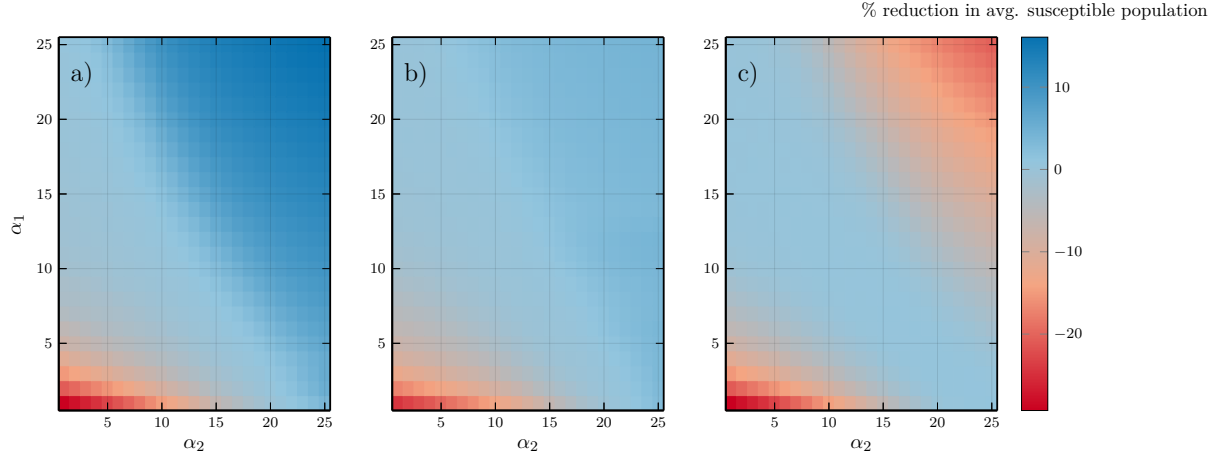


Figure 2.6: Percentage change in average susceptible (mature) forest population compared to no FTP with $\tau = 0.15, m = 8$, b) controlled burning with $\tau = 0.15, m = 8$, with respect to burning rates α_1, α_2 . FTP and CBP increase the average population of mature trees in many cases, in addition to reducing outbreak sizes.

mortality due to MPB outbreaks in forests prone to both fire and beetle outbreaks. Only a small intensity of thinning is required to see significant results. Prescribed burning has a similar, although less significant, effect on the age structure of the forest, and therefore similarly dampens MPB outbreaks. Prior to the arrival of European colonists, indigenous americans routinely burned areas in western North America [27], these practices were not recognized as beneficial by colonial governments, and were outlawed [42].

Implications for Fire/beetle management

Our work provides support for the practice of thinning forest stands to create more heterogeneity in age structure [108, 151], despite the absence of spatially explicit dynamics in our model. We show that even small changes to the demographics of forest stands can result in large shifts in forest dynamics, dampening out oscillating disturbance patterns and thereby increasing stand resilience. Using an abstract model for this purpose hopefully allows the evidence to generalize better over the wide range of possible ecosystem parameters.

Evidence in literature for dynamical regimes described

Broadly, our model can describe the current dynamical regime of stands of pine forests in the western interior with low fire susceptibility parameters α_1, α_2 (the bottom right-hand corner of Figure 2.2a) depending on the location and time. Our model represents a

single stand with autonomous parameters, and in reality, there are probably many possible dynamical regimes coexisting across the landscape and through time. Taylor and Carroll [214] studied the wildfire and MPB history of interior British Columbia, and also found this dynamic regime, albeit with decreasing prevalence of wildfire and increasing MPB outbreaks through the 20th century. They find that the low frequency and severity of wildfire has increased the percentage of pine in susceptible age classes to 55%, consistent with our estimate for low α_1, α_2 (see Figure 2.3a for an example of the large susceptible stands in this dynamical regime). Axelson et al. [21] records that, for their study area in southern interior British Columbia, there has been a fire-free interval of over 100 years. While this period is much longer than in our model, a trend towards higher variance in fire periods does match our model for the aforementioned parameter range, and a more complex fire model could potentially capture this additional complexity. They also record an average return time of 36 years for MPB in their area, consistent with our estimate for sufficiently low burning parameters. Kulakowski et al. [119] records a similar dynamic regime as [21] for the 20th century, but more frequent fire outbreaks, more closely matching this model.

Implications for Forest Ecosystems

The dry pine forest ecosystem that we model in this paper is home to many vertebrates who react to disturbance, biotic and otherwise, in different ways. Many wood-boring birds use MPB as a food source [153, 174]. Of these bird species, the three-toed woodpecker (*Picoides dorsalis*) and hairy woodpecker (*Leuconotopicus villosus*) depend significantly on bark beetles as a source of food [123]. Accounts estimate that they make up about 23% of the woodpeckers diet on an average year [33], although during outbreak years the fraction could be much larger [123]. Woodpeckers increase their reproduction rate during outbreak years of MPB [73], so dampening MPB outbreaks could be detrimental to bird populations, although there are feedbacks here that warrant further study. At least one predator of MPB, the black-backed woodpecker (*Picoides arcticus*), is heavily dependent on wildfires for habitat. Therefore, improving forest heterogeneity would likely also improve resilience in woodpecker populations which depend on these disturbances for habitat. Small mammals that inhabit western pine forests differ on their preference for burn-cleared habitat [250]. Mammals such as the deer mouse (*Peromyscus maniculatus*) strongly prefer burn clearing [251], while the red backed-vole (*Myodes gapperi*) favors undisturbed stands [250]. Increasing heterogeneity would improve the availability of both open stands for species which prefer the former habitat and closed, undisturbed stands for species which favor the latter. The impact of our results for these ecosystems are likely to be significant, but due to the complex feedbacks mentioned in these relationships, it is difficult to know without extending the model and further empirical data on the strength

of these feedbacks.

The primary goal of this paper was to build on work on the age structured models of beetle-infested stands[69] to a dynamical situation with a more complex disturbance regime that includes wildfire, a common feature of the forests inhabited by MPB. The modelling of fire spread is a very complex problem which is dependent on many variables which are not modelled here. Moreover, the beetle infestation model we used was relatively simple, necessitating use of a simple fire model as well in order to retain tractability of the model. We opted for a simple approach derived from the compartmental modelling literature. The dynamics we see here are an average case, so a more sophisticated fire model would yield more detailed results. The assumed impact of fire on all age classes, and the mechanism through which we model fire spread could also be refined in future work. Snags are also not considered burnable material, which may have an effect on some of the dynamics. We chose not to include these to reduce the number of parameters, especially parameters for which we don't have empirically-derived values. Lastly, the parameters which we drew from Duncan et al. [69] were not tested for sensitivity, and therefore our findings could be affected by these values.

A number of other approaches that relax our simplifying assumptions could be explored in future research. Other models combine annual difference equations with continuous time intra-year equations [210, 134, 54]. A continuous time summer phase is one way we could more accurately explicitly model a wildfire season. The FTP is straightforward and corroborates the findings of similar work with more complex mechanisms [210]. Nevertheless, our control strategies could be significantly more detailed and take into account fire-regimes and current susceptible population. Our goal was to illustrate that we can take advantage of the system dynamics by flattening the age distribution through burning a small percentage of juvenile trees, but more complex strategies might be more efficient. Spatial models would provide even more possibilities for control options. We did not explore the complex relationship between bark beetle emergence and temperature. MPB life-cycles are heavily regulated by temperature: warm years can cause more than one generation to emerge in a season, and severe cold can wipe out large populations. The higher precipitation and temperatures predicted by models of climate change imply conditions more conducive to MPB reproduction and therefore MPB outbreaks. Fire season intensity is also affected by temperature, and some evidence suggests that increasing temperatures and earlier snowmelts are probably creating worse fire seasons in this area [240]. Serotinous forests will be subject to very different environmental regimes in coming decades that involve multiple stressors. We have demonstrated how a model can explore the impact of fire and control protocols on tree stand age structure and thus MPB outbreaks. Future models that account for multiple disturbance mechanisms could be useful for anticipating how forests will respond

to novel environmental regimes in the rest of the twenty-first century.

Funding

This research was supported by an NSERC discovery grant to Chris T. Bauch and Madhur Anand.

Conflicts of interest/Competing interests

The authors declare no competing interests.

Availability of data and material

Not Applicable.

Code availability

(software application or custom code)

The source code for this work can be found at the author's public git repository: <https://git.uwaterloo.ca/pjentsch/fire-mitigates-bark-beetle-outbreaks-in-serotinous-forests>

Authors' contributions

All authors conceived ideas for the study. PCJ designed and coded the model, performed analyses, created figures, and drafted the manuscript. All authors revised the manuscript

Chapter 3

Prioritising COVID-19 vaccination in changing social and epidemiological landscapes: a mathematical modelling study

During the COVID-19 pandemic, authorities must decide which groups to prioritise for vaccination in a shifting social–epidemiological landscape in which the success of large-scale non-pharmaceutical interventions requires broad social acceptance. We aimed to compare projected COVID-19 mortality under four different strategies for the prioritisation of SARS-CoV-2 vaccines. We developed a coupled social–epidemiological model of SARS-CoV-2 transmission in which social and epidemiological dynamics interact with one another. We modelled how population adherence to non-pharmaceutical interventions responds to case incidence. In the model, schools and workplaces are also closed and reopened on the basis of reported cases. The model was parameterised with data on COVID-19 cases and mortality, SARS-CoV-2 seroprevalence, population mobility, and demography from Ontario, Canada (population 14.5 million). Disease progression parameters came from the SARS-CoV-2 epidemiological literature. We assumed a vaccine with 75% efficacy against disease and transmissibility. We compared vaccinating those aged 60 years and older first (oldest-first strategy), vaccinating those younger than 20 years first (youngest-first strategy), vaccinating uniformly by age (uniform strategy), and a novel contact-based strategy. The latter three strategies interrupt transmission, whereas the first targets a vulnerable group to reduce disease. Vaccination rates ranged from 0.5% to 5% of the population per week, beginning on either Jan 1 or Sept 1, 2021. Case no-

tifications, non-pharmaceutical intervention adherence, and lockdown undergo successive waves that interact with the timing of the vaccine programme to determine the relative effectiveness of the four strategies. Transmission-interrupting strategies become relatively more effective with time as herd immunity builds. The model predicts that, in the absence of vaccination, 72000 deaths (95% credible interval 40000–122000) would occur in Ontario from Jan 1, 2021, to March 14, 2025, and at a vaccination rate of 1.5% of the population per week, the oldest-first strategy would reduce COVID-19 mortality by 90.8% on average (followed by 89.5% in the uniform, 88.9% in the contact-based, and 88.2% in the youngest-first strategies). 60000 deaths (31000–108000) would occur from Sept 1, 2021, to March 14, 2025, in the absence of vaccination, and the contact-based strategy would reduce COVID-19 mortality by 92.6% on average (followed by 92.1% in the uniform, 91.0% in the oldest-first, and 88.3% in the youngest-first strategies) at a vaccination rate of 1.5% of the population per week. Interpretation The most effective vaccination strategy for reducing mortality due to COVID-19 depends on the time course of the pandemic in the population. For later vaccination start dates, use of SARS-CoV-2 vaccines to interrupt transmission might prevent more deaths than prioritising vulnerable age groups.

3.1 Introduction

The COVID-19 pandemic has imposed a massive global health burden as waves of infection to move through populations around the world [144]. Both empirical analyses and mathematical models conclude that non-pharmaceutical interventions (NPIs) are effective in reducing COVID-19 case incidence [18, 165, 223]. However, pharmaceutical interventions are highly desirable given the socio-economic costs of lockdown and physical distancing. Hence, dozens of vaccines are in development [133], and model-based analyses are exploring the question of which groups should get the COVID-19 vaccine first [46, 48].

When vaccines become available, we will face a very different epidemiological landscape from the early pandemic. Many populations will already have experienced one or more waves of COVID-19. As a result of natural immunity, the effective reproduction number R_{eff} (the average number of secondary infections produced per infected person) will be reduced from its original value of approximately $R_0 = 2.2$ in the absence of pre-existing immunity [100]. Epidemiological theory tells us that as R (or R_0) decline toward 1, the indirect benefits of transmission-blocking vaccines become stronger. For instance, if $R_{eff} \approx 1.5$, such as for seasonal influenza, only an estimated 33% percent of the population needs immunity for transmission to die out in a homogeneously mixing population [17, 70]. This effect was evidenced by the strong suppression of influenza incidence in Australia in Spring

2020 due to NPIs targeted against COVID-19 [20].

This effect has stimulated a literature comparing the vaccination of groups that are responsible for most transmission to vaccination of groups that are vulnerable to serious complications from the infection. Natural immunity to SARS-CoV-2 will likely continue to rise in many populations on account of further infection waves. Given these likely changes to the epidemiological landscape before the vaccine becomes available, we suggest this question is worthy of investigation in the context of COVID-19.

The social landscape will also look very different when vaccines become available and this aspect is crucial to understanding the pandemic. Scalable non-pharmaceutical interventions (NPIs) like physical distancing, hand-washing and masks are often one of the few available interventions when a novel pathogen emerges. Flattening the COVID-19 epidemic curve was possible due to a sufficient response by populations willing to adhere to public health recommendations. Therefore, pandemic waves are not simply imposed on populations – they are a creation of the population response to the pathogen. They exemplify coupled socio-epidemiological systems exhibiting two-way feedback between disease dynamics and behavioural dynamics interact with one another [166].

Approaches to modelling coupled social-epidemiological dynamics vary[187, 194, 81, 233, 82]. Some models have used evolutionary game theory to model this two-way feedback in a variety of coupled human-environment systems [166, 29, 102, 51, 14, 248, 6]. Evolutionary game theory captures how individuals learn social behaviours from others while weighing risks and benefits of different choices. In this framework, individuals who do not adopt NPIs can “free-ride” on the benefits of reduced transmission generated by individuals who do adopt NPIs [187].

Here, our objective is to compare projected COVID-19 mortality under four strategies for the prioritisation of COVID-19 vaccines: older individuals first, children first, uniform allocation, and a novel strategy based on the contact structure of the population. We use an age-structured model of SARS-CoV-2 transmission, including evolutionary game theory to model population adherence to NPIs and changes to mobility patterns. We use scenario and sensitivity analysis to identify how strategy effectiveness responds to possible changes in the social-epidemiological landscape that may occur before and after vaccines become available.

3.2 Model Overview

3.2.1 Structure and parameterisation

We developed an age-structured SEPAIR model (Susceptible, Exposed, Presymptomatic, Asymptomatic, Symptomatic, Removed) with ages in 5-year increments. Upon infection, individuals enter a latent period where they are infected but not yet infectious (“Exposed”). After the latent period, individuals become presymptomatically infectious, and then either symptomatically or asymptomatically infectious, before finally entering the Removed compartment when their infectiousness ends. We did not model testing or contact tracing explicitly, although we assume infected individuals are ascertained at some rate. Transmission occurs through an age-specific contact matrix, susceptibility to infection is age-specific, and we include seasonality due to changes in the contact patterns throughout the year. To infer model parameters, we fitted the model to Ontario COVID-19 case notifications stratified by age and time, Ontario seroprevalence data, and Ontario mobility data. Use of seroprevalence data ensured that our estimates of transmission were not biased by case under-reporting. Remaining model parameter values were fixed using Ontario demographic and mortality data, and literature on COVID-19 serial interval and incubation periods. Details of our model structure, parameterization, data sources, and model fits appear in the appendix, pp 1-11.

Both schools and workplaces are closed when the number of ascertained active cases surpasses 50%, 100%, 150%, 200%, or 250% of the peak ascertained active cases that occurred during the first wave (the “shutdown threshold”, T), and are re-opened again when cases fall below that threshold. Individuals interact with other individuals at a specified rate and switch between adherence and non-adherence to NPIs, including mobility restrictions, by comparing the cost of practicing NPIs against the cost of not practicing NPIs and thereby being subject to an increased risk of infection according to the prevalence of ascertained cases. Both school and workplace closure and population level of adherence to NPIs reduce transmission according to a specified efficacy (see Appendix, pp 1-5).

3.2.2 Vaccine scenarios

We considered two dates for the onset of vaccination: 1 March 2021 and 1 September 2021. These correspond to the end dates of a two-dose course of vaccination lasting two weeks. We assumed it was possible to vaccinate 0.5%, 1.0%, 1.5%, 2.5%, or 5.0% of the population per week (the “vaccination rate”, θ). Our baseline scenario assumed a vaccine with 75% efficacy in all ages, against both infection and transmission.

The “oldest first” strategy administers the vaccine to individuals 60 years of age or older, first. After all individuals in this group are vaccinated, the vaccine is administered uniformly to other ages. The “youngest first” strategy is similar, except it administers the vaccine to individuals younger than 20 years of age first. The “uniform” strategy administers vaccines to all age groups uniformly, from the very start. The “contact-based” strategy allocates vaccines according to the relative role played by different age groups in transmission. This tends to prioritise ages 15-19 primarily, 20-59 secondarily, and the least in older or younger ages (Appendix, pages 4, 12). The “oldest first” strategy targets a vulnerable age group while the other three strategies are designed to interrupt transmission. We also explored an optimal strategy that optimizes age-specific vaccine coverage to minimize the number of deaths over five years (Appendix, page 4). We also report on sensitivity analyses in the Results section.

3.3 Results

The Google mobility data that we use as a proxy for adherence to NPIs closely mirrors the COVID-19 case notification data over the time period used for fitting (Figure 1, open orange circles). Since a heightened perception of COVID-19 infection risk simulates the adoption of NPIs²⁶, which in turn reduces SARS-CoV-2 transmission [18, 165], this exemplifies a coupled social-epidemiological dynamic. The mirroring may furthermore represent convergence between social and epidemiological dynamics, which has been predicted for strongly coupled systems [203]. Moreover, the fit of the social submodel to the mobility data is as good as the fit of the epidemic submodel to case notification data (Figure 1), despite the fact that our social model consists of significantly fewer equations and a similar number of parameters as our epidemiological model. This shows how modelling population behaviour during a pandemic can be accomplished with relatively simple models.

The model predicts additional pandemic waves from Fall 2020 onward, not only with respect to COVID-19 cases but also population adherence to NPIs and periods of school and workplace closure (Figure 2). The impact of the four strategies on COVID-19 cases and deaths depends on when the vaccine becomes available and how quickly the population can get vaccinated. Broadly speaking, vaccinating 60+ year-olds first reduces mortality the most out of all four strategies if vaccination begins in March 2021, whereas the uniform or contact-based strategies reduce mortality the most if vaccination begins in September 2021, unless the vaccination rate is very small. More specifically, we identify three regimes for model dynamics. We explore them through plots of infection incidence over time (Figure 3); plots of the cumulative number of deaths under all four strategies, as they depend on

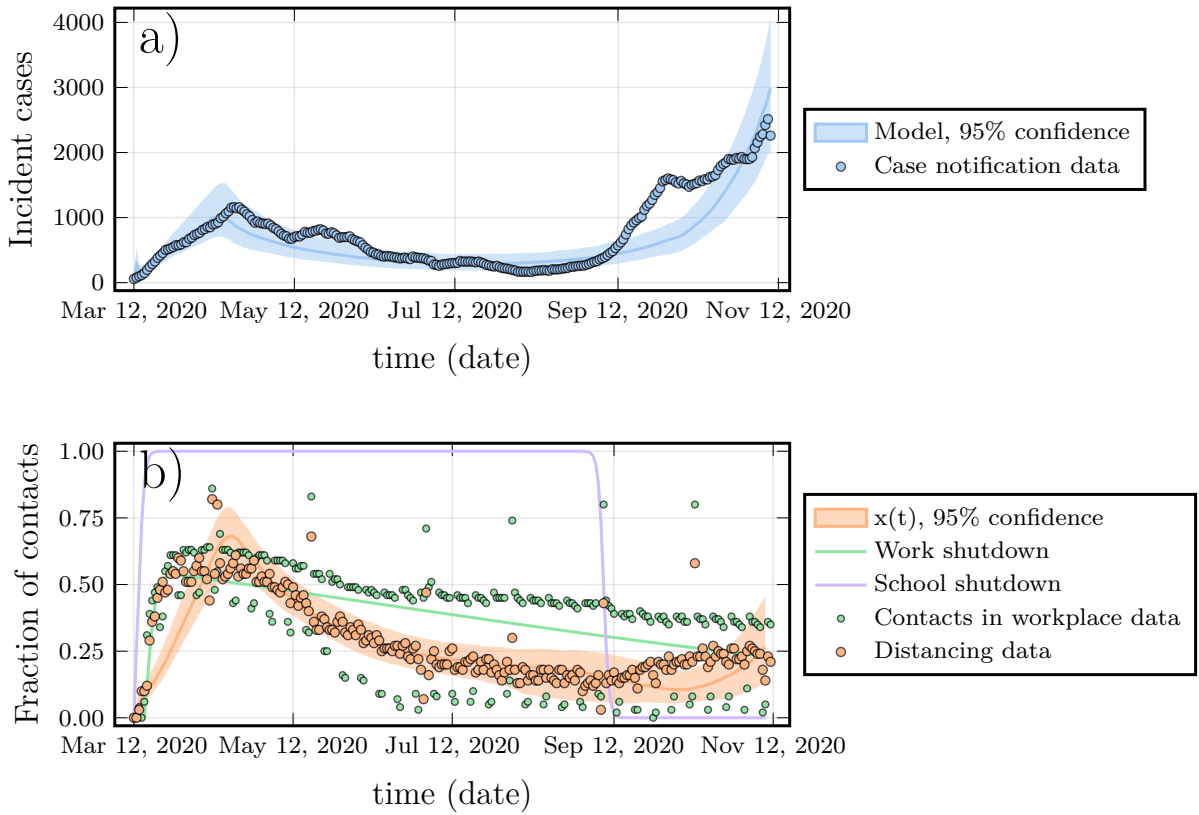


Figure 3.1: COVID-19 case numbers and proxy for adherence to non-pharmaceutical interventions. (A) COVID-19 case incidence by date of report in Ontario. Dots show the 7-day running average of case notification data, and the line represents the ascertained case incidence from best fitting models (with 95% credible intervals represented by the shaded region). (B) Each dot represents the proportional reduction in time spent at retail and recreation destinations and workplaces on the given date, compared with the 5-week average on corresponding days of the week 1 year ago, according to Google mobility data. Lines show the proportion of the population adhering to non-pharmaceutical interventions (with 95% credible intervals represented by the shaded region) as well as workplace and school shutdown curves from the fitted model. Methods and data sources are provided in the appendix (pp 1–11).

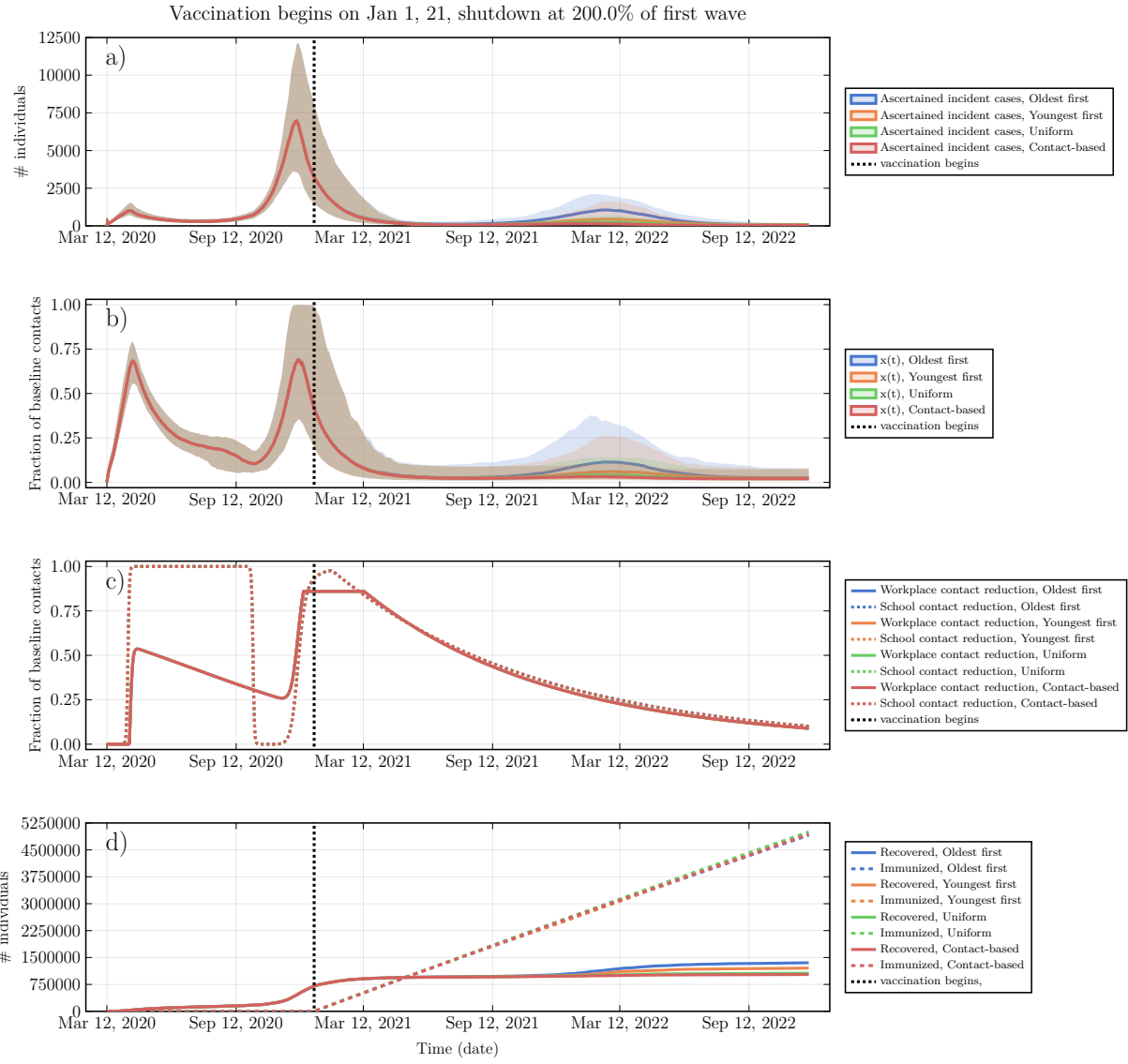


Figure 3.2: Effect of interaction of social and epidemiological dynamics on pandemic waves and vaccine strategy effectiveness over time. (A) Number of ascertained incident COVID-19 cases. (B) Proportion of the population practising non-pharmaceutical interventions. (C) Level of school and workplace closure (note that curves for different vaccination strategies overlap). (D) Number of individuals with natural or vaccine-derived immunity. Predictions are based on the Ontario population size (14.6 million), with vaccination beginning on Jan 1, 2021 (as indicated by the dashed vertical line in the graphs), shutdown occurring at 200% of peak cases in the first wave, and a vaccination rate of 0.5% of the population per week. Other parameter values are provided in the appendix (pp 1–11).

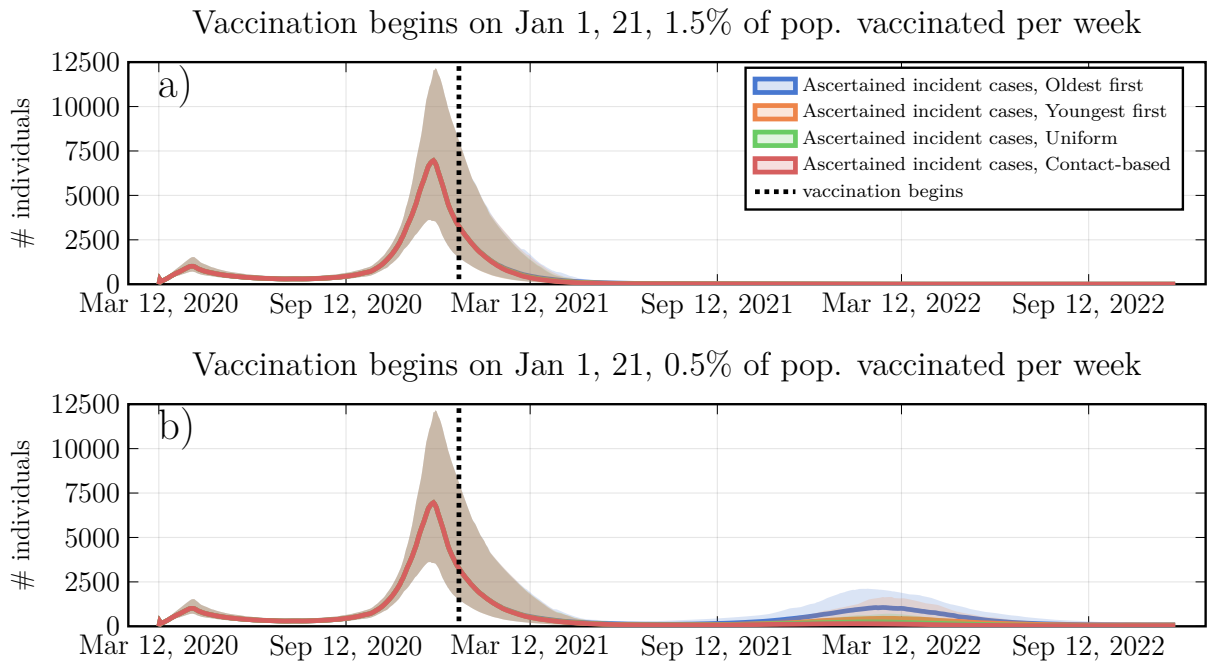


Figure 3.3: Incident cases by vaccination strategy across three model regimes. Projections of ascertained incident COVID-19 cases if vaccination begins in January (A, B) or September (C, D), and if the rate of vaccination is 1.5% (A, C) or 0.5% (B, D) of the population per week. These scenarios represent three main model regimes: timely vaccination (A), partial vaccination and indirect protection (B, C), and slow and late vaccination (D). Projections are based on the Ontario population size of 14.6 million and shutdown occurring at 200% of peak cases in the first wave. Other parameter values are provided in the appendix (pp 1–11).

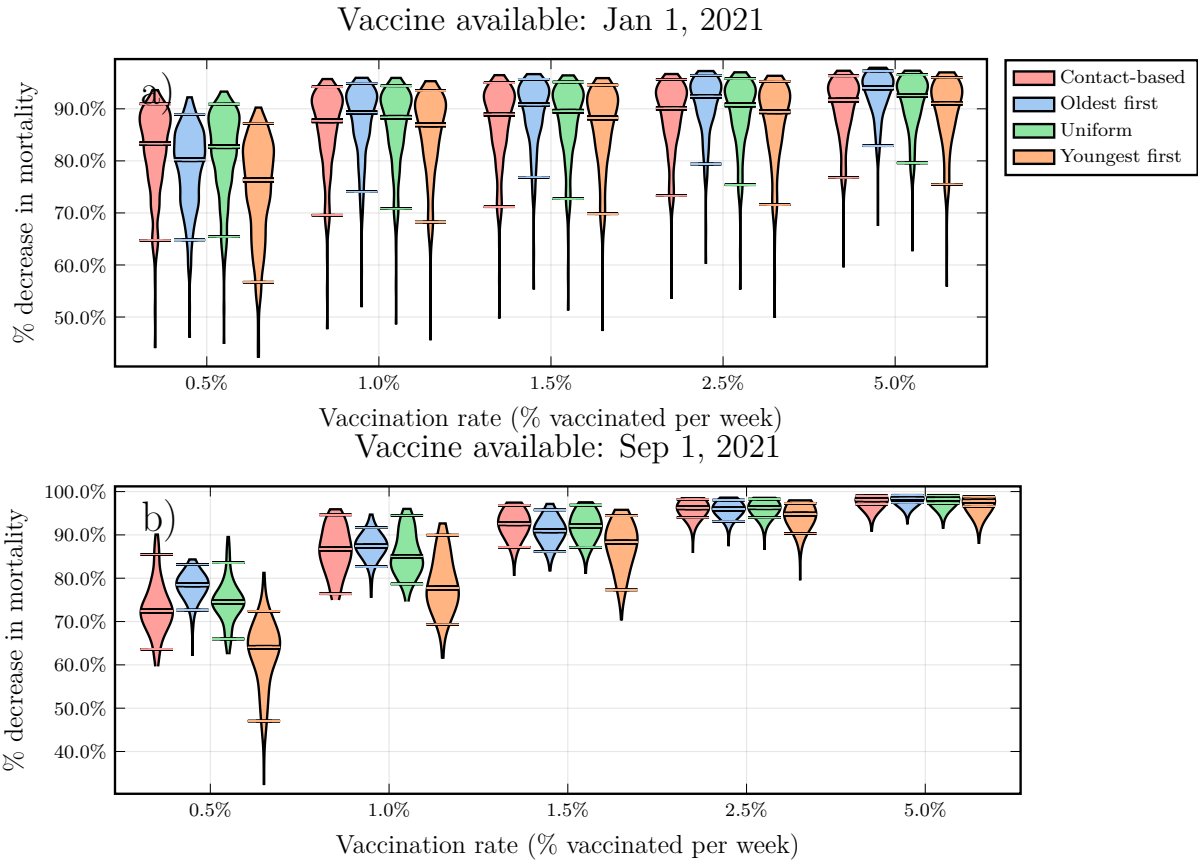
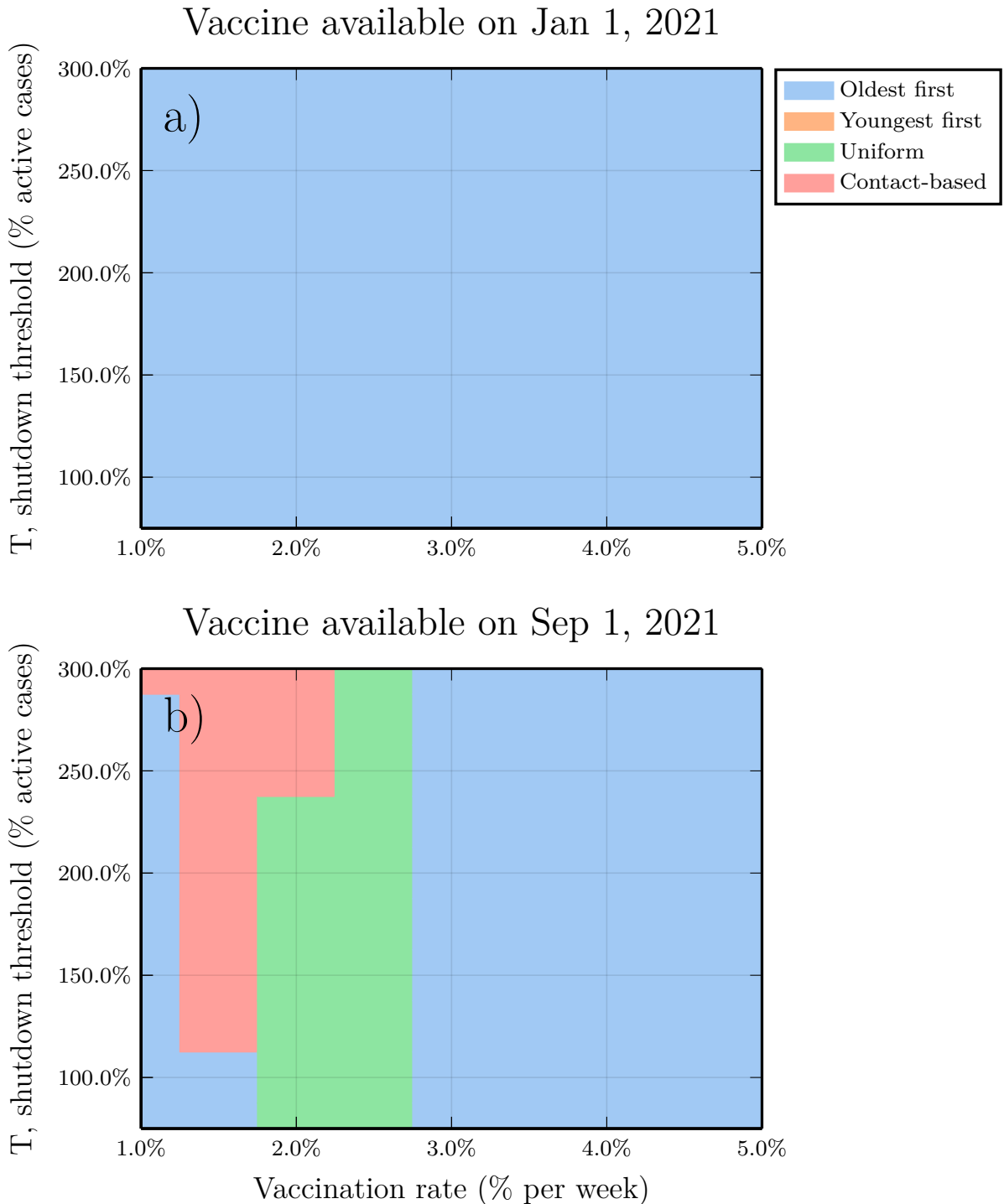


Figure 3.4: Effects of vaccination strategy and start date on percentage reduction in mortality. Violin plots of the percentage reduction in mortality under the four vaccine strategies, relative to no vaccination, as a function of the vaccination rate, for vaccination beginning on Jan 1, 2021 (A), and Sept 1, 2021 (B). Horizontal lines represent the median values and 95% credible intervals of posterior model projections. Projections are based on the Ontario population size of 14.6 million and shutdown occurring at 200% of peak cases in the first wave. Other parameter values are provided in the appendix (pp 1–11). The projected number of deaths in the absence of vaccination was 72000 (95% credible interval 40000–122000) from Jan 1, 2021, to March 14, 2025, and 60000 (31000–108000) from Sept 1, 2021, to March 14, 2025.



Best strategies for preventing deaths according to shutdown threshold and vaccination rate for vaccinations beginning in January (A) and September (B), 2021. Each parameter combination on the plane is colour coded according to which of the four strategies prevented the most deaths, on average, across all model realisations. Shutdown threshold is the number of active cases as a percentage of peak cases in the first wave. Other parameter values are provided in the appendix (pp 1–11).

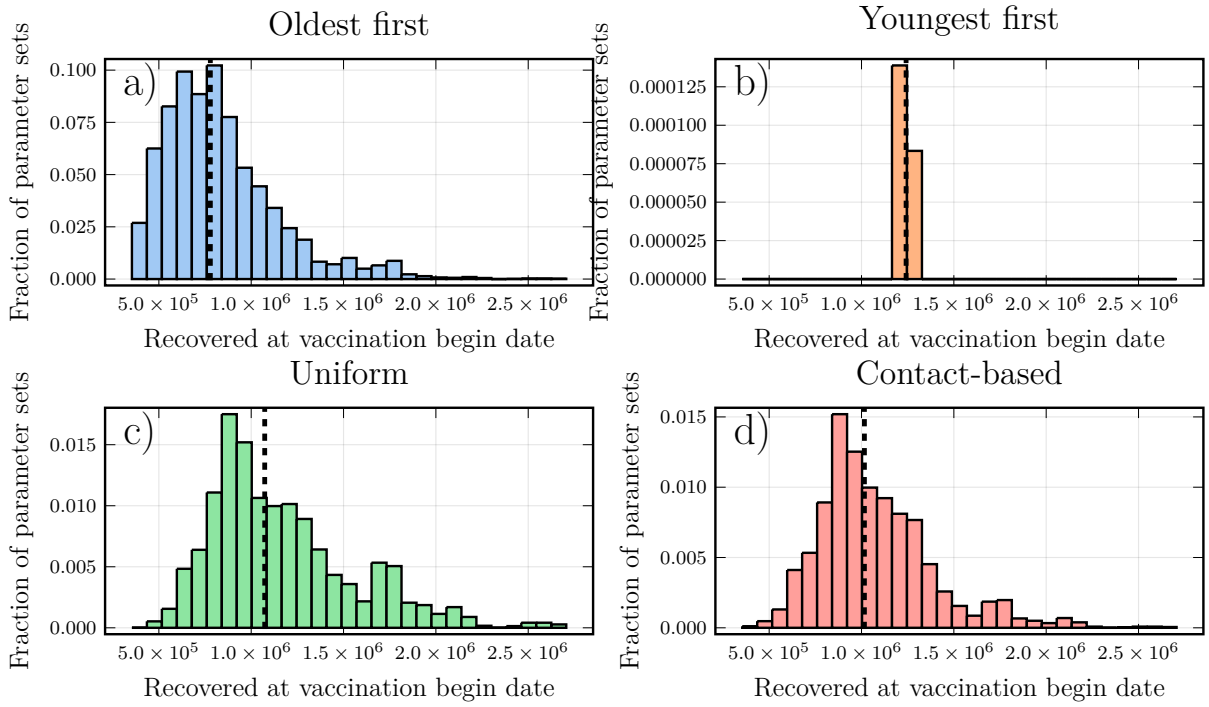


Figure 3.5: Effect of pre-existing natural immunity on the effectiveness of transmission-interrupting strategies. Frequency histogram of the proportion of the population with natural immunity for each strategy, taken from simulations where that strategy reduced mortality most effectively, for oldest-first (A), youngest-first (B), uniform (C), and contact-based strategies (D). The most effective strategy is defined as the one that reduced mortality the most across the largest number of model realisations. Vertical dashed lines denote median values of the distribution. Other parameter values are provided in the appendix (pp 1–11).

the vaccination rate (Figure 4) and shutdown threshold (Appendix, pp. 16-17); and plots showing which of the four strategies is the most effective (in terms of reducing mortality) as a function of the shutdown threshold and the vaccination rate (Figure 5).

In the first regime, vaccination starts soon and the vaccination rate is relatively high (March availability, vaccinating 1.5% or more of the population per week). A third wave in Fall 2021/Winter 2022 is thereby prevented (Figure 3a and appendix, page 13). In this regime, enough people are vaccinated sufficiently far in advance to prevent a third wave, therefore it does not matter which age group is vaccinated first. All four strategies have very similar effectiveness, although “oldest first” has a slight edge over the other strategies (Figure 4a, 5a).

In the second regime, either vaccination starts soon but the vaccination rate is lower (March availability, 1% or less vaccinated per week, Figure 3b and Figure 2), or vaccination starts later but the vaccination rate is high (September availability, vaccinating 1.5% or more of the population per week, Figure 3c and appendix, page 14). In this intermediate scenario, a sufficient proportion of the population is vaccinated for indirect protection from the vaccine to become important, but not enough individuals are vaccinated to completely prevent a third wave. As a result, the uniform and contact-based strategies are significantly more effective than the 60+ first strategy, while the “youngest first” strategy does worst of all (Figure 4, 5). The under-performance of the youngest first strategy occurs because in populations with strong age-assortative mixing [179], the indirect benefits of vaccination are “wasted” if vaccination is first concentrated in specific age groups before being extended to the rest of the population. The 60+ first strategy is less affected by this because the COVID-19 case fatality rate is high in this age group.

In the third regime, vaccination starts late and the vaccination rate is low (September availability, 1% or less vaccinated per week; Figure 3d and appendix, page 15). This scenario does not allow enough time for indirect protection from vaccination to become strong. As a result, the oldest first strategy has significantly higher effectiveness than the other three strategies (Figure 4b, 5b). Overall mortality is higher for all strategies, on account of the delayed rollout of the vaccine.

The relative performance of the strategies observed in these three regimes is generally unchanged across the full range of values for the shutdown threshold (Appendix, pp. 16-17). Some of our violin plots show a dominant lobe and a smaller secondary lobe, on account of the fact that different intervention settings can generate a different number or timing of pandemic waves. The optimized strategy always does best, by definition (Appendix, pp. 16-17). But it can be instructive to study how the optimized strategy allocates vaccines among the age groups. The optimal vaccine strategy allocates vaccines mostly to the 25-44

age group and secondly to 70+, depending on the vaccination rate (Appendix, page 18). These patterns suggest that the optimal strategy includes transmission interruption as a mechanism.

Frequency histograms across all stochastic model realizations showing what percentage of the population has natural immunity at the start of a vaccine program, when a particular strategy was shown to work best, illustrate the role of indirect protection (Figure 6). In simulations where the oldest first strategy did best, the percentage of the population with natural immunity tends to be relatively low. This is expected, since indirect protection from vaccines is weaker when few people have natural immunity upon which vaccine indirect protection can build. But when the uniform or contact-based strategy does best, more simulations exhibit a high level of natural immunity at the start of vaccination. We note that the variance in these histograms is high, however, which underscores the role of other factors in the model such as timing and interaction between social and epidemiological dynamics. Studying model predictions under variation in the basic reproduction number, R_0 [17], also illustrates the role of indirect protection. As R_0 is increased from 1.5 to 2.5 we observe that the vaccine becomes less effective in reducing mortality across all strategies, as expected (Appendix, page 19). This occurs because when R_0 is larger the indirect protection of vaccines is weaker [17]. As a result, the effectiveness of the “oldest first” strategy is less compromised by the increase in R_0 than the other strategies, at least when vaccination starts in September.

We also studied how the best strategy changes depending on vaccine efficacy ranging from 40-90% in 60+ year-olds and in < 60 year-olds (Appendix, pp. 20-21). The uniform or contact-based strategies were the most effective in these ranges, except when (a) vaccination starts in September at 1% per week and efficacy in < 60 year-olds is less than 70%, and (b) vaccination starts in March at 2.5% per week and efficacy is greater in 60+ year-olds than in < 60 year-olds. We note that (b) is unlikely since vaccine efficacy typically falls with age, and (a) is expected since this places the model in the third dynamical regime.

We also modelled dynamics of vaccinating behaviour after vaccines become available (Appendix, pp 4, 22-25). Due to lack of empirical data, we explored a wide range for the social learning rate and the relative cost of vaccination versus infection. Either the uniform or contact-based strategies were most effective, except when the relative cost of the vaccine is very low, in which case oldest first is the best strategy (Appendix, pp 22). Vaccine refusal increases as the vaccine cost rises (Appendix, pp 23-25). Since vaccine refusal in the targeted age group forces vaccination of other age groups instead, it makes all strategies behave more like the uniform strategy, although age-specific behaviours could change these predictions.

Our baseline inferred value of $R_0 \approx 1.7$ was lower than many published estimates [100]. We ran simulations with $R_0 = 2.5$ for December 2020 onward and found that “oldest first” was somewhat more effective across a broader region of parameter space for September availability, particularly at higher vaccination rates (Appendix, pp 26). Finally, we also ran simulations with 30% higher and lower ascertainment for December 2020 onward to capture potential changes to COVID-19 testing and found that it had little impact on which strategy was most effective (Appendix, pp 27-28).

3.4 Discussion

Our social-epidemiological model suggests that if a COVID-19 vaccine becomes available later in the pandemic, using SARS-CoV-2 vaccines to interrupt transmission might prevent more COVID-19 deaths than using the vaccines to target those 60+ years of age, depending on when the vaccine becomes available and how quickly the population can be vaccinated. These results are driven by the fact that the vaccine may only become available after populations have had one or more waves of immunizing infections. As a result, the effective reproduction number R_{eff} could be significantly closer to 1 than the basic reproduction number $R_0 \approx 2.2$ that applies to susceptible populations. In this regime, vaccines have disproportionately large indirect protective effects [17].

Several studies have used compartmental models to study prioritisation of age groups for COVID-19 vaccination [46, 48, 138]. These models vary widely in terms of study populations, representation of population heterogeneity, interventions, and assumptions about when vaccination starts. Similar to our results, Matrajt et al [138] find that the level of pre-existing immunity strongly dictates outcomes: when pre-existing immunity is high, the optimal strategy distributes the vaccine more evenly across age groups rather than prioritising older age groups. Buckner et al [48] find that targeting 60+ year-olds is best for reducing mortality. They assumed that vaccination begins in December 2020, and they base initial conditions on case notifications in the United States in that month. Similarly, Bubar et al [46] find that vaccinating 60+ year-olds works best for reducing mortality for vaccine programs starting in July 2020 in Belgium, or August 2020 in New York City. Our results agree with Refs. [46, 48] for the scenario of March 2021 vaccine availability. However, we find it makes sense to switch to vaccinating other age groups by September 2021. Such a late vaccine start date was not analyzed in Refs. [46, 48] although their findings might change if the models were re-initialized to accommodate vaccination starting in September 2021.

Our analysis was limited by its focus on prioritisation of age groups. We did not model

other sources of heterogeneity such as geography, socio-economic status, sex, or ethnicity—all of which are important determinants of disease burden in this highly unequal pandemic. We did not model outbreaks in long-term care facilities, where the dynamics of transmission and indirect protection differ from the general population. Similarly, we did not distinguish healthcare or other essential workers. However, many of these individuals are working age adults, and thus vaccinating them first among other working adults is consistent with our uniform and contact-based strategies. Our mortality estimates assume ICU capacity is not exceeded. If ICU capacity is exceeded in the second wave, then our projected deaths will be an under-estimate, although we speculate that the relative performance of the four strategies would not change. We used a single population model, but inter-population mobility can influence transmission dynamics: a large influx of infectious persons from another population can weaken the indirect protection afforded by vaccines.

We used changes to baseline time spent at retail and recreational outlets to represent population adherence to NPIs. Such mobility data is an imperfect proxy for physical distancing and will not capture mask use or hand-washing. We did not have high resolution mobility data on these practices, although in future it may be possible to infer information about these practices by combining information from phone surveys with online social media data. Our simple ascertainment process in the model was designed to implicitly capture the effects of COVID-19 PCR testing, contact tracing and isolation (TTI). But without explicitly representing them, it is impossible for us to study combined strategies of vaccination and TTI, or to anticipate how specific changes to TTI would influence our findings.

Finally, the model was parameterised with data from Ontario, Canada. The projected impact of the four vaccine strategies may differ in settings with different epidemiological or social characteristics. At the same time, we note that our findings rely upon a robust epidemiological effect that occurs when R_{eff} becomes small. Therefore, the only thing that may change in other settings is the timing of the switch to vaccine strategies that interrupt transmission.

We opted for a coupled social-epidemiological model on account of the importance of interactions between population behaviour and disease dynamics for the control of COVID-19 in the absence of preventive pharmaceutical interventions. Our model generated significantly different projections in our sensitivity analysis where population behaviour was assumed constant, which is similar to conventional approaches to transmission modelling. Our social model is less complicated than our epidemiological model and despite this, the coupled social-epidemiological model fitted population-level behaviour as readily as it fitted the epidemic curve. Predicting behaviour is fraught with uncertainty, but so is predicting an epidemic curve. Moreover, digital data on behaviour and sentiment that can be used

to model social dynamics is increasingly available [193]. Given this, we suggest a role for more widespread use of social-epidemiological models during pandemics.

To apply these results to COVID-19 pandemic mitigation, large-scale seroprevalence surveys before the onset of vaccination could ascertain the level of a population’s natural immunity. Age-structured compartmental models could be initialized with this information to generate population-specific projections. In populations where SARS-CoV-2 seropositivity is high due to a Fall/Winter 2020 wave, vaccinating to interrupt transmission may reduce COVID-19 mortality more effectively than targeting vulnerable groups.

3.5 Appendix

3.5.1 Model Equations

Transmission dynamics are given by an SEPAIR model, modified to take population adherence to NPIs and school/workplace closure into account, and divided into age classes $i \in [1, 16]$, where each age class contains a 5 year cohort, except for the oldest age group which comprises the ages 75 and over. The model equations are:

$$\frac{dS_i^1}{dt} = -r\rho_i \left[1 + s \sin \left(\frac{2\pi}{365}(t - \phi) - \frac{\pi}{2} \right) \right] S_i^1 \sum_{j=1}^{16} C_{ij}(t) \left(\frac{I_{s_j} + I_{a_j} + P_j}{N_j} \right) - \tau S_i^1 \quad (3.1)$$

$$\frac{dS_i^2}{dt} = -r\rho_i \left[1 + s \sin \left(\frac{2\pi}{365}(t - \phi) - \frac{\pi}{2} \right) \right] S_i^2 \sum_{j=1}^{16} C_{ij}(t) \left(\frac{I_{s_j} + I_{a_j} + P_j}{N_j} \right) - \tau S_i^2 \quad (3.2)$$

$$\frac{dE_i}{dt} = r_i \left[1 + s \sin \left(\frac{2\pi}{365}(t - \phi) - \frac{\pi}{2} \right) \right] (S_i^1 + S_i^2) \sum_{j=1}^{16} C_{ij}(t) \left(\frac{I_{s_j} + I_{a_j} + P_j}{N_j} \right) - \sigma_0 E_i + \tau (S_i^1 + S_i^2) \quad (3.3)$$

$$\frac{dP_i}{dt} = \sigma_0 E_i - \sigma_1 P_i \quad (3.4)$$

$$\frac{dI_{a_i}}{dt} = \eta \sigma_1 E_i - \gamma_a I_{a_i} \quad (3.5)$$

$$\frac{dI_{s_i}}{dt} = (1 - \eta) \sigma_1 E_i - \gamma_s I_{s_i} \quad (3.6)$$

$$\frac{dR_i}{dt} = \gamma_a I_{a_i} + \gamma_s I_{s_i} \quad (3.7)$$

$$\frac{dD_i}{dt} = \Omega(D(t)) \quad (3.8)$$

Parameter values are defined in Table 3.1. The vaccination dynamics are an impulsive process applied each day, described below. S_i^1 is the number of unvaccinated susceptible individuals in age group i , and S_i^2 is the number of susceptible individuals in age group i who have received a standard two dose course of vaccination but were not immunized. $E_i(t)$ is the number of exposed but not yet infectious individuals in age group i (i.e., individuals in the latent period). $I_{a_i}(t)$ is the number of asymptomatic infectious individuals in age group i and $I_{s_i}(t)$ is the number of symptomatic infectious individuals in age group i . $R_i(t)$ is the number of Removed (recovered, vaccinated, and deceased) individuals in compartment i .

The variable $D(t) \in [0, 1]$ in the model equation $dD(t)/dt = \Omega(D(t))$ represents the public health authority's reaction to the prevalence of ascertained cases and it evolves according to:

$$\Omega(D(t)) = \begin{cases} k_1(1 - D(t)) & \sum_{i=1}^{16} \alpha_i(I_{a_i} + I_{s_i}) > T \\ -k_2 D(t) & \sum_{i=1}^{16} \alpha_i(I_{a_i} + I_{s_i}) \leq T \end{cases} \quad (3.9)$$

This represents closure being triggered when ascertained cases exceed a threshold T , and being lifted when cases drop below that threshold again.

The proportion x of individuals who practice NPIs such as mask wearing, handwashing, and physical distancing, starts off at $x(0) = 0.01$ and evolves as:

$$\frac{dx}{dt} = \kappa x(1 - x) \left(\frac{\sum_{i=1}^{16} \alpha_i(I_{a_i} + I_{s_i})}{\sum_{i=1}^{16} N_i} - cx \right) + p_{ul}(1 - 2x) \quad (3.10)$$

where κ is the social learning rate, c is the incentive to not practice NPIs, and α_i is the fraction of total cases ($I_a + I_s$) that are reported, also known as the ascertainment rate. The p_{ul} term is a phenomenological term that represents the effects of social heterogeneity and influence from external populations that prevents the system from remaining arbitrarily close to $x = 0$ or $x = 1$ for unrealistic periods of time. These equations describe a population where individual sample other individuals at some time rate and switch between adherence and non-adherence to NPIs with a probability proportional to the expected gain in utility $\sum_{i=1}^{16} \alpha_i(I_{a_i} + I_{s_i}) - cx$. We refer the reader to existing literature for details on the derivation of this equation [29, 102, 216, 30, 160].

$C_{ij}(t, x)$ is the average number of contacts per day and consists of contacts at workplaces, schools, households, and other locations, which vary depending on government shutdown policies as well as individual adherence to NPIs like physical distancing and mask use:

$$C_{ij}(t, x) = C_{ij}^W(t) + C_{ij}^S(t) + (1 - \epsilon_P x)(\bar{C}_{ij}^O + \bar{C}_{ij}^H) \quad (3.11)$$

The contacts in each of the aforementioned places can vary as follows. At workplaces, which can be closed by public health authorities:

$$C_{ij}^W(t) = \begin{cases} (1 - \epsilon_W)\bar{C}_{ij}^W & t - t_{delay} > t_{close}, t - t_{delay} < t_{open}^w \\ \bar{C}_{ij}^W & t - t_{delay} < t_{close}^w \\ (1 - D(t)(1 - \epsilon_W))\bar{C}_{ij}^W & t - t_{delay} > t_{open}^w \end{cases} \quad (3.12)$$

where \bar{C}_{ij}^W is the normal (non-pandemic) number of contact-hours per day between individuals of age i and j at the workplace [247]; $\bar{C}_{ij}^W(1 - D(t)\epsilon_P)$ is the reduced rate under workplace closure efficacy $0 < \epsilon_W < 1$ and closure level $D(t)$; and t_{delay} represents the delay between the decision to adopt NPIs and their impact on transmission [128]. Lower than perfect efficacy may stem either from occasional use of workplace for critical needs or non-authorized access, workplaces that remain open because they provide essential services, etc. t_{close}^W and t_{open}^W are the times of closing and re-opening workplaces, respectively. Similarly, for schools we have:

$$C_{ij}^S(t) = \begin{cases} 0 & t - t_{delay} > t_{close}^s, t - t_{delay} < t_{open}^s \\ \bar{C}_{ij}^S & t - t_{delay} < t_{close}^s \\ (1 - D(t))\bar{C}_{ij}^S & t - t_{delay} > t_{open}^s \end{cases} \quad (3.13)$$

All other places of exposure are governed by social processes with imperfect ability of public health authorities to enforce mandates, and hence are governed by voluntary population adherence to NPIs such as mask use and physical distancing as per the $\epsilon_P x(t)$ term in the equation, where ϵ_P is efficacy of individual adoption of NPIs. In principle, contact hours spent at home should increase as workplaces and schools are closed, but we assume that infection probabilities will saturate rapidly with contact hours in the home. Each of the conditional functions in equations (3.12,3.13), are represented in the model as a smoothed step function with a steep slope, and we restrict them between 0 and 1 if the smoothing process would cause the closure level $D(t)$ to exceed 1.0. Finally, our interventions (school and workplace shutdown) do not distinguish between preventing contacts in "home" versus "other" locations. We assume the same efficacy of NPIs in home as in "other" locations. On one hand, individuals are less likely to use NPIs at home. On the other hand, contacts at home are repeated and thus there is a saturating effect that can somewhat reduce the infection risk, compared to the diversity of contacts experienced in the general community. Additionally, our case notifications are not broken down by the location of infection and thus we have limited ability to parameterize two difference NPI efficacy in home and "other" locations. As a result, we assume the same efficacy in both settings.

3.5.2 Vaccination process

Each day, the total number of individuals vaccinated is equal to $\sum_{i=1}^{16} \phi \frac{S_i(t)}{N_i}$, and the number of individuals immunized against transmission of the virus is $\sum_{i=1}^{16} v_{T_i} \frac{S_i(t)}{N_i - V_i}$ on account of imperfect vaccination. The factor $\frac{S_i(t)}{N_i - V_i}$ represents vaccination of each person with equal probability, so the probability of vaccinating a susceptible person decreases with the fraction of susceptible individuals out of the non-vaccinated people. If there are less than ϕ_i individuals in group S_i^1 , then the remainder of the vaccine is spread evenly among the remaining non-vaccinated groups. Individuals who are vaccinated but not immunized due to imperfect efficacy are moved to the corresponding S_i^2 . We assume that a course of vaccination will not be administered to a person more than twice.

The fraction of people who are vaccinated against disease but not against transmissibility is $v_{D_i} - v_{T_i}$. We assume this fraction of people is still able to transmit the disease normally, and therefore we account for them by reducing the mortality rate (see Supp. Mortality computation).

3.5.3 Differences between parameters in the first and second wave

To account for the differences in social response, to the first and second waves of the infection, we assume that the social dynamics variables κ (the social learning rate), and c (the incentive not to distance). We assume that these variables are functions of time, which transition between two values at a time $t_{switch} = 160$ days after the beginning of the pandemic.

$$\kappa = \kappa(t) = \kappa_2 \left(\frac{\tanh(k_s(t - t_{switch})) + 1}{2} \right) + \kappa_1 \left(1 - \frac{\tanh(k_s(t - t_{switch})) + 1}{2} \right) \quad (3.14)$$

$$c = c(t) = c_2 \left(\frac{\tanh(k_s(t - t_{switch})) + 1}{2} \right) + c_1 \left(1 - \frac{\tanh(k_s(t - t_{switch})) + 1}{2} \right) \quad (3.15)$$

We chose the rate of switch, $k_s = 0.05$ to take 2 - 4 weeks.

3.5.4 Case under-ascertainment

Case under-ascertainment of the i th age group is represented by the following function:

$$\alpha_i(t) = \begin{cases} \alpha_{i,2} & t > t_{switch} \\ \alpha_{i,1} \left(\frac{t_{switch}-t}{t_{switch}} \right) & t \leq t_{switch} \end{cases} \quad (3.16)$$

where where $\alpha_{1,1}, \alpha_{2,1}, \alpha_{3,1}$ corresponds to the ascertainment in the age groups $(0, 20), (20, 60), > 60$ at $t = 0$, respectively. We assume that the ascertainment rises to a value of $\alpha_{1,2}, \alpha_{2,2}, \alpha_{3,2}$ in the age groups $(0, 20), (20, 60), > 60$ respectively, at $t = t_{switch}$, denoting the increase in ascertainment throughout the first wave and into the second wave. We multiply the infections in each age group i at time t by the corresponding $\alpha_i(t)$ after the simulation is finished.

3.5.5 Baseline transmission rate

We can compute r as a function of the next-generation matrix, $M = -\Theta\Sigma^{-1}$ [63], where Θ and Σ are defined as in equations 3.17, 3.18, and so M is a function of $R_0, \sigma_0, \sigma_1, \gamma_a, \gamma_s, \eta, C(t)$, and N . These matrices come from the rate at which infected individuals enter and leave the infection compartments when the system is linearized about the $I_a = 0, I_s = 0, P = 0$ equilibrium. The basic reproduction ratio, R_0 , of the infection is the spectral radius of M , written $\rho(M)$. We can pull r out of this expression and write r in terms of the other

parameters: $r = \frac{R_0}{\rho(M)}$.

$$\Theta = \begin{bmatrix} 0 & \dots & 0 & \frac{rC_{1,1}(0)N_1}{N_1} & \dots & \frac{rC_{1,n}(0)N_1}{N_n} & \frac{rC_{1,1}(0)N_1}{N_1} & \dots & \frac{rC_{1,n}(0)N_1}{N_n} & \frac{rC_{1,1}(0)N_1}{N_1} \\ \dots & \frac{rC_{1,n}(0)N_1}{N_n} & & & & & & & & & \\ \vdots & \ddots & \vdots & \vdots & \vdots & \ddots & \vdots & \ddots & \vdots & \vdots & \vdots \\ \ddots & \vdots & & & & & & & & & \\ 0 & \dots & 0 & \frac{rC_{1,n}(0)N_n}{N_1} & \dots & \frac{rC_{n,n}(0)N_n}{N_n} & \frac{rC_{1,n}(0)N_n}{N_1} & \dots & \frac{rC_{n,n}(0)N_n}{N_n} & \frac{rC_{1,n}(0)N_n}{N_1} & \\ \dots & \frac{rC_{n,n}(0)N_n}{N_n} & & & & & & & & & \\ 0 & \dots & 0 & 0 & \dots & 0 & 0 & \dots & 0 & 0 & \\ \dots & 0 & & & & & & & & & \\ \vdots & \ddots & \vdots & \vdots & \ddots & \vdots & \vdots & \ddots & \vdots & \vdots & \vdots \\ \ddots & \vdots & & & & & & & & & \\ 0 & \dots & 0 & 0 & \dots & 0 & 0 & \dots & 0 & 0 & \\ \dots & 0 & & & & & & & & & \\ 0 & \dots & 0 & 0 & \dots & 0 & 0 & \dots & 0 & 0 & \\ \dots & 0 & & & & & & & & & \\ \vdots & \ddots & \vdots & \vdots & \ddots & \vdots & \vdots & \ddots & \vdots & \vdots & \vdots \\ \ddots & \vdots & & & & & & & & & \\ 0 & \dots & 0 & 0 & \dots & 0 & 0 & \dots & 0 & 0 & \\ \dots & 0 & & & & & & & & & \end{bmatrix} \quad (3.17)$$

$$\Sigma = \begin{bmatrix} -\sigma_0 & \dots & 0 & 0 & \dots & 0 & 0 & \dots & 0 & 0 \\ \dots & 0 & & & & & & & & \\ \vdots & -\sigma_0 & \vdots & \vdots & \ddots & \vdots & \vdots & 0 & \vdots & \vdots \\ 0 & \vdots & & & & & & & & \\ 0 & \dots & -\sigma_0 & 0 & \dots & 0.0 & 0 & \dots & 0 & 0 \\ \dots & 0 & & & & & & & & \\ 0 & \dots & 0 & -\sigma_1 & \dots & 0 & 0 & \dots & 0 & 0 \\ \dots & 0 & & & & & & & & \\ \vdots & \ddots & \vdots & \vdots & -\sigma_1 & \vdots & \vdots & \ddots & \vdots & \vdots \\ \ddots & \vdots & & & & & & & & \\ 0 & \dots & 0 & 0 & \dots & -\sigma_1 & 0 & \dots & 0 & 0 \\ \dots & 0 & & & & & & & & \\ 0 & \dots & 0 & \eta\sigma_1 & \dots & 0 & -\gamma_a & \dots & 0 & 0 \\ \dots & 0 & & & & & & & & \\ \vdots & \ddots & \vdots & \vdots & \eta\sigma_1 & \vdots & \vdots & -\gamma_a & \vdots & \vdots \\ \ddots & \vdots & & & & & & & & \\ 0 & \dots & 0 & 0 & \dots & \eta\sigma_1 & 0 & \dots & -\gamma_a & 0 \\ \dots & 0 & & & & & & & & \\ 0 & \dots & 0 & (1-\eta)\sigma_1 & \dots & 0 & 0 & \dots & 0 & -\gamma_s \\ \dots & 0 & & & & & & & & \\ \vdots & \ddots & \vdots & \vdots & (1-\eta)\sigma_1 & \vdots & \vdots & \ddots & \vdots & \vdots \\ -\gamma_s & \vdots & & & & & & & & \\ 0 & \dots & 0 & 0 & \dots & (1-\eta)\sigma_1 & 0 & \dots & 0 & 0 \\ \dots & -\gamma_s & & & & & & & & \end{bmatrix} \quad (3.18)$$

3.5.6 Disease progression parameters

Transition rates for the duration of the asymptomatic infectious period and the proportion of symptomatic cases were obtained from COVID-19 epidemiological literature [152, 122, 218]. We computed the mortality due to COVID-19 by applying the case fatality rate obtained from [158], interpolated to 16 age groups.

3.5.7 Initial conditions

The point $t = 0$ was chosen to be the day at which the province of Ontario recorded more than 50 cases, March 10th 2020, to reduce the effects of stochasticity in the early case

counts. Let the number of observed cases of COVID-19 in age group i on March 10th 2020 be ω_i . We use the age distribution of ω_i to determine the age distribution for $I_a(t) + I_s(t)$. The true number of cases that day is ω_i/α_i , where α_i is the ascertainment rate of cases in group i . Since we do not know the actual number of active cases, $I_{a_i}(t) + I_{s_i}(t)$ at $t = 0$, we assume the number of active cases is equal to the true number of incident cases multiplied by a constant I_0 , which is also treated as a model variable to be fitted. Therefore, $I_{s_i}(0) = \eta I_0 \frac{\omega_i}{\alpha_i}$ and $I_{a_i}(0) = (1 - \eta) I_0 \frac{\omega_i}{\alpha_i}$. Similarly, we assumed that the numbers of presymptomatic and exposed cases at $t = 0$ are proportional to the number of ascertained incident cases in each age group, ω_i . We fit the variables P_0 and E_0 so that $P(0) = P_0 \frac{\omega_i}{\alpha_i}$ and $E(0) = E_0 \frac{\omega_i}{\alpha_i}$. We assumed that $S_i^1(0) = N_i - (I_a(0) + I_s(0) + E(0) + P(0))$, so the total number of susceptible, unvaccinated individuals $\sum_{i=1}^{16} S_i^1(0)$ is the population of the region (minus the number who begin in the infected compartments), and $S_i^2(0) = 0$, $E_i(0) = 0$, $R_i(0) = 0$ for all i . Lastly, we assumed that at $t = 0$, only 1% of individuals are physical distancing, so $x(0) = 0.01$, and that $D(0) = 0$.

3.5.8 Particle filtering

We calibrated the model with data from Ontario, Canada. Since the workplace closure opening and closing rates, k_1 and k_2 , are not coupled with the model, we fit a step function of the form

$$f(t) = \epsilon_W (\tanh k_1(t - t_{close}^W) - \tanh k_2(t - t_{close}^W))$$

to the "workplaces_percent_change_from_baseline" field of the Google mobility data [87] for the province. We applied a particle filtering approach using intervals around selected parameters. Intervals used for sampling appear in Table 3.1. We fit the 7-day moving average of incident cases on each day across all age groups to the number of cases registered by Public Health Ontario on that day [222], and also the total number of cases at the end of the fitting window for each age group. The decrease in contact-hours due to social distancing, $x(t)$, was fit to the decrease in the "Retail and Recreation" hours recorded by Google mobility [87]. The 1.1% (0.8%, 1.3%) of Ontario residents seropositive for COVID-19 in June 2021 was also used as a fitting criterion [182]. The posterior distribution of the parameters was estimated with the approximate Bayesian computation scheme described in [225], with uniform priors and 200 particles, using the KissABC [10] library for the Julia language. The acceptance threshold was chosen to given acceptable variation and evaluation time.

3.5.9 Vaccination refusal dynamics

In an extension to the model explored the dynamics of the model with the added complication of vaccine refusal. We introduce a variable $y(t)$ to represent that fraction of the population willing to be vaccinated for the virus, governed by imitation dynamics similar to the social distancing equation 3.10. We add the following equation 3.19 to the rest of the model equations [29, 30].

$$\frac{dy}{dt} = \kappa_{vac}y(1 - y) \left(\frac{\sum_{i=1}^{16} \alpha_i(I_{a_i} + I_{s_i})}{\sum_{i=1}^{16} N_i} - c_{vac} \right) \quad (3.19)$$

In the above equation, the vaccination decisions of the population are governed by a payoff function, where c_{vac} is the payoff not to vaccinate, and the payoff to vaccinate is proportional to current the number of ascertained active infections. The initial condition for this variable, y_0 is assumed to be 0.67 from [137].

The population in age group i that refuses to be vaccinated is $N_i(1 - y(t))$. We implement this mechanic in the model by assuming that the number of people vaccinated each day in age group i , ψ_i is unchanged, except that the compartment $S_{v_i}^1$ is considered to be empty when $N_i(1 - y(t))$ people remain.

3.5.10 Model extension for vaccine efficacy against disease only

We conducted the sensitivity analysis scenario distinguishing vaccine efficacy against disease only versus vaccine efficacy against both infectivity and disease by adjusting the case fatality rates according to vaccine coverage in the population and assumed efficacies. The adjustment factor is determined by the relative sizes of $S_1(t)$ and $S_2(t)$. Let $\xi_1(S_1(t)) = \xi S_1(t)$ be the rate at which individuals in $S_1(t)$ are infected, and similarly $\xi_2 = \xi S_2(t)$ the rate at which individuals in $S_2(t)$ are infected. Let $S_3(t)$ be the number of people at t who are immunized but still able to transmit the virus, and $\xi_3 = \xi S_3(t)$. We also assume that

$$\frac{\xi_1(t)}{\xi_3(t)} = \frac{1 - v_{D_i}}{v_{D_i} - v_{T_i}} \quad (3.20)$$

which applies given that the timescale of infection in individuals is fast compared to the whole duration of the pandemic. The proportion of unvaccinated people who are infected at t is $\frac{\xi_1(t)}{\xi_1(t) + \xi_2(t) + \xi_3(t)}$, and the fraction of vaccinated but not immunized people infected at t is $\frac{\xi_2(t)}{\xi_1(t) + \xi_2(t) + \xi_3(t)}$. From equation 3.20, and the model equations, we can adjust the

probability that a given person who is infected also dies at time t as

$$\text{Adjusted mortality at } t \text{ for age group } i = \frac{S_{1i}(t) + S_{2i}(t)}{S_{1i}(t) + S_{2i}(t) \frac{1-v_{Ti}}{1-v_{Di}}} \times \text{Cases at } t \times \text{measured CFR} \quad (3.21)$$

Table 3.1: Parameter definitions, values, particle filtering ranges, and sources.

Parameter	Meaning	Value [Range]
N_i	Population in age group i	0 – 4: 790 10 – 14: 7 20 – 24: 1 30 – 34: 1 40 – 44: 9 50 – 54: 1 60 – 64: 8 70 – 74: 5
μ_i	COVID-19 case fatality rate in age group i	0 – 4: 0.00 10 – 14: 0 20 – 24: 0 30 – 34: 0 40 – 44: 0 50 – 54: 0 60 – 64: 0 70 – 74: 0
C_{ij}	contact rate between class i and j	see Supp.
R_0	basic reproduction rate of infection	calibrated
r	probability of transmission per contact	derived from
σ_0	inverse of latent period for exposed individuals	calibrated
σ_1	inverse of latent period for presymptomatic individuals	calibrated
γ_a	inverse of infectious period for asymptomatic individuals	0.25/day
γ_s	inverse of infectious period for symptomatic individuals	calibrated
$\alpha_{1,1}$	Ascertainment rate of class i in the first wave (before t_{switch})	calibrated
$\alpha_{1,2}$	Ascertainment rate of class i in the first wave (before t_{switch})	calibrated
$\alpha_{1,3}$	Ascertainment rate of class i in the first wave (before t_{switch})	calibrated
$\alpha_{2,1}$	Ascertainment rate of class i in the second wave (after t_{switch})	calibrated
$\alpha_{2,2}$	Ascertainment rate of class i in the second wave (after t_{switch})	calibrated
$\alpha_{2,3}$	Ascertainment rate of class i in the second wave (after t_{switch})	calibrated
ρ_1	Age-specific susceptibility modifier, ages 0-20	calibrated
ρ_2	Age-specific susceptibility modifier, ages 20-60	calibrated
ρ_3	Age-specific susceptibility modifier, ages 60+	calibrated
η	fraction of symptomatic infections	0.15
ϵ_P	efficacy of physical distancing	calibrated
κ	social learning rate	calibrated
s	seasonality	calibrated
ϕ	seasonality phase	-30 days
v_{T_i}	Vaccine efficacy against transmissibility and disease for individuals in group i ⁶³	75%
v_{D_i}	Vaccine efficacy against disease only for individuals in group i	75%
I_0	Initial ratio of active cases to incident cases	calibrated
P_0	Initial ratio of presymptomatic cases to incident cases	calibrated
E_0	Initial ratio of exposed cases to incident cases	calibrated
ψ_i	Number of vaccines allocated for individuals in group i each day	varied by
T	Threshold in active reported cases for school/workplace closure	varied by

References

- [1]
- [2]
- [3] Mountain pine beetle (factsheet). *Natural Resources Canada*, Feb 2017.
- [4] James K Agee. The influence of forest structure on fire behavior. In *Proceedings of the 17th annual forest vegetation management conference*, pages 52–68. University of California, Shasta County Cooperative Extension Redding, CA, 1996.
- [5] Michelle C Agne, Travis Woolley, and Stephen Fitzgerald. Fire severity and cumulative disturbance effects in the post-mountain pine beetle lodgepole pine forests of the pole creek fire. *Forest Ecology and Management*, 366:73–86, 2016.
- [6] Muntasir Alam, KM Ariful Kabir, and Jun Tanimoto. Based on mathematical epidemiology and evolutionary game theory, which is more effective: quarantine or isolation policy? *Journal of Statistical Mechanics: Theory and Experiment*, 2020(3):033502, 2020.
- [7] Alen Alexanderian, Matthias K Gobbert, K Renee Fister, Holly Gaff, Suzanne Lenhart, and Elsa Schaefer. An age-structured model for the spread of epidemic cholera: analysis and simulation. *Nonlinear Analysis: Real World Applications*, 12(6):3483–3498, 2011.
- [8] René I Alfaro, Rochelle Campbell, Paula Vera, Brad Hawkes, Terry L Shore, et al. Dendroecological reconstruction of mountain pine beetle outbreaks in the chilcotin plateau of british columbia. In *Mountain Pine Beetle Symposium: Challenges and solutions. TL Shore, JE Brooks, and JE Stone (editors)*. Kelowna, BC, pages 245–256, 2003.

- [9] Qasim Ali, Chris T Bauch, and Madhur Anand. Coupled human-environment dynamics of forest pest spread and control in a multi-patch, stochastic setting. *PLoS one*, 10(10):e0139353, 2015.
- [10] Francesco Allemano. Kissabc.jl. <https://github.com/JuliaApproxInference/KissABC.jl>, 2020.
- [11] Craig D Allen. Interactions across spatial scales among forest dieback, fire, and erosion in northern new mexico landscapes. *Ecosystems*, 10(5):797–808, 2007.
- [12] EA Allen and LM Humble. Nonindigenous species introductions: a threat to canada’s forests and forest economy1. *Canadian Journal of Plant Pathology*, 24(2):103–110, 2002.
- [13] Jennifer L Allen, Sara Wesser, Carl J Markon, and Kenneth C Winterberger. Stand and landscape level effects of a major outbreak of spruce beetles on forest vegetation in the copper river basin, alaska. *Forest Ecology and Management*, 227(3):257–266, 2006.
- [14] Marco A Amaral, Marcelo M de Oliveira, and Marco A Javarone. An epidemiological model with voluntary quarantine strategies governed by evolutionary game dynamics. *arXiv preprint arXiv:2008.05979*, 2020.
- [15] GD Amman and JA Logan. Silvicultural control of mountain pine beetle: prescriptions and the influence of microclimate. *American Entomologist*, 44(3):166–178, 1998.
- [16] Elizabeth S Anderson. What is the point of equality? *Ethics*, 109(2):287–337, 1999.
- [17] Roy M Anderson, B Anderson, and Robert M May. *Infectious diseases of humans: dynamics and control*. Oxford university press, 1992.
- [18] Sean C Anderson, Andrew M Edwards, Madi Yerlanov, Nicola Mulberry, Jessica Stockdale, Sarafa A Iyaniwura, Rebeca C Falcao, Michael C Otterstatter, Michael A Irvine, Naveed Z Janjua, et al. Estimating the impact of COVID-19 control measures using a bayesian model of physical distancing. *medRxiv*, 2020.
- [19] M Ya Antonovsky, RA Fleming, Yu A Kuznetsov, and WC Clark. Forest-pest interaction dynamics: the simplest mathematical models. *Theoretical Population Biology*, 37(2):343–367, 1990.

- [20] Australian Government, Department of Health. Australian influenza surveillance report. 2(20 April to 3 May 2020), 2020.
- [21] Jodi N Axelson, René I Alfaro, and Brad C Hawkes. Influence of fire and mountain pine beetle on the dynamics of lodgepole pine stands in british columbia, canada. *Forest Ecology and Management*, 257(9):1874–1882, 2009.
- [22] Jodi N Axelson, René I Alfaro, and Brad C Hawkes. Changes in stand structure in uneven-aged lodgepole pine stands impacted by mountain pine beetle epidemics and fires in central british columbia. *The Forestry Chronicle*, 86(1):87–99, 2010.
- [23] Ana Babus, Sanmay Das, and SangMok Lee. The optimal allocation of COVID-19 vaccines. *medRxiv*, 2020.
- [24] William L Baker and Thomas T Veblen. Spruce beetles and fires in the nineteenth-century subalpine forests of western colorado, usa. *Arctic and Alpine Research*, pages 65–80, 1990.
- [25] Shweta Bansal, Babak Pourbohloul, and Lauren Ancel Meyers. A comparative analysis of influenza vaccination programs. *PLoS Med*, 3(10):e387, 2006.
- [26] Lee-Ann Barlow, Jacob Cecile, Chris T Bauch, and Madhur Anand. Modelling interactions between forest pest invasions and human decisions regarding firewood transport restrictions. *PLoS One*, 9(4):e90511, 2014.
- [27] Stephen W Barrett and Stephen F Arno. Indian fires as an ecological influence in the northern rockies. *Journal of Forestry*, 80(10):647–651, 1982.
- [28] Enric Batllori, Miquel De Cáceres, Lluís Brotons, David D Ackerly, Max A Moritz, and Francisco Lloret. Cumulative effects of fire and drought in mediterranean ecosystems. *Ecosphere*, 8(8), 2017.
- [29] Chris T Bauch. Imitation dynamics predict vaccinating behaviour. *Proceedings of the Royal Society B: Biological Sciences*, 272(1573):1669–1675, 2005.
- [30] Chris T Bauch and Samit Bhattacharyya. Evolutionary game theory and social learning can determine how vaccine scares unfold. *PLoS Comput Biol*, 8(4):e1002452, 2012.
- [31] Chris T Bauch and Alison P Galvani. Social factors in epidemiology. *Science*, 342(6154):47–49, 2013.

- [32] BC Ministry of Forests, Mines and Lands. *The state of british columbia's forests*, 3rd ed., 2010.
- [33] Foster Ellenborough Lascelles Beal. *Food of the woodpeckers of the United States*. Number 37. US Department of Agriculture, Biological Survey, 1911.
- [34] Barbara J Bentz, Jacques Régnière, Christopher J Fettig, E Matthew Hansen, Jane L Hayes, Jeffrey A Hicke, Rick G Kelsey, Jose F Negrón, and Steven J Seybold. Climate change and bark beetles of the western united states and canada: direct and indirect effects. *BioScience*, 60(8):602–613, 2010.
- [35] Melvyn S Berger. *Nonlinearity and functional analysis: lectures on nonlinear problems in mathematical analysis*, volume 74. Academic press, 1977.
- [36] Alan A Berryman. Theoretical explanation of mountain pine beetle dynamics in lodgepole pine forests. *Environmental entomology*, 5(6):1225–1233, 1976.
- [37] Souvik Bhattacharya and Maia Martcheva. Oscillations in a size-structured prey-predator model. *Mathematical biosciences*, 228(1):31–44, 2010.
- [38] Julie C Blackwood, Alan Hastings, and Peter J Mumby. A model-based approach to determine the long-term effects of multiple interacting stressors on coral reefs. *Ecological Applications*, 21(7):2722–2733, 2011.
- [39] Julie C Blackwood, Alan Hastings, and Peter J Mumby. The effect of fishing on hysteresis in caribbean coral reefs. *Theoretical Ecology*, 5(1):105–114, 2012.
- [40] Nancy K Bockino and Daniel B Tinker. Interactions of white pine blister rust and mountain pine beetle in whitebark pine ecosystems in the southern greater yellowstone area. *Natural Areas Journal*, 32(1):31–40, 2012.
- [41] Donald J Bogucki, FH Bormann, EO Box, SP Bratton, R Dolan, CP Dunn, RTT Forman, GK Gruendlung, GR Guntenspergen, TD Hayes, et al. *Landscape heterogeneity and disturbance*, volume 64. Springer Science & Business Media, 2012.
- [42] Robert Boyd. Indians, fire and the land.
- [43] Tim Bradley and Paul Tueller. Effects of fire on bark beetle presence on jeffrey pine in the lake tahoe basin. *Forest Ecology and Management*, 142(1):205–214, 2001.
- [44] Ulrik Brandes. On variants of shortest-path betweenness centrality and their generic computation. *Social Networks*, 30(2):136–145, 2008.

- [45] John S Brownstein, Ken P Kleinman, and Kenneth D Mandl. Identifying pediatric age groups for influenza vaccination using a real-time regional surveillance system. *American Journal of Epidemiology*, 162(7):686–693, 2005.
- [46] Kate M Bubar, Stephen M Kissler, Marc Lipsitch, Sarah Cobey, Yonatan Grad, and Daniel B Larremore. Model-informed COVID-19 vaccine prioritization strategies by age and serostatus. *medRxiv*, 2020.
- [47] James H Buck and Jordan M Marshall. Hitchhiking as a secondary dispersal pathway for adult emerald ash borer, *agrilus planipennis*. *Gt Lakes Entomol*, 41:197–199, 2009.
- [48] Jack H Buckner, Gerardo H Chowell, and Michael R Springborn. Optimal dynamic prioritization of scarce COVID-19 vaccines. *medRxiv*, 2020.
- [49] B Buma. Disturbance interactions: characterization, prediction, and the potential for cascading effects. *Ecosphere*, 6(4):1–15, 2015.
- [50] Bureau of Labor Statistics. American time use survey — 2018 results. <https://www.bls.gov/news.release/pdf/atus.pdf>, 2018. accessed 4 April 2020.
- [51] Thomas M Bury, Chris T Bauch, and Madhur Anand. Charting pathways to climate change mitigation in a coupled socio-climate model. *PLoS computational biology*, 15(6):e1007000, 2019.
- [52] Canadian Food Inspection Agency (CFIA). <https://www.inspection.gc.ca/plants/plant-pests-invasive-species/insects/emerald-ash-borer/areas-regulated/eng/1347625322705/1367860339942>, 2019.
- [53] David Cappaert, Deborah G McCullough, Therese M Poland, and Nathan W Siegert. Emerald ash borer in north america: a research and regulatory challenge. *American Entomologist*. 51 (3): 152-165., 51(3), 2005.
- [54] Renato Casagrandi and Sergio Rinaldi. A minimal model for forest fire regimes. *The American Naturalist*, 153(5):527–539, 1999.
- [55] B Chen-Charpentier and MCA Leite. A model for coupling fire and insect outbreak in forests. *Ecological modelling*, 286:26–36, 2014.
- [56] Richard C Cobb and Margaret R Metz. Tree diseases as a cause and consequence of interacting forest disturbances. *Forests*, 8(5):147, 2017.

- [57] H Ken Cordell. The latest trends in nature-based outdoor recreation. *Forest History Today, Spring 2008*, 2008.
- [58] H Ken Cordell. Outdoor recreation trends and futures: a technical document supporting the forest service 2010 rpa assessment. *Gen. Tech. Rep. SRS-150. Asheville, NC: US Department of Agriculture Forest Service, Southern Research Station*, 167 p., 150:1–167, 2012.
- [59] H Ken Cordell, Carter Betz, and Gary T Green. Nature-based outdoor recreation trends and wilderness. *International Journal of Wilderness, August 2008, Volume 14, Number 2, Page 7-13*, 2008.
- [60] Michael G Crandall and Paul H Rabinowitz. Bifurcation from simple eigenvalues. *Journal of Functional Analysis*, 8(2):321–340, 1971.
- [61] Michael G Crandall and Paul H Rabinowitz. Bifurcation, perturbation of simple eigenvalues, itand linearized stability. *Archive for Rational Mechanics and Analysis*, 52(2):161–180, 1973.
- [62] Don G Despain and William H Romme. Ecowgy and management of high-intensity fires in yelwwstone national park.
- [63] Odo Diekmann, JAP Heesterbeek, and Michael G Roberts. The construction of next-generation matrices for compartmental epidemic models. *Journal of the Royal Society Interface*, 7(47):873–885, 2010.
- [64] Daniel C Donato, Martin Simard, William H Romme, Brian J Harvey, and Monica G Turner. Evaluating post-outbreak management effects on future fuel profiles and stand structure in bark beetle-impacted forests of greater yellowstone. *Forest Ecology and Management*, 303:160–174, 2013.
- [65] J Douglas and FA Milner. Numerical methods for a model of population dynamics. *Calcolo*, 24(3-4):247–254, 1987.
- [66] C Ronnie Drever, Garry Peterson, Christian Messier, Yves Bergeron, and Mike Flanagan. Can forest management based on natural disturbances maintain ecological resilience? *Canadian Journal of Forest Research*, 36(9):2285–2299, 2006.
- [67] Barbara Drossel and Franz Schwabl. Self-organized critical forest-fire model. *Physical review letters*, 69(11):1629, 1992.

- [68] Danielle Dube, Kiho Kim, Alisa P Alker, and C Drew Harvell. Size structure and geographic variation in chemical resistance of sea fan corals *gorgonia ventalina* to a fungal pathogen. *Marine Ecology Progress Series*, 231:139–150, 2002.
- [69] Jacob P Duncan, James A Powell, Luis F Gordillo, and Joseph Eason. A model for mountain pine beetle outbreaks in an age-structured forest: Predicting severity and outbreak-recovery cycle period. *Bulletin of mathematical biology*, 77(7):1256–1284, 2015.
- [70] Jonathan Dushoff, Joshua B Plotkin, Cecile Viboud, Lone Simonsen, Mark Miller, Mark Loeb, and JD David. Vaccinating to protect a vulnerable subpopulation. *PLoS Med*, 4(5):e174, 2007.
- [71] Paul FJ Eagles. Trends in park tourism: Economics, finance and management. *Journal of sustainable tourism*, 10(2):132–153, 2002.
- [72] Leah Edelstein-Keshet. *Mathematical models in biology*, volume 46. SIAM, 1988.
- [73] Amanda B Edworthy, Mark C Drever, and Kathy Martin. Woodpeckers increase in abundance but maintain fecundity in response to an outbreak of mountain pine bark beetles. *Forest Ecology and Management*, 261(2):203–210, 2011.
- [74] CM Elkin and Mary L Reid. Low energy reserves and energy allocation decisions affect reproduction by mountain pine beetles, *dendroctonus ponderosae*. *Functional Ecology*, 19(1):102–109, 2005.
- [75] Jon C Emery, Timothy W Russel, Yang Liu, Joel Hellewell, Carl AB Pearson, Gwen M Knight, Rosalind M Eggo, Adam J Kucharski, Sebastian Funk, Stefan Flasche, et al. The contribution of asymptomatic sars-cov-2 infections to transmission-a model-based analysis of the diamond princess outbreak. *medRxiv*, 2020.
- [76] SG Field, AW Schoettle, JG Klutsch, SJ Tavener, and MF Antolin. Demographic projection of high-elevation white pines infected with white pine blister rust: a non-linear disease model. *Ecological Applications*, 22(1):166–183, 2012.
- [77] P Fong and PW Glynn. A dynamic size-structured population model: does disturbance control size structure of a population of the massive coral *gardineroseris planulata* in the eastern pacific? *Marine biology*, 130(4):663–674, 1998.

- [78] Linton C Freeman. A set of measures of centrality based on betweenness. *Sociometry*, pages 35–41, 1977.
- [79] Lee E Frelich. *Forest dynamics and disturbance regimes: studies from temperate evergreen-deciduous forests*. Cambridge University Press, 2002.
- [80] Feng Fu, Daniel I Rosenbloom, Long Wang, and Martin A Nowak. Imitation dynamics of vaccination behaviour on social networks. *Proceedings of the Royal Society B: Biological Sciences*, 278(1702):42–49, 2011.
- [81] Sebastian Funk, Erez Gilad, Chris Watkins, and Vincent AA Jansen. The spread of awareness and its impact on epidemic outbreaks. *Proceedings of the National Academy of Sciences*, 106(16):6872–6877, 2009.
- [82] Sebastian Funk, Marcel Salathé, and Vincent AA Jansen. Modelling the influence of human behaviour on the spread of infectious diseases: a review. *Journal of the Royal Society Interface*, 7(50):1247–1256, 2010.
- [83] Estella Gilbert, James A Powell, Jesse A Logan, and Barbara J Bentz. Comparison of three models predicting developmental milestones given environmental and individual variation. *Bulletin of Mathematical Biology*, 66(6):1821, 2004.
- [84] Globalnews. The dates and staggered starts for all GTA schools. September 2020. <https://globalnews.ca/news/6668240/coronavirus-ontario-schools-closed/>.
- [85] Globalnews Canada. Coronavirus: All publicly funded schools in ontario closing for 2 weeks due to COVID-19. March 2020. <https://globalnews.ca/news/6668240/coronavirus-ontario-schools-closed/>.
- [86] Martin Golubitsky, Ian Stewart, and David G Schaeffer. *Singularities and groups in bifurcation theory*, volume 2. Springer Science & Business Media, 2012.
- [87] Google, Inc. COVID-19 community mobility reports, September 2020. Available at <https://www.google.com/{COVID}19/mobility/>.
- [88] Tim R Gottwald, Gareth Hughes, James H Graham, Xiaoan Sun, and Tim Riley. The citrus canker epidemic in florida: the scientific basis of regulatory eradication policy for an invasive species. *Phytopathology*, 91(1):30–34, 2001.

- [89] K Gower, JB Fontaine, C Birnbaum, and NJ Enright. Sequential disturbance effects of hailstorm and fire on vegetation in a mediterranean-type ecosystem. *Ecosystems*, 18(7):1121–1134, 2015.
- [90] Robert A Haack, Kenneth R Law, Victor C Mastro, H Sharon Ossenburghen, and Bernard J Raimo. New york’s battle with the asian long-horned beetle. *Journal of Forestry*. 95 (12): 11-15., 2(12), 1997.
- [91] Robert A Haack, Toby R Petrice, and Alex C Wiedenhoeft. Incidence of bark-and wood-boring insects in firewood: a survey at michigan’s mackinac bridge. *Journal of Economic Entomology*, 103(5):1682–1692, 2010.
- [92] Aric Hagberg, Pieter Swart, and Daniel S Chult. Exploring network structure, dynamics, and function using networkx. Technical report, Los Alamos National Lab.(LANL), Los Alamos, NM (United States), 2008.
- [93] M Elizabeth Halloran and Ira M Longini. Community studies for vaccinating schoolchildren against influenza, 2006.
- [94] Frank G Hawkesworth. Diseases of lodgepole pine. In: *Proceedings, Society of American Foresters, Division of Forest Management; Denver, Colorado; 1964. Society of American Foresters*. p. 125-127., pages 125–127, 1964.
- [95] Kirsten A Henderson, Madhur Anand, and Chris T Bauch. Carrot or stick? modelling how landowner behavioural responses can cause incentive-based forest governance to backfire. *PloS one*, 8(10):e77735, 2013.
- [96] Daniel A Herms and Deborah G McCullough. Emerald ash borer invasion of north america: history, biology, ecology, impacts, and management. *Annual review of entomology*, 59:13–30, 2014.
- [97] Herbert W Hethcote. The mathematics of infectious diseases. *SIAM review*, 42(4):599–653, 2000.
- [98] Jeffrey A Hicke, Morris C Johnson, Jane L Hayes, and Haiganoush K Preisler. Effects of bark beetle-caused tree mortality on wildfire. *Forest Ecology and Management*, 271:81–90, 2012.
- [99] Jeffrey A Hicke, Jesse A Logan, James Powell, and Dennis S Ojima. Changing temperatures influence suitability for modeled mountain pine beetle (*dendroctonus ponderosae*) outbreaks in the western united states. *Journal of Geophysical Research: Biogeosciences*, 111(G2), 2006.

- [100] Joe Hilton and Matt J Keeling. Estimation of country-level basic reproductive ratios for novel coronavirus (COVID-19) using synthetic contact matrices. *medRxiv*, 2020.
- [101] Josef Hofbauer and Karl Sigmund. *Evolutionary games and population dynamics*. Cambridge university press, 1998.
- [102] Clinton Innes, Madhur Anand, and Chris T Bauch. The impact of human-environment interactions on the stability of forest-grassland mosaic ecosystems. *Scientific reports*, 3(1):1–10, 2013.
- [103] P-E Jabin, V Lemesle, and D Aurelle. A continuous size-structured red coral growth model. *Mathematical models and methods in applied sciences*, 18(11):1927–1944, 2008.
- [104] William R Jacobi, JG Hardin, BA Goodrich, and CM Cleaver. Retail firewood can transport live tree pests. *Journal of economic entomology*, 105(5):1645–1658, 2012.
- [105] WR Jacobi, BA Goodrich, CM Cleaver, et al. Firewood transport by national and state park campers: a risk for native or exotic tree pest movement. *Arboriculture and Urban Forestry*, 37(3):126, 2011.
- [106] Patrick James, Louis-Etienne Robert, B Mike Wotton, David L Martell, and Richard A Fleming. Lagged cumulative spruce budworm defoliation affects the risk of fire ignition in ontario, canada. *Ecological applications*, 27(2):532–544, 2017.
- [107] Michael J. Jenkins, Elizabeth Hebertson, Wesley Page, and C. Arik Jorgensen. Bark beetles, fuels, fires and implications for forest management in the intermountain west. *Forest Ecology and Management*, 254(1):16–34, 2008.
- [108] Michael J Jenkins, Wesley G Page, Elizabeth G Hebertson, and Martin E Alexander. Fuels and fire behavior dynamics in bark beetle-attacked forests in western north america and implications for fire management. *Forest Ecology and Management*, 275:23–34, 2012.
- [109] Peter C Jentsch. <https://git.uwaterloo.ca/pjentsch/prioritizing-covid-19-vaccination-in-changing-social-and-epidemiological-landscapes> 2020.
- [110] Steven G. Johnson. The NLOpt nonlinear-optimization package, 2020. Available at <http://github.com/stevengj/nlopt>.

- [111] Jeffrey M Kane, J Morgan Varner, Margaret R Metz, and Phillip J van Mantgem. Characterizing interactions between fire and other disturbances and their impacts on tree mortality in western us forests. *Forest Ecology and Management*, 405:188–199, 2017.
- [112] Vadim A Karatayev, Madhur Anand, and Chris T Bauch. Local lockdowns outperform global lockdown on the far side of the COVID-19 epidemic curve. *Proceedings of the National Academy of Sciences*, 2020.
- [113] Merrill R Kaufmann et al. The status of our scientific understanding of lodgepole pine and mountain pine beetles: a focus on forest ecology and fire behavior. 2008.
- [114] Barbara Lee Keyfitz and Nathan Keyfitz. The mckendrick partial differential equation and its uses in epidemiology and population study. *Mathematical and Computer Modelling*, 26(6):1–9, 1997.
- [115] Frank H Koch, Denys Yemshanov, Robert A Haack, and Roger D Magarey. Using a network model to assess risk of forest pest spread via recreational travel. *PloS one*, 9(7):e102105, 2014.
- [116] Cynthia S Kolar and David M Lodge. Progress in invasion biology: predicting invaders. *Trends in ecology & evolution*, 16(4):199–204, 2001.
- [117] Kent F Kovacs, Robert G Haight, Deborah G McCullough, Rodrigo J Mercader, Nathan W Siegert, and Andrew M Liebhold. Cost of potential emerald ash borer damage in us communities, 2009–2019. *Ecological Economics*, 69(3):569–578, 2010.
- [118] Kent F Kovacs, Robert G Haight, Rodrigo J Mercader, and Deborah G McCullough. A bioeconomic analysis of an emerald ash borer invasion of an urban forest with multiple jurisdictions. *Resource and Energy Economics*, 36(1):270–289, 2014.
- [119] Dominik Kulakowski, Daniel Jarvis, Thomas T Veblen, and Jeremy Smith. Stand-replacing fires reduce susceptibility of lodgepole pine to mountain pine beetle outbreaks in colorado. *Journal of Biogeography*, 39(11):2052–2060, 2012.
- [120] Toshikazu Kuniya. Existence of a nontrivial periodic solution in an age-structured sir epidemic model with time periodic coefficients. *Applied Mathematics Letters*, 27:15–20, 2014.
- [121] Alexander Lachmann. Correcting under-reported COVID-19 case numbers. *medRxiv*, 2020.

- [122] Stephen A Lauer, Kyra H Grantz, Qifang Bi, Forrest K Jones, Qulu Zheng, Hannah R Meredith, Andrew S Azman, Nicholas G Reich, and Justin Lessler. The incubation period of coronavirus disease 2019 (COVID-19) from publicly reported confirmed cases: estimation and application. *Annals of internal medicine*, 2020.
- [123] Dave Leatherman, I Aguayo, and TM Mehall. Mountain pine beetle. *Colorado Birds*, page 33, 2012.
- [124] Mark A Lewis, William Nelson, and Cailin Xu. A structured threshold model for mountain pine beetle outbreak. *Bulletin of mathematical biology*, 72(3):565–589, 2010.
- [125] Chao Li and Michael J Apps. Effects of contagious disturbance on forest temporal dynamics. *Ecological Modelling*, 87(1-3):143–151, 1996.
- [126] Chao Li, Hugh J Barclay, Brad C Hawkes, and SW Taylor. Lodgepole pine forest age class dynamics and susceptibility to mountain pine beetle attack. *Ecological Complexity*, 2(3):232–239, 2005.
- [127] Jia Li. Dynamics of age-structured predator-prey population models. *Journal of mathematical analysis and applications*, 152(2):399–415, 1990.
- [128] You Li, Harry Campbell, Durga Kulkarni, Alice Harpur, Madhurima Nundy, Xin Wang, Harish Nair, Usher Network for COVID, et al. The temporal association of introducing and lifting non-pharmaceutical interventions with the time-varying reproduction number (r) of sars-cov-2: a modelling study across 131 countries. *The Lancet Infectious Diseases*, 2020.
- [129] Andrew M Liebhold and Patrick C Tobin. Population ecology of insect invasions and their management. *Annu. Rev. Entomol.*, 53:387–408, 2008.
- [130] Shuguang Liu, Ben Bond-Lamberty, Jeffrey A Hicke, Rodrigo Vargas, Shuqing Zhao, Jing Chen, Steven L Edburg, Yueming Hu, Jinxun Liu, A David McGuire, et al. Simulating the impacts of disturbances on forest carbon cycling in north america: Processes, data, models, and challenges. *Journal of Geophysical Research: Biogeosciences*, 116(G4), 2011.
- [131] James E Lotan, James K Brown, and Leon F Neuenschwander. Role of fire in lodgepole pine forests. 1985.

- [132] Donald Ludwig, Dixon D Jones, Crawford S Holling, et al. Qualitative analysis of insect outbreak systems: the spruce budworm and forest. *Journal of animal ecology*, 47(1):315–332, 1978.
- [133] Nicole Lurie, Melanie Saville, Richard Hatchett, and Jane Halton. Developing COVID-19 vaccines at pandemic speed. *New England Journal of Medicine*, 382(21):1969–1973, 2020.
- [134] Heather J Lynch, Roy A Renkin, Robert L Crabtree, and Paul R Moorcroft. The influence of previous mountain pine beetle (*dendroctonus ponderosae*) activity on the 1988 yellowstone fires. *Ecosystems*, 9(8):1318–1327, 2006.
- [135] Junling Ma and David JD Earn. Generality of the final size formula for an epidemic of a newly invading infectious disease. *Bulletin of mathematical biology*, 68(3):679–702, 2006.
- [136] Monia Makhoul, Houssein H Ayoub, Hiam Chemaitelly, Shaheen Seedat, Ghina R Mumtaz, Sarah Al-Omari, and Laith J Abu-Raddad. Epidemiological impact of sars-cov-2 vaccination: mathematical modeling analyses. *medRxiv*, 2020.
- [137] Amyn A. Malik, SarahAnn M. McFadden, Jad Elharake, and Saad B. Omer. Determinants of covid-19 vaccine acceptance in the us. *EClinicalMedicine*, 26:100495, 2020.
- [138] Laura Matrajt, Julie Eaton, Tiffany Leung, and Elizabeth R Brown. Vaccine optimization for COVID-19, who to vaccinate first? *medRxiv*, 2020.
- [139] Daniel J McGrail, Jianli Dai, Kathleen M McAndrews, and Raghu Kalluri. Enacting national social distancing policies corresponds with dramatic reduction in COVID19 infection rates. *PloS one*, 15(7):e0236619, 2020.
- [140] Daniel W McKenney, John H Pedlar, Denys Yemshanov, Kathy L Campbell, and Kevin Lawrence. Estimates of the potential cost of emerald ash borer (*agrilus planipennis fairmairei*) in canadian municipalities. 2012.
- [141] Garrett W Meigs, Harold SJ Zald, John L Campbell, William S Keeton, and Robert E Kennedy. Do insect outbreaks reduce the severity of subsequent forest fires? *Environmental Research Letters*, 11(4):045008, 2016.
- [142] Johan A Metz and Odo Diekmann. *The dynamics of physiologically structured populations*, volume 68. Springer, 2014.

- [143] Gerard Meurant. *The ecology of natural disturbance and patch dynamics*. Academic press, 2012.
- [144] Ian F Miller, Alexander D Becker, Bryan T Grenfell, and C Jessica E Metcalf. Disease and healthcare burden of COVID-19 in the United States. *Nature Medicine*, 26(8):1212–1217, 2020.
- [145] Kenji Mizumoto, Katsushi Kagaya, Alexander Zarebski, and Gerardo Chowell. Estimating the asymptomatic proportion of coronavirus disease 2019 (COVID-19) cases on board the diamond princess cruise ship, yokohama, japan, 2020. *Eurosurveillance*, 25(10):2000180, 2020.
- [146] Christopher J Moran and Mark A Cochrane. Do mountain pine beetle outbreaks change the probability of active crown fire in lodgepole pine forests? comment. *Ecology*, 93(4):939–941, 2012.
- [147] Joël Mossong, Niel Hens, Mark Jit, Philippe Beutels, Kari Auranen, Rafael Mikola-jczyk, Marco Massari, Stefania Salmaso, Gianpaolo Scalia Tomba, Jacco Wallinga, et al. Social contacts and mixing patterns relevant to the spread of infectious diseases. *PLoS medicine*, 5(3), 2008.
- [148] Jim R Muirhead, Brian Leung, Colin van Overdijk, David W Kelly, Kanavillil Nandakumar, Kenneth R Marchant, and Hugh J MacIsaac. Modelling local and long-distance dispersal of invasive emerald ash borer *agrilus planipennis* (coleoptera) in north america. *Diversity and Distributions*, 12(1):71–79, 2006.
- [149] National Invasive Species Council (NISC). Fiscal year 2007 interagency invasive species performance budget. Online source, 2007.
- [150] Brian Nearing. Checkpoint tries to halt wood traffic. *timesunion*, 2012.
- [151] José F Negrón, Kurt K Allen, Angie Ambourn, Blaine Cook, and Kenneth Marchand. Large-scale thinnings, ponderosa pine, and mountain pine beetle in the black hills, usa. *Forest Science*, 63(5):529–536, 2017.
- [152] Hiroshi Nishiura, Natalie M Linton, and Andrei R Akhmetzhanov. Serial interval of novel coronavirus (COVID-19) infections. *International journal of infectious diseases*, 2020.
- [153] Andrea R Norris and Kathy Martin. Mountain pine beetle presence affects nest patch choice of red-breasted nuthatches. *The Journal of Wildlife Management*, 72(3):733–737, 2008.

- [154] Magnus Nyström and Carl Folke. Spatial resilience of coral reefs. *Ecosystems*, 4(5):406–417, 2001.
- [155] Magnus Nyström, Carl Folke, and Fredrik Moberg. Coral reef disturbance and resilience in a human-dominated environment. *Trends in Ecology & Evolution*, 15(10):413–417, 2000.
- [156] Ministry of Sustainable Resource Management. British columbia’s forests: A geographical snapshot. 2003.
- [157] Tom Oliver, David B Roy, Jane K Hill, Tom Brereton, and Chris D Thomas. Heterogeneous landscapes promote population stability. *Ecology letters*, 13(4):473–484, 2010.
- [158] Ontario Agency for Health Protection and Promotion (Public Health Ontario). COVID-19 case fatality, case identification, and attack rates in ontario. <https://www.publichealthontario.ca/-/media/documents/ncov/epi/2020/06/COVID19-epi-case-identification-age-only-template.pdf?la=en>, 2020.
- [159] Ontario Ministry of Natural Resources. Are you moving firewood? important information you should read, 2011.
- [160] Tamer Oraby, Vivek Thampi, and Chris T Bauch. The influence of social norms on the dynamics of vaccinating behaviour for paediatric infectious diseases. *Proceedings of the Royal Society B: Biological Sciences*, 281(1780):20133172, 2014.
- [161] Organisation for Economic Co-operation and Development. Oecd intensive care bed capacity, <https://www.oecd.org/coronavirus/en/data-insights/intensive-care-beds-capacity>, accessed 25 september 2020, 2020.
- [162] World Health Organization. Who target product profiles for COVID-19 vaccines, [https://www.who.int/who-documents-detailredirect/ who-target-product-profiles-for-COVID-19-vaccines](https://www.who.int/who-documents-detailredirect/who-target-product-profiles-for-COVID-19-vaccines), accessed 25 september 2020, 2020.
- [163] George D Papadopoulos and Fotini-Niovi Pavlidou. A comparative review on wildfire simulators. *IEEE systems Journal*, 5(2):233–243, 2011.
- [164] Serge Payette, Najat Bhiry, Ann Delwaide, and Martin Simard. Origin of the lichen woodland at its southern range limit in eastern canada: the catastrophic impact of insect defoliators and fire on the spruce-moss forest. *Canadian Journal of Forest Research*, 30(2):288–305, 2000.

- [165] Corey M Peak, Rebecca Kahn, Yonatan H Grad, Lauren M Childs, Ruoran Li, Marc Lipsitch, and Caroline O Buckee. Individual quarantine versus active monitoring of contacts for the mitigation of COVID-19: a modelling study. *The Lancet Infectious Diseases*, 2020.
- [166] Sansao A Pedro, Frank T Ndjomatchoua, Peter Jentsch, Jean M Tcheunche, Madhur Anand, and Chris T Bauch. Conditions for a second wave of COVID-19 due to interactions between disease dynamics and social processes. *medRxiv*, 2020.
- [167] Debra PC Peters, Ariel E Lugo, F Stuart Chapin, Steward TA Pickett, Michael Duniway, Adrian V Rocha, Frederick J Swanson, Christine Laney, and Julia Jones. Cross-system comparisons elucidate disturbance complexities and generalities. *Ecosphere*, 2(7):1–26, 2011.
- [168] Debra PC Peters, Roger A Pielke, Brandon T Bestelmeyer, Craig D Allen, Stuart Munson-McGee, and Kris M Havstad. Cross-scale interactions, nonlinearities, and forecasting catastrophic events. *Proceedings of the National Academy of Sciences of the United States of America*, 101(42):15130–15135, 2004.
- [169] Garry D Peterson. Contagious disturbance, ecological memory, and the emergence of landscape pattern. *Ecosystems*, 5(4):329–338, 2002.
- [170] Kim Peterson and Andrea Diss-Torrance. Motivation for compliance with environmental regulations related to forest health. *Journal of environmental management*, 112:104–119, 2012.
- [171] Toby R Petrice and Robert A Haack. Effects of cutting date, outdoor storage conditions, and splitting on survival of agrilus planipennis (coleoptera: Buprestidae) in firewood logs. *Journal of Economic Entomology*, 99(3):790–796, 2006.
- [172] David Pimentel, Rodolfo Zuniga, and Doug Morrison. Update on the environmental and economic costs associated with alien-invasive species in the united states. *Ecological economics*, 52(3):273–288, 2005.
- [173] Therese M Poland and Deborah G McCullough. Emerald ash borer: invasion of the urban forest and the threat to north america’s ash resource. *Journal of Forestry*, 104(3):118–124, 2006.
- [174] Hugh DW Powell, Sallie J Hejl, and Diana L Six. Measuring woodpecker food: a simple method for comparing wood-boring beetle abundance among fire-killed trees. *Journal of Field Ornithology*, 73(2):130–140, 2002.

- [175] James A Powell and Barbara J Bentz. Connecting phenological predictions with population growth rates for mountain pine beetle, an outbreak insect. *Landscape Ecology*, 24(5):657–672, 2009.
- [176] James A Powell, Jesse A Logan, and Barbara J Bentz. Local projections for a global model of mountain pine beetle attacks. *Journal of Theoretical Biology*, 179(3):243–260, 1996.
- [177] Anantha M Prasad, Louis R Iverson, Matthew P Peters, Jonathan M Bossenbroek, Stephen N Matthews, T Davis Sydnor, and Mark W Schwartz. Modeling the invasive emerald ash borer risk of spread using a spatially explicit cellular model. *Landscape ecology*, 25(3):353–369, 2010.
- [178] Kiesha Prem, Alex R Cook, and Mark Jit. Projecting social contact matrices in 152 countries using contact surveys and demographic data. *PLoS computational biology*, 13(9):e1005697, 2017.
- [179] Kiesha Prem, Kevin van Zandvoort, Petra Klepac, Rosalind M Eggo, Nicholas G Davies, Alex R Cook, Mark Jit, et al. Projecting contact matrices in 177 geographical regions: an update and comparison with empirical data for the COVID-19 era. *medRxiv*, 2020.
- [180] Provincial government of Ontario, Canada. Reopening ontario in stages, 2020. Available at <https://www.ontario.ca/page/reopening-ontario-stages>.
- [181] Public Health Agency of Canada. Daily epidemiological update. <https://www.canada.ca/content/dam/phac-aspc/documents/services/diseases-maladies/2019-novel-coronavirus-infection/COVID19-epi-update-eng-2020-04-03.pdf>, 2020. accessed 4 April 2020.
- [182] Public Health Ontario. Covid-19 serosurveillance summary: Covid-19 seroprevalence in ontario: March 27, 2020 to june 30, 2020, 2020.
- [183] Erin J Questad and Bryan L Foster. Coexistence through spatio-temporal heterogeneity and species sorting in grassland plant communities. *Ecology letters*, 11(7):717–726, 2008.
- [184] Christopher Rackauckas and Qing Nie. Differentialequations. jl—a performant and feature-rich ecosystem for solving differential equations in julia. *Journal of Open Research Software*, 5(1), 2017.

- [185] Kenneth F Raffa, Brian H Aukema, Barbara J Bentz, Allan L Carroll, Jeffrey A Hicke, Monica G Turner, and William H Romme. Cross-scale drivers of natural disturbances prone to anthropogenic amplification: the dynamics of bark beetle eruptions. *AIBS Bulletin*, 58(6):501–517, 2008.
- [186] Nick Reid. Roadside checkpoints to monitor illegal firewood transport in new hampshire. *Concord Monitor*, 2017.
- [187] Timothy C Reluga. Game theory of social distancing in response to an epidemic. *PLoS Comput Biol*, 6(5):e1000793, 2010.
- [188] Suzanne L Robertson, Shandelle M Henson, Timothy Robertson, and JM Cushing. A matter of maturity: To delay or not to delay? continuous-time compartmental models of structured populations in the literature 2000–2016. *Natural Resource Modeling*, 2018.
- [189] Christopher T Rota, Joshua J Millspaugh, Mark A Rumble, Chad P Lehman, and Dylan C Kesler. The role of wildfire, prescribed fire, and mountain pine beetle infestations on the population dynamics of black-backed woodpeckers in the black hills, south dakota. *PloS one*, 9(4), 2014.
- [190] Les Safranyik et al. Mountain pine beetle epidemiology in lodgepole pine. In *Mountain pine beetle symposium: Challenges and solutions*, pages 33–40, 2003.
- [191] Les Safranyik, Douglas A Linton, Terry L Shore, BC Hawkes, et al. *The effects of prescribed burning on mountain pine beetle in lodgepole pine*, volume 391. 2001.
- [192] Les Safranyik, Bill Wilson, et al. *The mountain pine beetle: a synthesis of biology, management and impacts on lodgepole pine*. Canadian Forest Service, 2007.
- [193] Marcel Salathe, Linus Bengtsson, Todd J Bodnar, Devon D Brewer, John S Brownstein, Caroline Buckee, Ellsworth M Campbell, Ciro Cattuto, Shashank Khandelwal, Patricia L Mabry, et al. Digital epidemiology. *PLoS Comput Biol*, 8(7):e1002616, 2012.
- [194] Marcel Salathé and Sebastian Bonhoeffer. The effect of opinion clustering on disease outbreaks. *Journal of The Royal Society Interface*, 5(29):1505–1508, 2008.
- [195] Charles Sartwell and Robert E. Stevens. Mountain pine beetle in ponderosa pine—prospects for silvicultural control in second-growth stands. *Journal of Forestry*, 73(3):136–140, 1975.

- [196] Akiko Satake, Heather M Leslie, Yoh Iwasa, and Simon A Levin. Coupled ecological–social dynamics in a forested landscape: Spatial interactions and information flow. *Journal of theoretical biology*, 246(4):695–707, 2007.
- [197] Melissa Savage and Joy Nystrom Mast. How resilient are southwestern ponderosa pine forests after crown fires? *Canadian Journal of Forest Research*, 35(4):967–977, 2005.
- [198] Boris Schling. *The Boost C++ Libraries*. XML Press, 2011.
- [199] Donald R Schoolmaster Jr. Resource competition and coexistence in heterogeneous metacommunities: many-species coexistence is unlikely to be facilitated by spatial variation in resources. *PeerJ*, 1:e136, 2013.
- [200] Rupert Seidl, Daniel C Donato, Kenneth F Raffa, and Monica G Turner. Spatial variability in tree regeneration after wildfire delays and dampens future bark beetle outbreaks. *Proceedings of the National Academy of Sciences*, page 201615263, 2016.
- [201] Rupert Seidl, Dominik Thom, Markus Kautz, Dario Martin-Benito, Mikko Peltoniemi, Giorgio Vacchiano, Jan Wild, Davide Ascoli, Michal Petr, Juha Honkaniemi, et al. Forest disturbances under climate change. *Nature climate change*, 7(6):395, 2017.
- [202] Colorado Forest Service. Report on the health of colorado’s forests. 2016.
- [203] Ram Sigdel, Madhur Anand, and Chris T Bauch. Convergence of socio-ecological dynamics in disparate ecological systems under strong coupling to human social systems. *Theoretical Ecology*, 12(3):285–296, 2019.
- [204] Juha Siikamäki. Contributions of the us state park system to nature recreation. *Proceedings of the National Academy of Sciences*, 108(34):14031–14036, 2011.
- [205] Martin Simard, William H Romme, Jacob M Griffin, and Monica G Turner. Do mountain pine beetle outbreaks change the probability of active crown fire in lodgepole pine forests? *Ecological Monographs*, 81(1):3–24, 2011.
- [206] Martin Simard, William H Romme, Jacob M Griffin, and Monica G Turner. Do mountain pine beetle outbreaks change the probability of active crown fire in lodgepole pine forests? reply. *Ecology*, 93(4):946–950, 2012.
- [207] Statistics Canada. Census profile, 2016 census, <https://www12.statcan.gc.ca/>, accessed 25 september 2020, 2020.

- [208] Robert S Steneck, Michael H Graham, Bruce J Bourque, Debbie Corbett, Jon M Erlandson, James A Estes, and Mia J Tegner. Kelp forest ecosystems: biodiversity, stability, resilience and future. *Environmental conservation*, 29(4):436–459, 2002.
- [209] M Henry H Stevens and Walter P Carson. Resource quantity, not resource heterogeneity, maintains plant diversity. *Ecology Letters*, 5(3):420–426, 2002.
- [210] S Strohm, ML Reid, and RC Tyson. Impacts of management on mountain pine beetle spread and damage: A process-rich model. *Ecological Modelling*, 337:241–252, 2016.
- [211] Andrew L Sullivan. Wildland surface fire spread modelling, 1990–2007. 3: Simulation and mathematical analogue models. *International Journal of Wildland Fire*, 18(4):387–403, 2009.
- [212] Krister Svanberg. A class of globally convergent optimization methods based on conservative convex separable approximations. *SIAM journal on optimization*, 12(2):555–573, 2002.
- [213] Hui Tang and Zhihua Liu. Hopf bifurcation for a predator-prey model with age structure. *Applied Mathematical Modelling*, 40(2):726–737, 2016.
- [214] Stephen W Taylor, Allan L Carroll, et al. Disturbance, forest age, and mountain pine beetle outbreak dynamics in bc: A historical perspective. In *Mountain pine beetle symposium: Challenges and solutions*, volume 3031. Natural Resources Canada, Canadian Forest Service, Pacific Forestry Centre . . . , 2003.
- [215] MJ Tegner and PK Dayton. Population structure, recruitment and mortality of two sea urchins (*Strongylocentrotus franciscanus* and *s. purpuratus*) in a kelp forest. *Marine Ecology Progress Series*, pages 255–268, 1981.
- [216] Vivek A Thampi, Madhur Anand, and Chris T Bauch. Socio-ecological dynamics of caribbean coral reef ecosystems and conservation opinion propagation. *Scientific reports*, 8(1):1–11, 2018.
- [217] James William Thomas. *Numerical partial differential equations: finite difference methods*, volume 22. Springer Science & Business Media, 2013.
- [218] Lauren Tindale, Michelle Coombe, Jessica E Stockdale, Emma Garlock, Wing Yin Venus Lau, Manu Saraswat, Yen-Hsiang Brian Lee, Louxin Zhang, Dongxuan Chen, Jacco Wallinga, et al. Transmission interval estimates suggest pre-symptomatic spread of COVID-19. *medRxiv*, 2020.

- [219] Patrick C Tobin. Cost analysis and biological ramifications for implementing the gypsy moth slow the spread program. *Gen. Tech. Rep. NRS-37. Newtown Square, PA: US Department of Agriculture, Forest Service, Northern Research Station.* 21 p., 37, 2008.
- [220] Patrick C Tobin, Andrea Diss-Torrance, Laura M Blackburn, and Brian D Brown. What does “local” firewood buy you? managing the risk of invasive species introduction. *Journal of economic entomology*, 103(5):1569–1576, 2010.
- [221] Diana F Tomback, Jane Kees Clary, James Koehler, Raymond J Hoff, and Stephen F Arno. The effects of blister rust on post-fire regeneration of whitebark pine: the sundance burn of northern idaho (usa). *Conservation Biology*, 9(3):654–664, 1995.
- [222] Treasury Board Secretariat of Ontario. Confirmed positive cases of COVID-19 in Ontario, September 2020. Available at <https://data.ontario.ca/dataset/confirmed-positive-cases-of-{COVID}-19-in-ontario/resource/455fd63b-603d-4608-8216-7d8647f43350>.
- [223] Ashleigh R Tuite, David N Fisman, and Amy L Greer. Mathematical modelling of COVID-19 transmission and mitigation strategies in the population of ontario, canada. *CMAJ*, 192(19):E497–E505, 2020.
- [224] Jean J Turgeon, Mary Orr, Cara Grant, Yunke Wu, and Ben Gasman. Decade-old satellite infestation of anoplophora glabripennis motschulsky (coleoptera: Cerambycidae) found in ontario, canada outside regulated area of founder population. *The Coleopterists Bulletin*, 69(4):674–679, 2015.
- [225] Brandon M Turner and Per B Sederberg. Approximate Bayesian computation with differential evolution. *Journal of Mathematical Psychology*, 56(5):375–385, 2012.
- [226] Monica G Turner, Robert H Gardner, Virginia H Dale, and Robert V O’Neill. Predicting the spread of disturbance across heterogeneous landscapes. *Oikos*, pages 121–129, 1989.
- [227] Monica G Turner and William H Romme. Landscape dynamics in crown fire ecosystems. *Landscape ecology*, 9(1):59–77, 1994.
- [228] United States Centers for Disease Control. Coronavirus disease 2019 (COVID-19). <https://www.cdc.gov/coronavirus/2019-ncov/cases-updates/cases-in-us.html>, 2020. accessed 4 April 2020.

- [229] United States Department of Agriculture Animal and Plant Health Inspection Service. Risk assessment of the movement of firewood within the united states, 2011.
- [230] US Centers for Disease Control. Severe outcomes among patients with coronavirus disease 2019 (COVID-19) — united states, february 12–march 16, 2020. <https://www.cdc.gov/mmwr/volumes/69/wr/pdfs/mm6912e2-h.pdf>. *MMWR*, 69(12):343–346, 2020.
- [231] Pauline Van den Driessche and James Watmough. Reproduction numbers and sub-threshold endemic equilibria for compartmental models of disease transmission. *Mathematical biosciences*, 180(1-2):29–48, 2002.
- [232] Thomas T Veblen, Keith S Hadley, Elizabeth M Nel, Thomas Kitzberger, Marion Reid, and Ricardo Villalba. Disturbance regime and disturbance interactions in a rocky mountain subalpine forest. *Journal of Ecology*, pages 125–135, 1994.
- [233] Frederik Verelst, Lander Willem, and Philippe Beutels. Behavioural change models for infectious disease transmission: a systematic review (2010–2015). *Journal of The Royal Society Interface*, 13(125):20160820, 2016.
- [234] Robert Verity, Lucy C Okell, Ilaria Dorigatti, Peter Winskill, Charles Whittaker, Natsuko Imai, Gina Cuomo-Dannenburg, Hayley Thompson, Patrick Walker, Han Fu, et al. Estimates of the severity of COVID-19 disease. *medRxiv*, 2020.
- [235] CE Van Wagner. Conditions for the start and spread of crown fire. *Canadian Journal of Forest Research*, 7(1):23–34, 1977.
- [236] CE Van Wagner. Age-class distribution and the forest fire cycle. *Canadian Journal of Forest Research*, 8(2):220–227, 1978.
- [237] Zhen Wang, Chris T Bauch, Samit Bhattacharyya, Alberto d’Onofrio, Piero Manfredi, Matjaž Perc, Nicola Perra, Marcel Salathe, and Dawei Zhao. Statistical physics of vaccination. *Physics Reports*, 664:1–113, 2016.
- [238] Laren Weber. Checkpoint tries to halt wood traffic. *The Toledo Blade*, 2006.
- [239] Earl E Werner and James F Gilliam. The ontogenetic niche and species interactions in size-structured populations. *Annual review of ecology and systematics*, 15(1):393–425, 1984.

- [240] Anthony L Westerling, Hugo G Hidalgo, Daniel R Cayan, and Thomas W Swetnam. Warming and earlier spring increase western us forest wildfire activity. *science*, 313(5789):940–943, 2006.
- [241] Peter S White and Anke Jentsch. The search for generality in studies of disturbance and ecosystem dynamics. In *Progress in botany*, pages 399–450. Springer, 2001.
- [242] Peter S White and S TA Pickett. *Natural disturbance and patch dynamics: An introduction*. Springer, 1985.
- [243] John RU Wilson, Eleanor E Dormontt, Peter J Prentis, Andrew J Lowe, and David M Richardson. Something in the way you move: dispersal pathways affect invasion success. *Trends in ecology & evolution*, 24(3):136–144, 2009.
- [244] Toby Wise, Tomislav Damir Zbozinek, Giorgia Michelini, Cindy C Hagan, et al. Changes in risk perception and protective behavior during the first week of the COVID-19 pandemic in the united states. 2020.
- [245] Denys Yemshanov, Robert G Haight, Frank H Koch, Bo Lu, Robert Venette, D Barry Lyons, Taylor Scarr, and Krista Ryall. Optimal allocation of invasive species surveillance with the maximum expected coverage concept. *Diversity and Distributions*, 21(11):1349–1359, 2015.
- [246] Denys Yemshanov, Frank H Koch, Daniel W McKenney, Marla C Downing, and Frank Sapi. Mapping invasive species risks with stochastic models: a cross-border united states-canada application for sirex noctilio fabricius. *Risk Analysis: An International Journal*, 29(6):868–884, 2009.
- [247] Emilio Zagheni, Francesco C Billari, Piero Manfredi, Alessia Melegaro, Joel Mossong, and W John Edmunds. Using time-use data to parameterize models for the spread of close-contact infectious diseases. *American journal of epidemiology*, 168(9):1082–1090, 2008.
- [248] Shi Zhao, Lewi Stone, Daozhou Gao, Salihu S Musa, Marc KC Chong, Daihai He, and Maggie H Wang. Imitation dynamics in the mitigation of the novel coronavirus disease (COVID-19) outbreak in wuhan, china from 2019 to 2020. *Annals of Translational Medicine*, 8(7), 2020.
- [249] RD Zinck and V Grimm. More realistic than anticipated: a classical forest-fire model from statistical physics captures real fire shapes. *The Open Ecology Journal*, 1(1), 2008.

- [250] Rafał Zwolak. A meta-analysis of the effects of wildfire, clearcutting, and partial harvest on the abundance of north american small mammals. *Forest Ecology and Management*, 258(5):539–545, 2009.
- [251] Rafał Zwolak and Kerry R Foresman. Deer mouse demography in burned and unburned forest: no evidence for source–sink dynamics. *Canadian Journal of Zoology*, 86(2):83–91, 2008.

Appendix

Appendix A

Appendix C

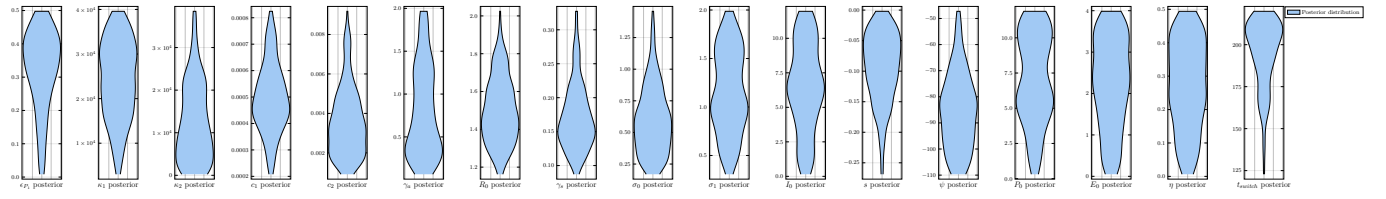


Figure A.1: Posterior distributions on inferred non-age structured model parameters for baseline model. Posteriors are composed of 200 candidate parameter sets from the particle filtering, the model was evaluated at these points for all future runs.

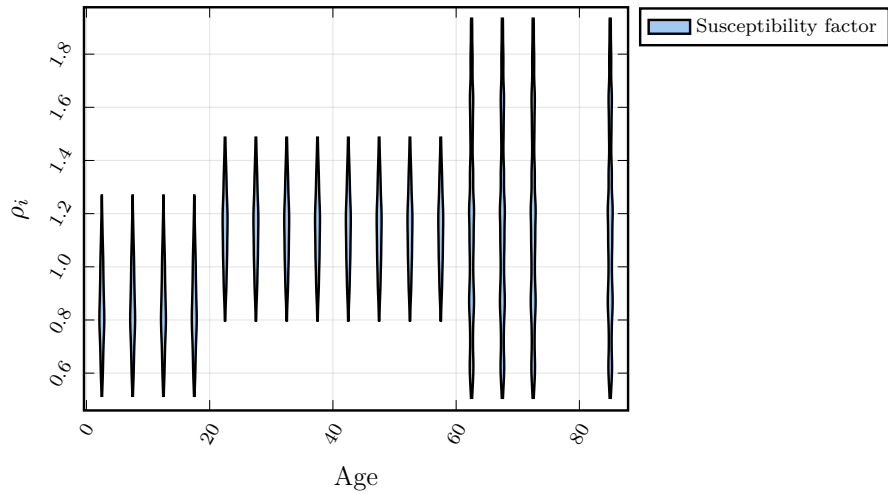


Figure A.2: Posterior distributions on inferred age-specific susceptibility modifier parameter ρ_i for baseline model. Three age-specific susceptibility parameters shown here, ρ_1, ρ_2, ρ_3 , were also inferred from particle filtering on the case and mobility data, corresponding to the age brackets 0-20, 20-60, 60+.

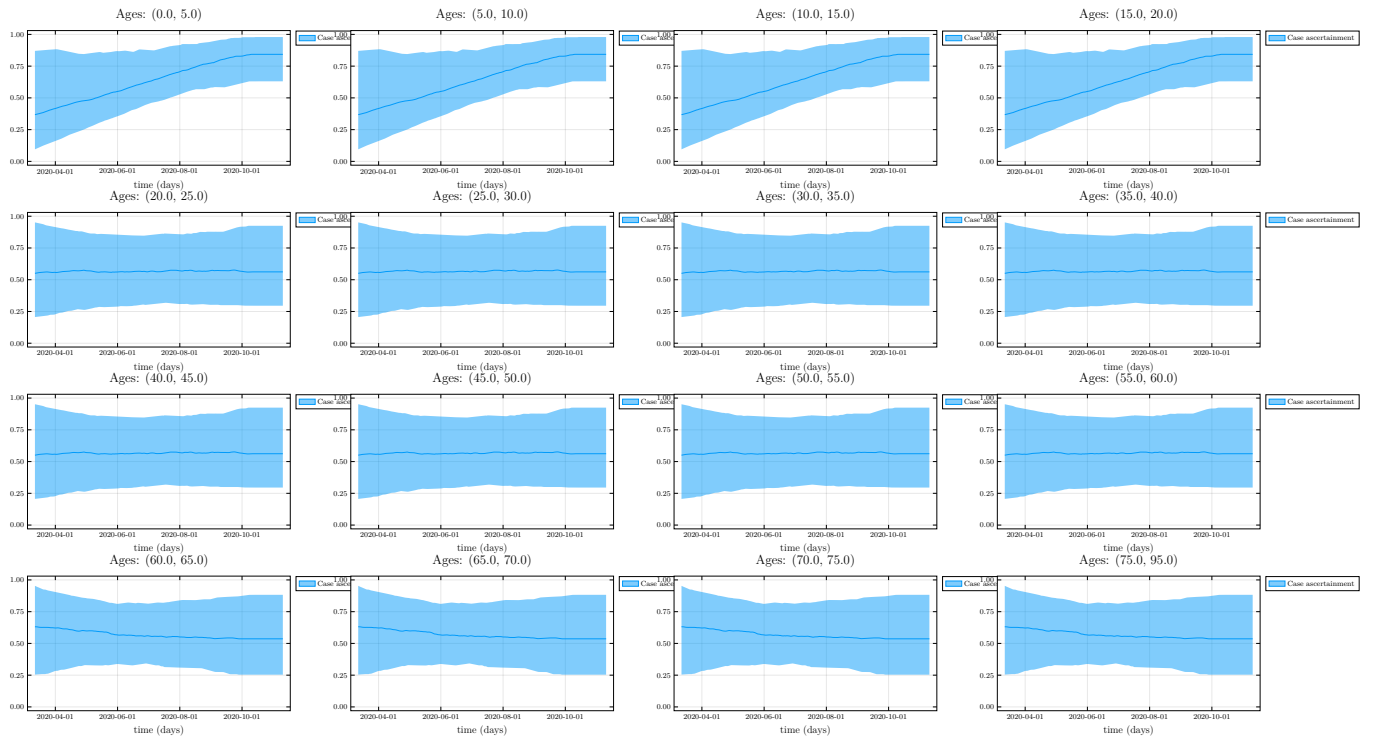


Figure A.3: Posterior distributions on inferred age-specific ascertainment rate over time for baseline model. Time dependent ascertainment rates inferred from the data, corresponding to the fraction of actual cases detected by the Ontario testing system.

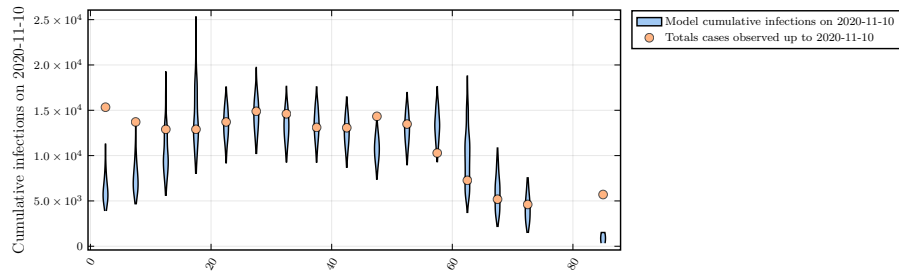


Figure A.4: Empirical data of cumulative infections due to COVID-19 by age and model posterior predictions. The age-specific total cases at the end of the fitting window, were used to calibrate the model, in an age dependent way. We used only three parameters to capture age specific effects and therefore trade-off some accuracy in the youngest and oldest age groups.

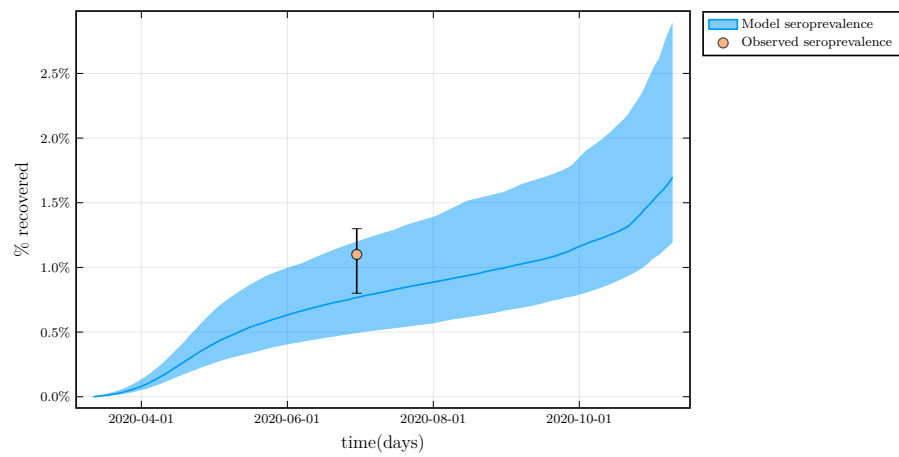


Figure A.5: Average of model posterior population seropositivity over time, compared to empirical data. Total seroprevalence in Ontario was assessed during the month of June. We used this value to calibrate the model further.

Contact-based vaccination strategy

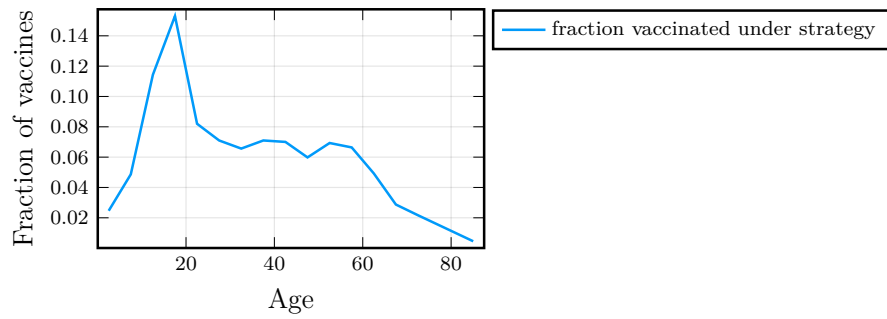


Figure A.6: **Age distribution of vaccination under the contact-based strategy.** This strategy vaccinates proportionally to the leading eigenvector of the full contact matrix, $C(0)$, to vaccinate people who will, approximately, produce the most secondary infections in a linearized regime.

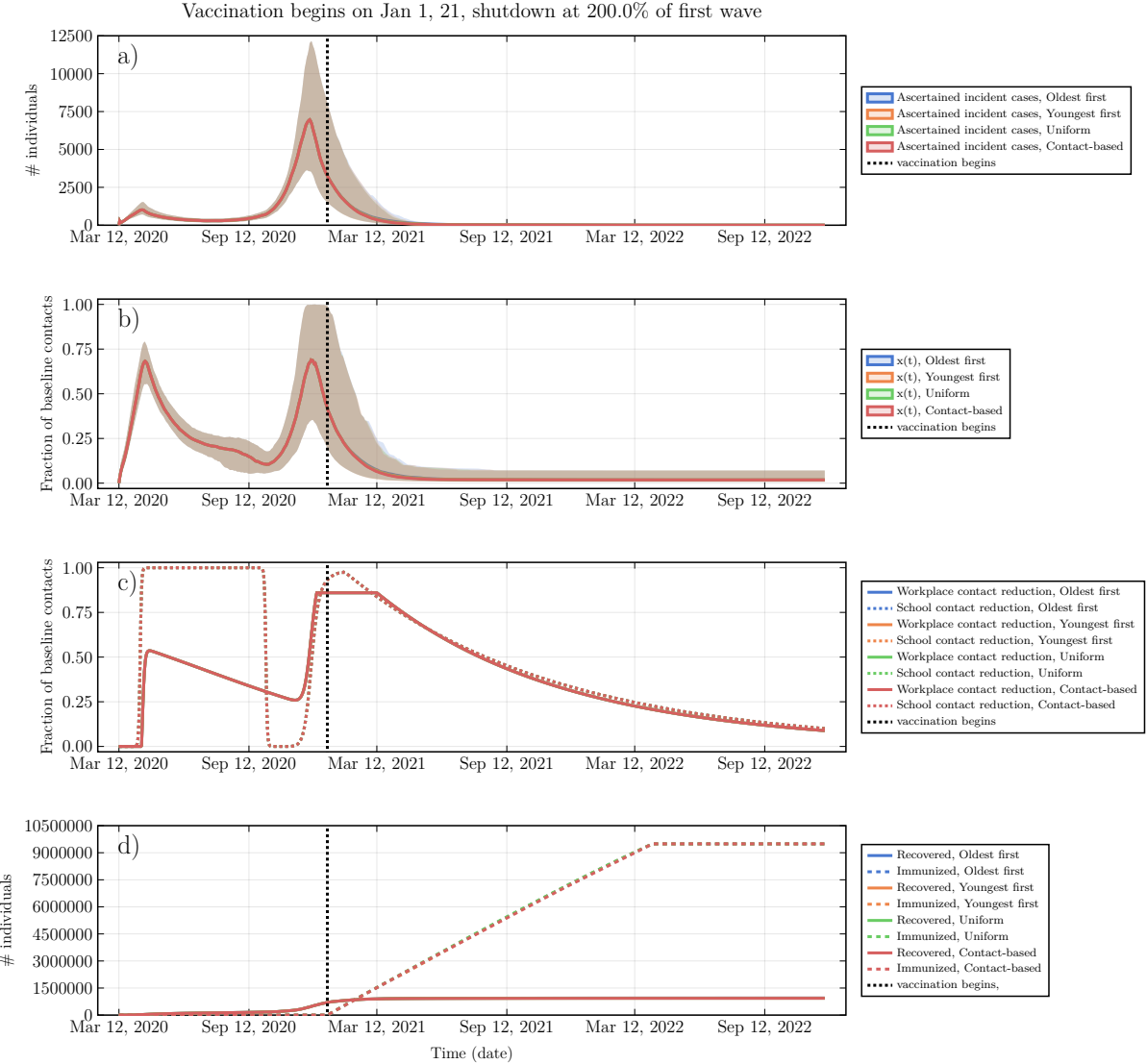


Figure A.7: Social and epidemic dynamics for early vaccine availability and high vaccination rate. (a) Ascertained incident COVID-19 cases, (b) proportion x of the population practicing NPIs, (c) Intensity of school and workplace closure, (d) percentage of population with natural or vaccine-derived immunity versus time. $T = 200\%$, $\psi_0 = 1.5\%$ per week, vaccine available in January 2021. Other parameters are in Table 3.1.

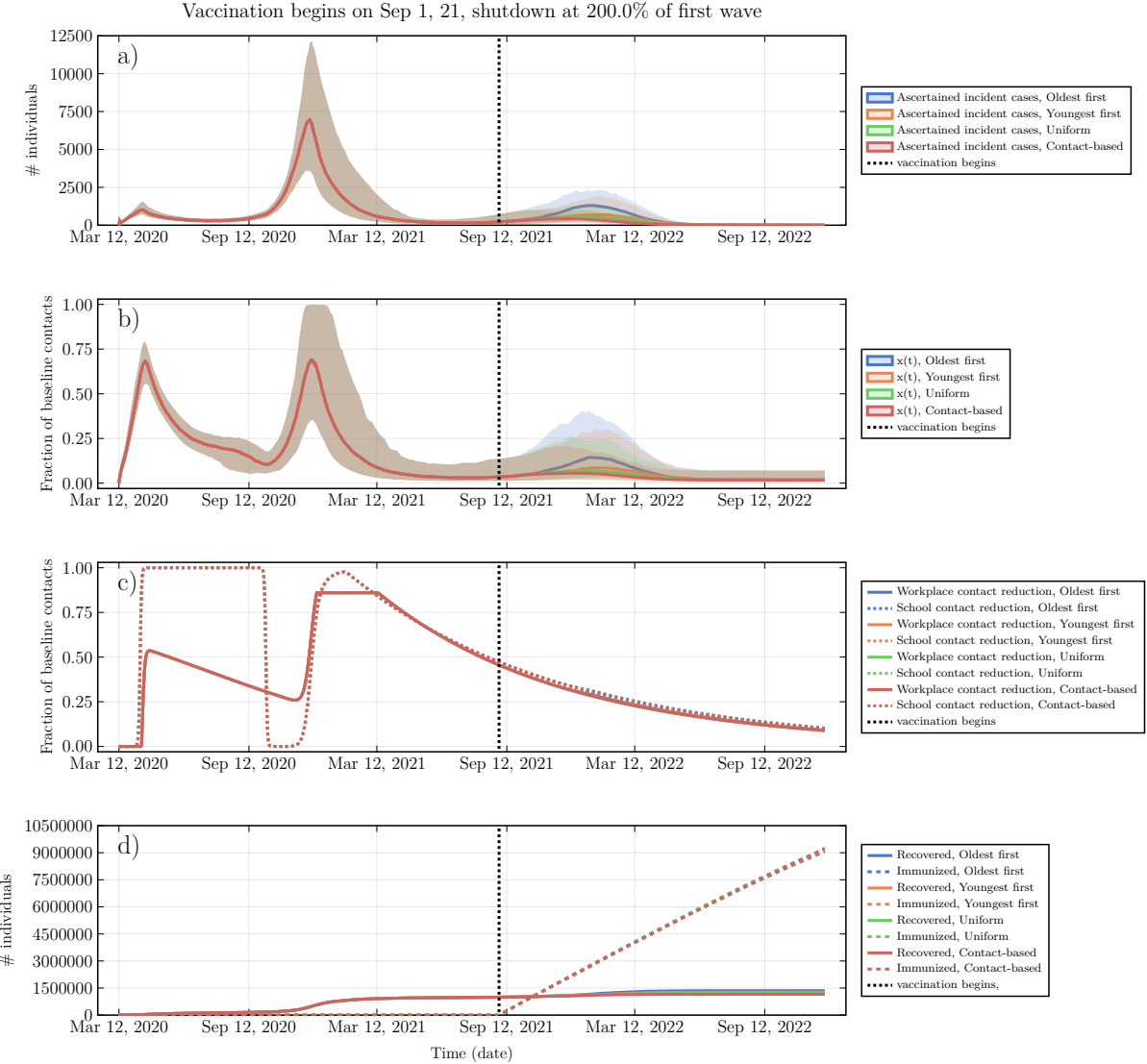


Figure A.8: Social and epidemic dynamics for late vaccine availability and high vaccination rate. (a) Ascertained incident COVID-19 cases, (b) proportion x of the population practicing NPIs, (c) Intensity of school and workplace closure, (d) percentage of population with natural or vaccine-derived immunity versus time. $T = 200\%$, $\psi_0 = 1.5\%$ per week, vaccine available in September 2021. Other parameters are in Table 3.1.

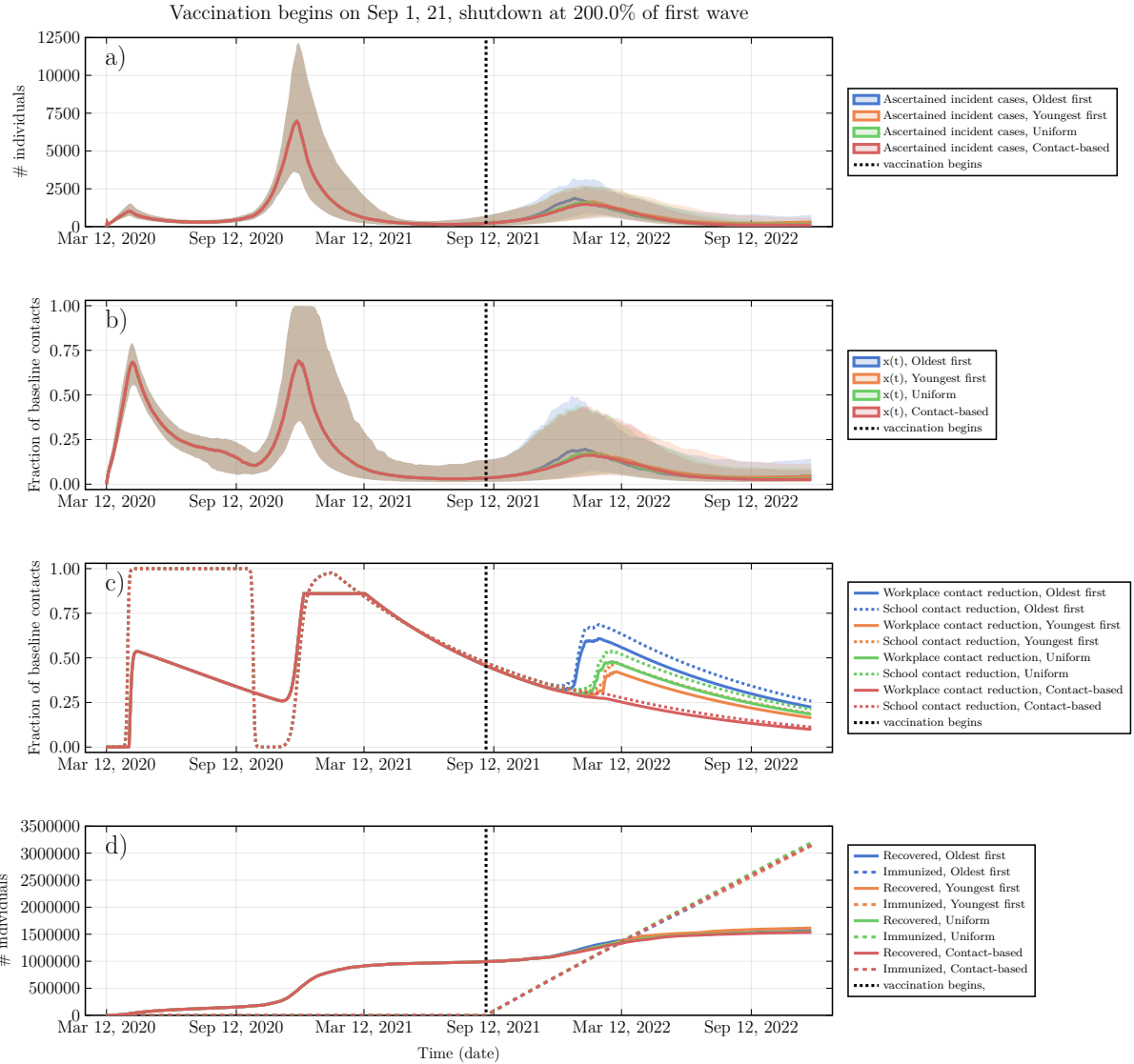


Figure A.9: Social and epidemic dynamics for late vaccine availability and low vaccination rate. (a) Ascertained incident COVID-19 cases, (b) proportion x of the population practicing NPIs, (c) Intensity of school and workplace closure, (d) percentage of population with natural or vaccine-derived immunity versus time. $T = 200\%$, $\psi_0 = 0.5\%$ per week, vaccine available in September 2021. Other parameters are in Table 3.1.

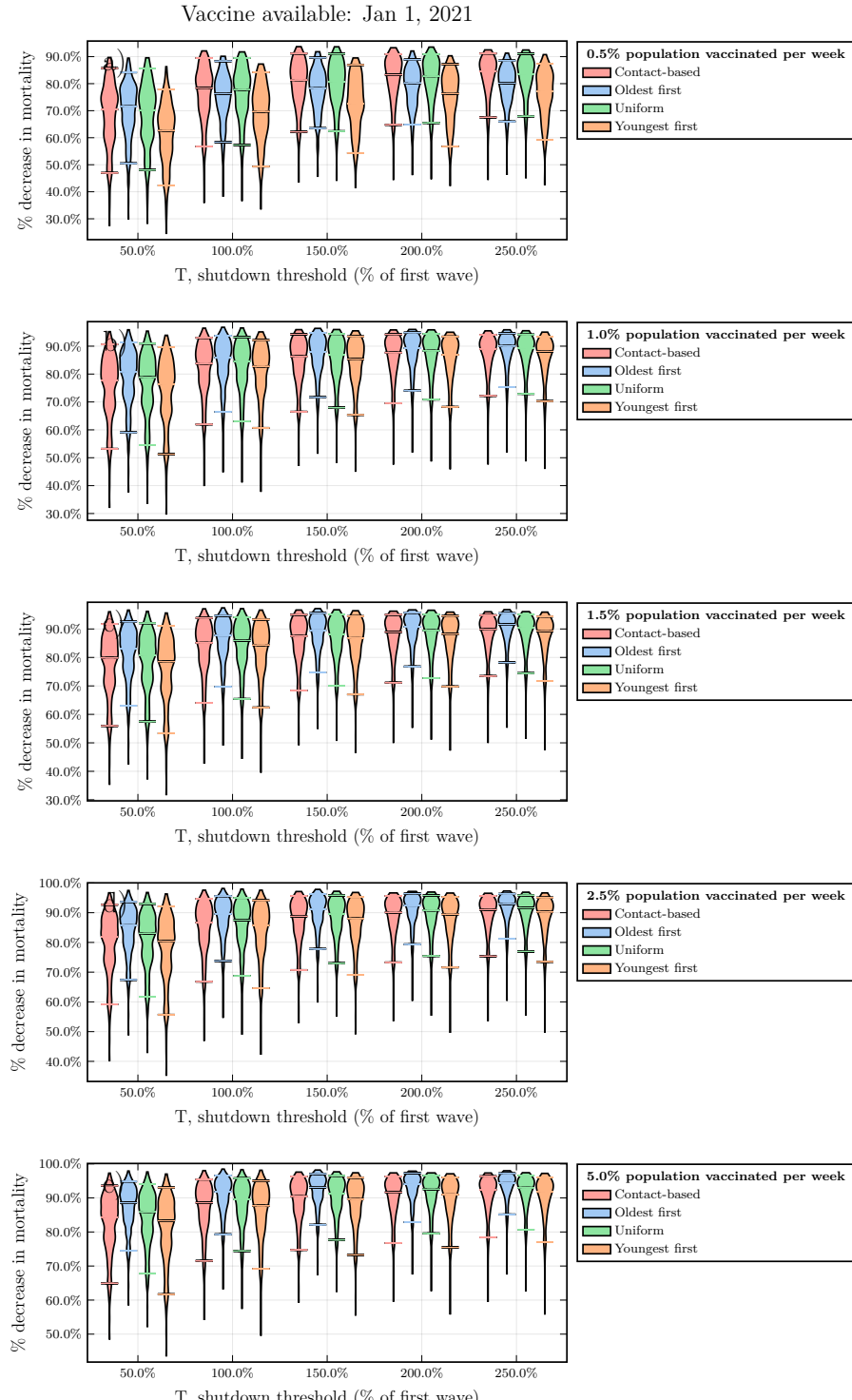


Figure A.10: Mortality reductions under various values of T and ψ_0 , early vaccine availability. Violin plots of the percent reduction in mortality under the four vaccine strategies, relative to no vaccination, as a function of the vaccination rate ψ_0 , for January 2021 availability. Horizontal lines represent median values of posterior model projections. Other parameter values in Table S1. Percentage reductions are relative to no vaccination. Projected number of deaths in the absence of vaccination were 35597.2 (CI: 57465.9–19507.9), 48518.8 (CI: 26252.9–22225.7), 61320.1 (CI: 196623.9–24612.5), 72007.3

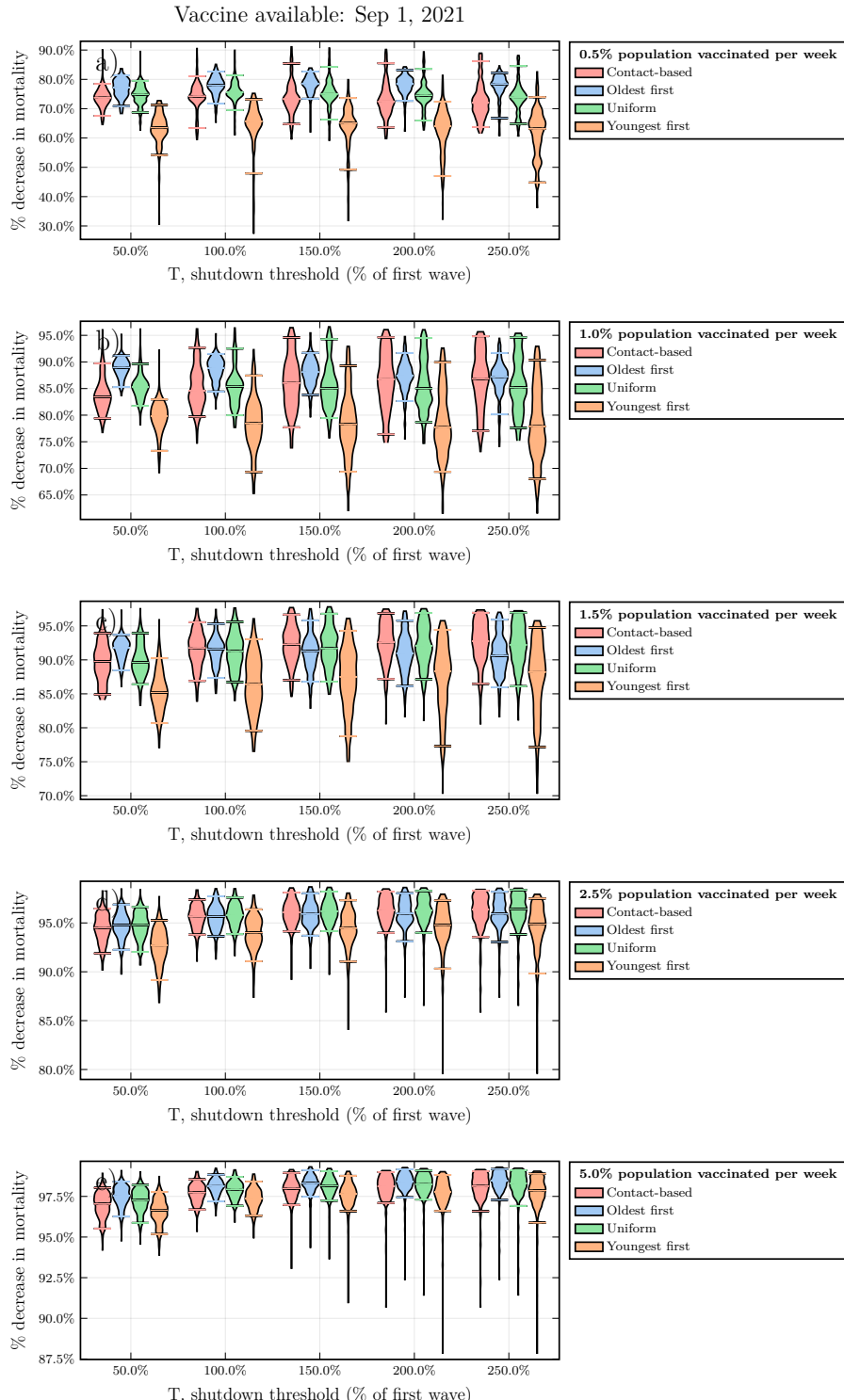


Figure A.11: Mortality reductions under various values of T and ψ_0 , late vaccine availability. Violin plots of the percent reduction in mortality under the four vaccine strategies, relative to no vaccination, as a function of the vaccination rate ψ_0 , for September 2021 availability. Horizontal lines represent median values of posterior model projections. Other parameter values in Table S1. Percentage reductions are relative to no vaccination. Projected number of deaths in the absence of vaccination were 25478.8 (CI:

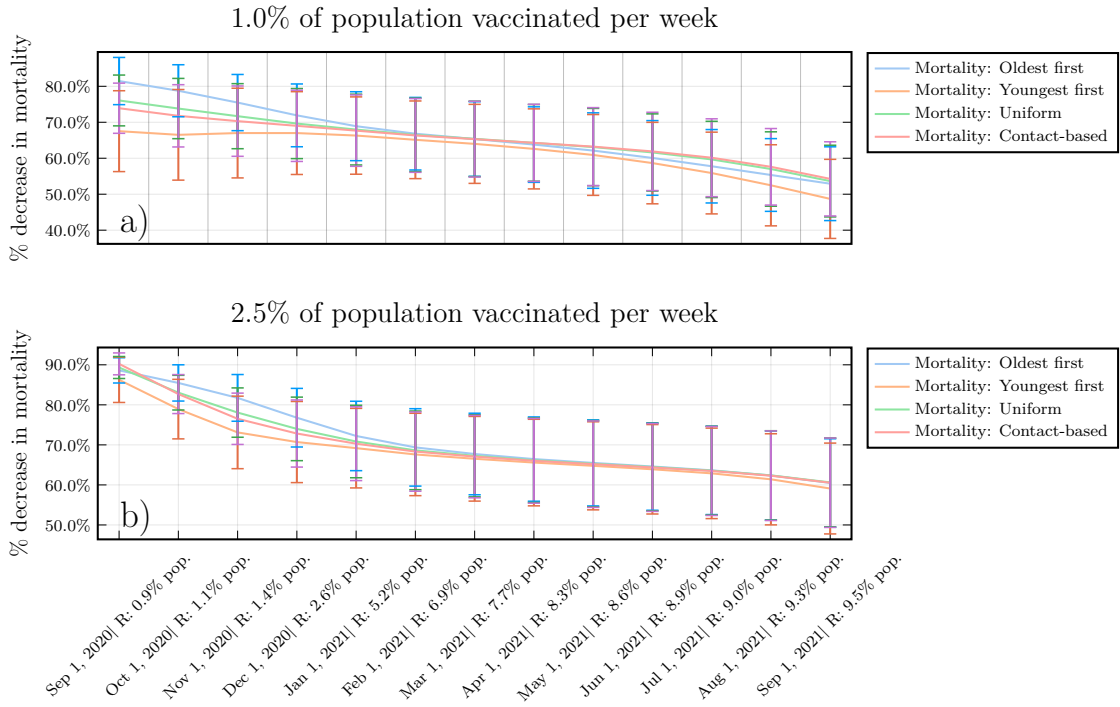


Figure A.12: A higher level of natural immunity increases the relative advantage of transmission-interrupting strategies. Median and standard deviation of the percent reduction in mortality under the four vaccine strategies, relative to no vaccination, as a function of the vaccination start date and percent recovered at that time, for (a) $\phi_0 = 1.0\%$ vaccinated per week and (b) $\phi_0 = 2.5\%$ vaccinated per week. Shutdown threshold $T = 200\%$, and other parameter values in Appendix, Table S1.

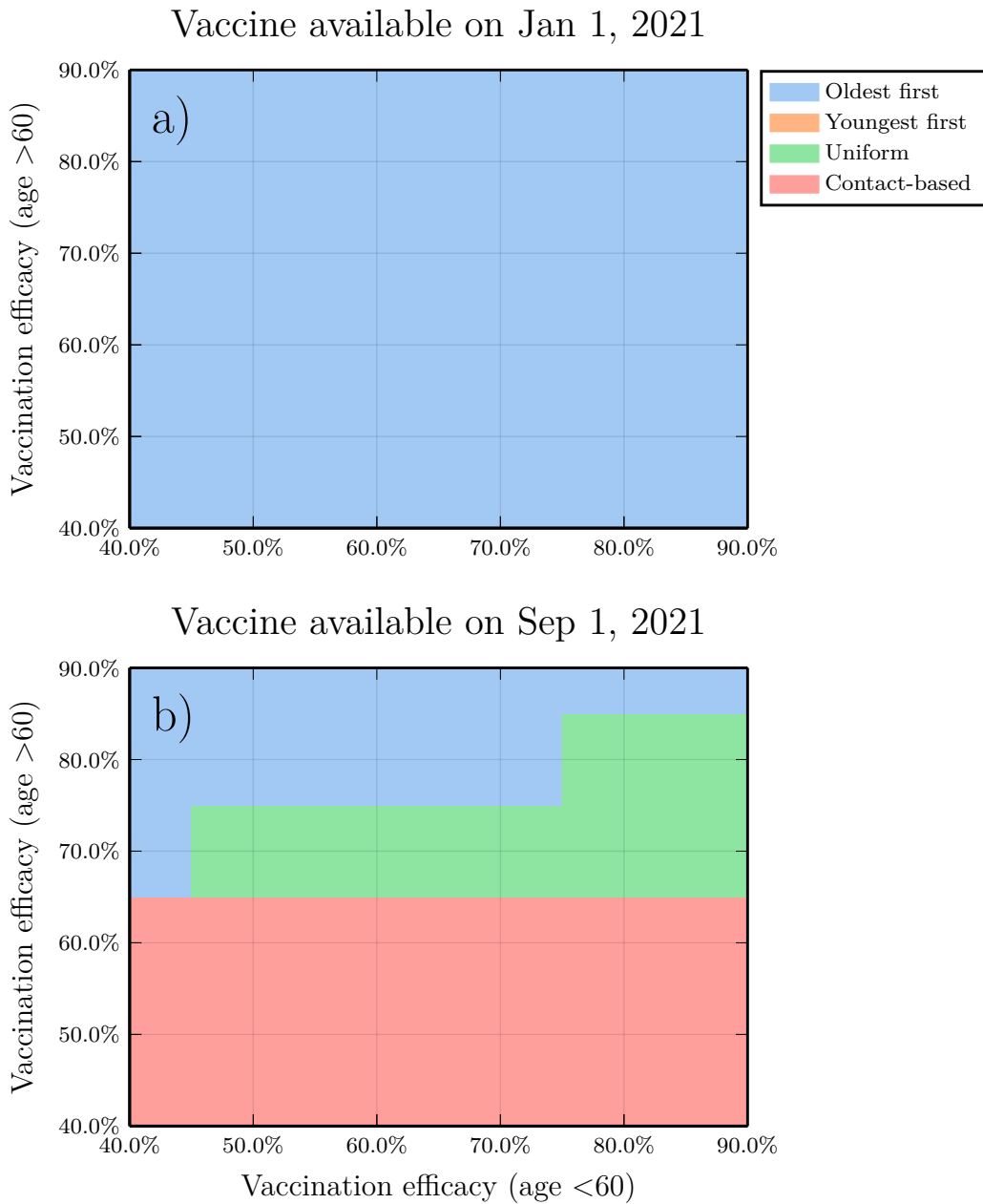


Figure A.13: **Sensitivity analysis exploring a range of vaccine efficacy values, for vaccination rate $\phi_0 = 2.5\%$ per week.** Subpanels are parameter planes for January and September availability showing the vaccination strategy that reduces COVID-19 mortality the most as a function of vaccine efficacy in 60+ year-olds versus vaccine efficacy in other age groups. Other parameter values as in Table S1.

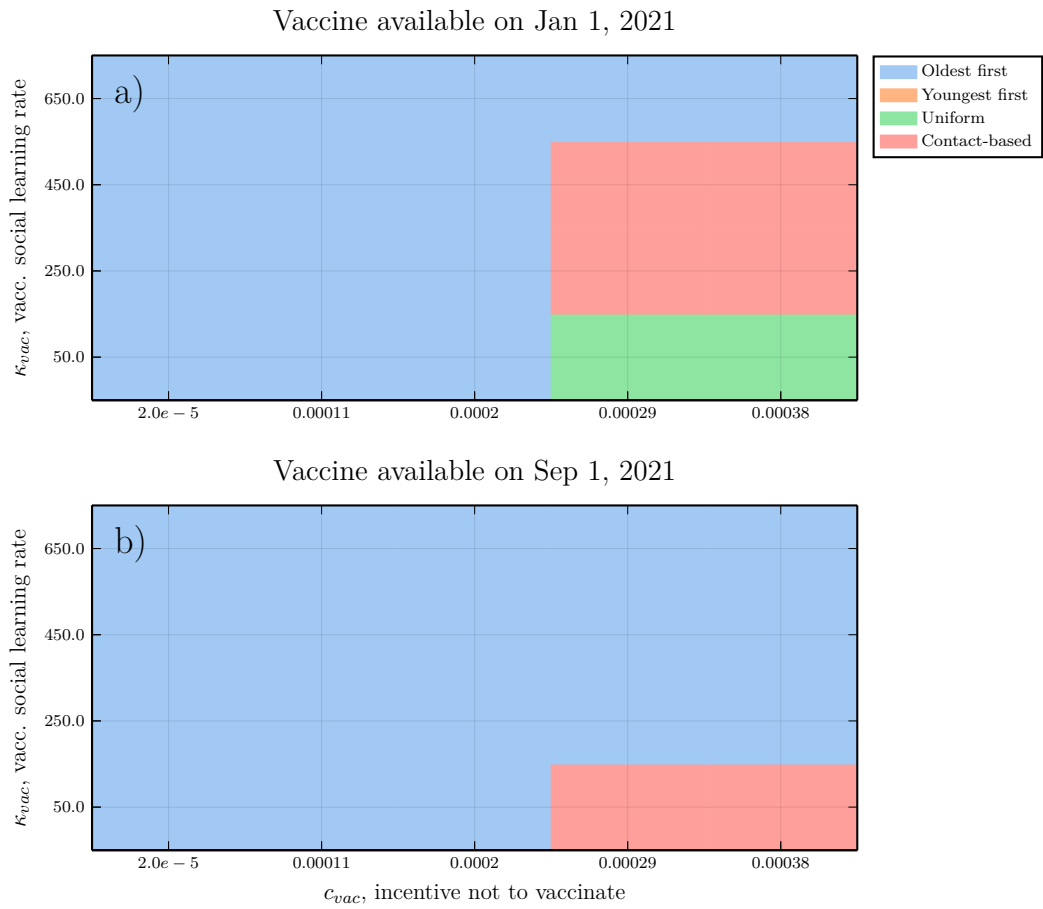


Figure A.14: Sensitivity analysis exploring impact of vaccinating behaviour dynamics. $\phi_0 = 2.5\%$ per week, $T = 200\%$. Subpanels are parameter planes for January and September availability showing the vaccination strategy that reduces COVID-19 mortality the most as a function of vaccine social learning rate κ_{vac} and vaccine cost parameter c_{vac} . Other parameter values as in Table S1.

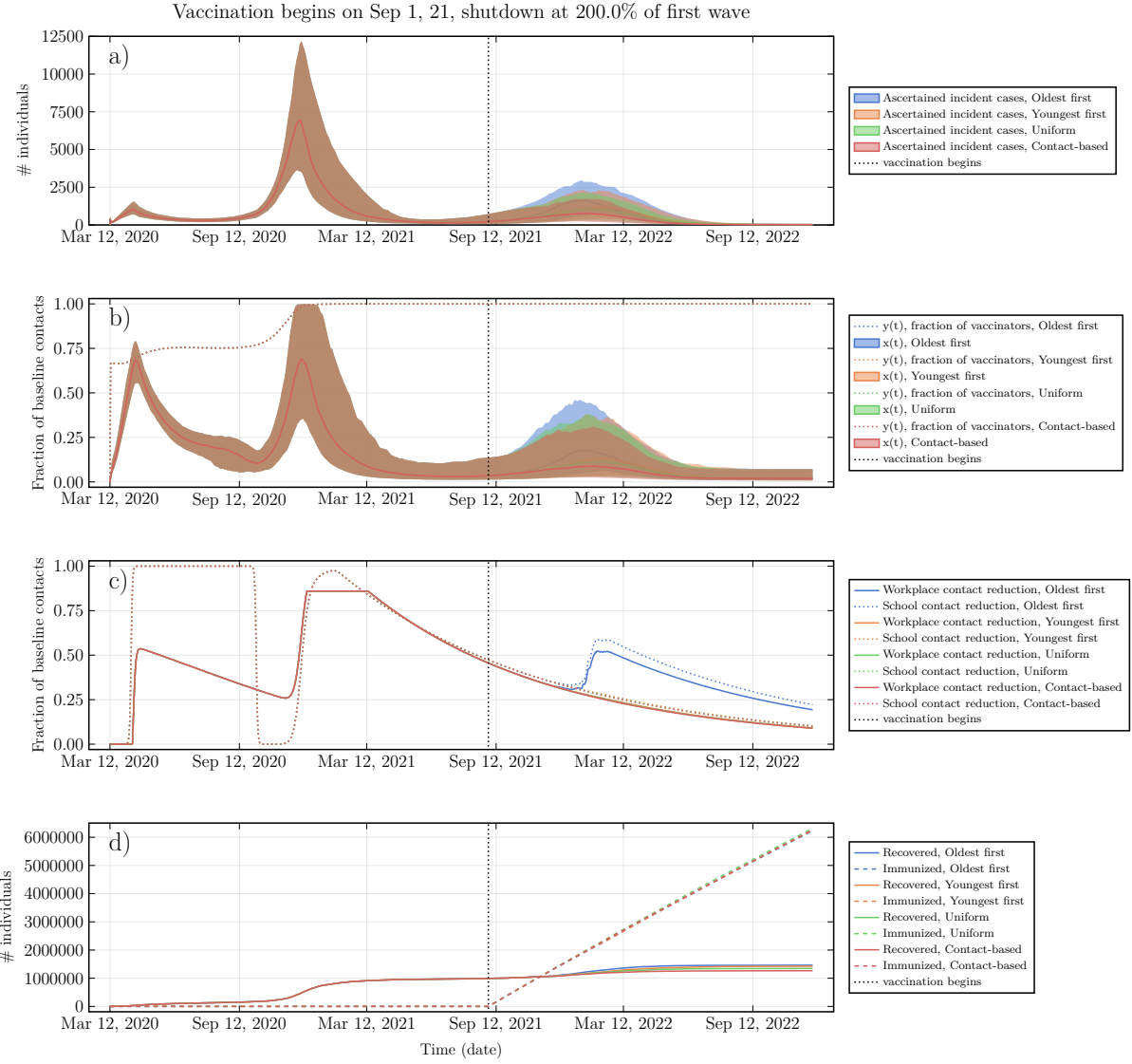


Figure A.15: Epidemic dynamics and social dynamics for both NPI adherence and vaccinating behaviour, when vaccine cost is small, $c_{vac} = 1.1 \times 10^{-4}$. (a) Ascertained incident COVID-19 cases, (b) proportion x of the population practicing NPIs, (c) Intensity of school and workplace closure, (d) percentage of population with natural or vaccine-derived immunity versus time. $T = 200\%$, $\psi_0 = 1.0\%$ per week (maximum rate in absence of vaccine refusal), vaccine available in September 2021, $\kappa_{vac} = 50/\text{day}$. Other parameters are in Table 3.1.

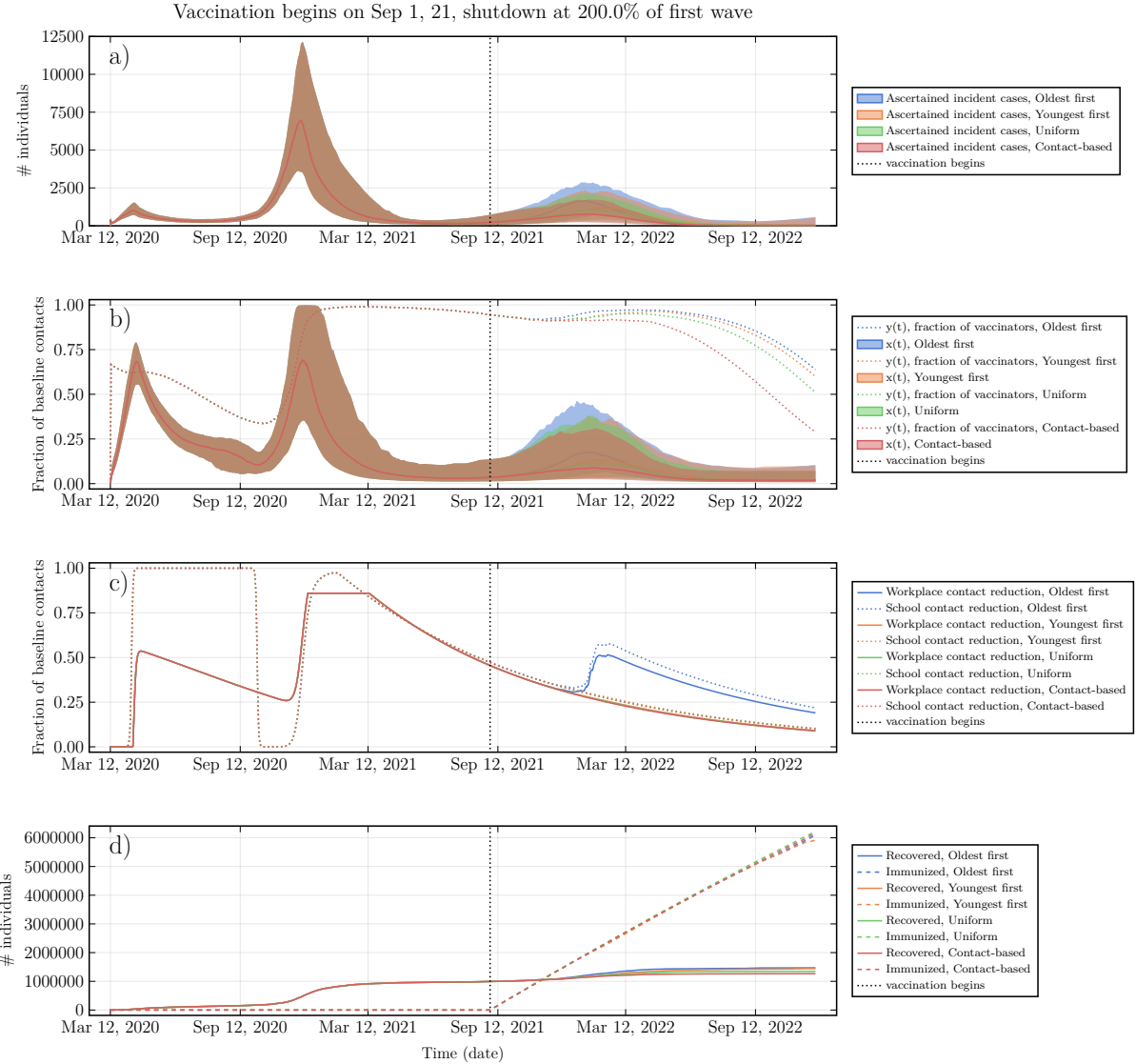


Figure A.16: Epidemic dynamics and social dynamics for both NPI adherence and vaccinating behaviour, when vaccine cost is moderate, $c_{vac} = 2.9 \times 10^{-4}$. (a) Ascertained incident COVID-19 cases, (b) proportion x of the population practicing NPIs, (c) Intensity of school and workplace closure, (d) percentage of population with natural or vaccine-derived immunity versus time. $T = 200\%$, $\psi_0 = 1.0\%$ per week (maximum rate in absence of vaccine refusal), vaccine available in September 2021, $\kappa_{vac} = 50/\text{day}$. Other parameters are in Table 3.1.

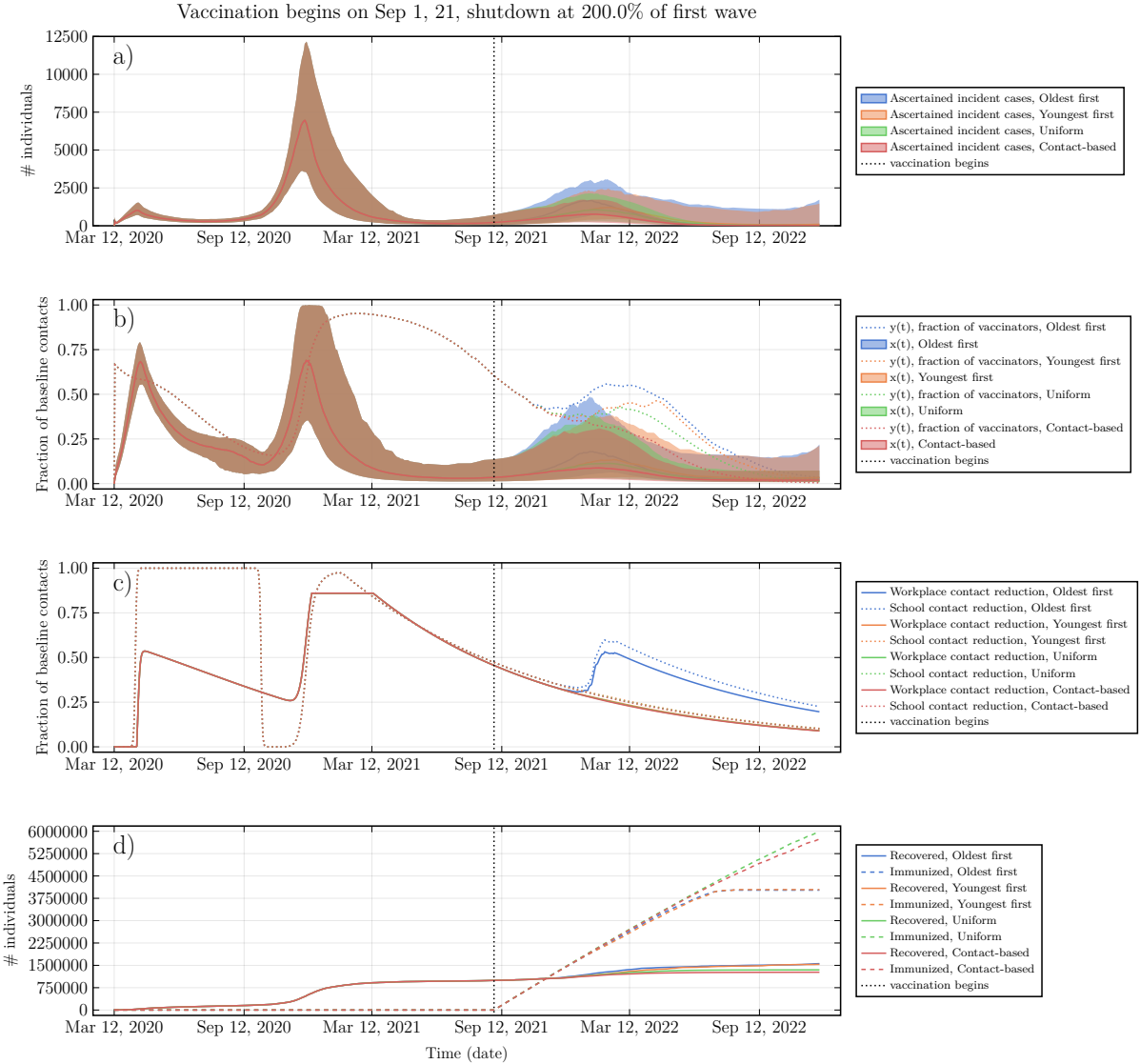


Figure A.17: Epidemic dynamics and social dynamics for both NPI adherence and vaccinating behaviour, when vaccine cost is high, $c_{vac} = 3.8 \times 10^{-4}$. (a) Ascertained incident COVID-19 cases, (b) proportion x of the population practicing NPIs, (c) Intensity of school and workplace closure, (d) percentage of population with natural or vaccine-derived immunity versus time. $T = 200\%$, $\psi_0 = 1.0\%$ per week (maximum rate in absence of vaccine refusal), vaccine available in September 2021, $\kappa_{vac} = 50/\text{day}$. Other parameters are in Table 3.1.

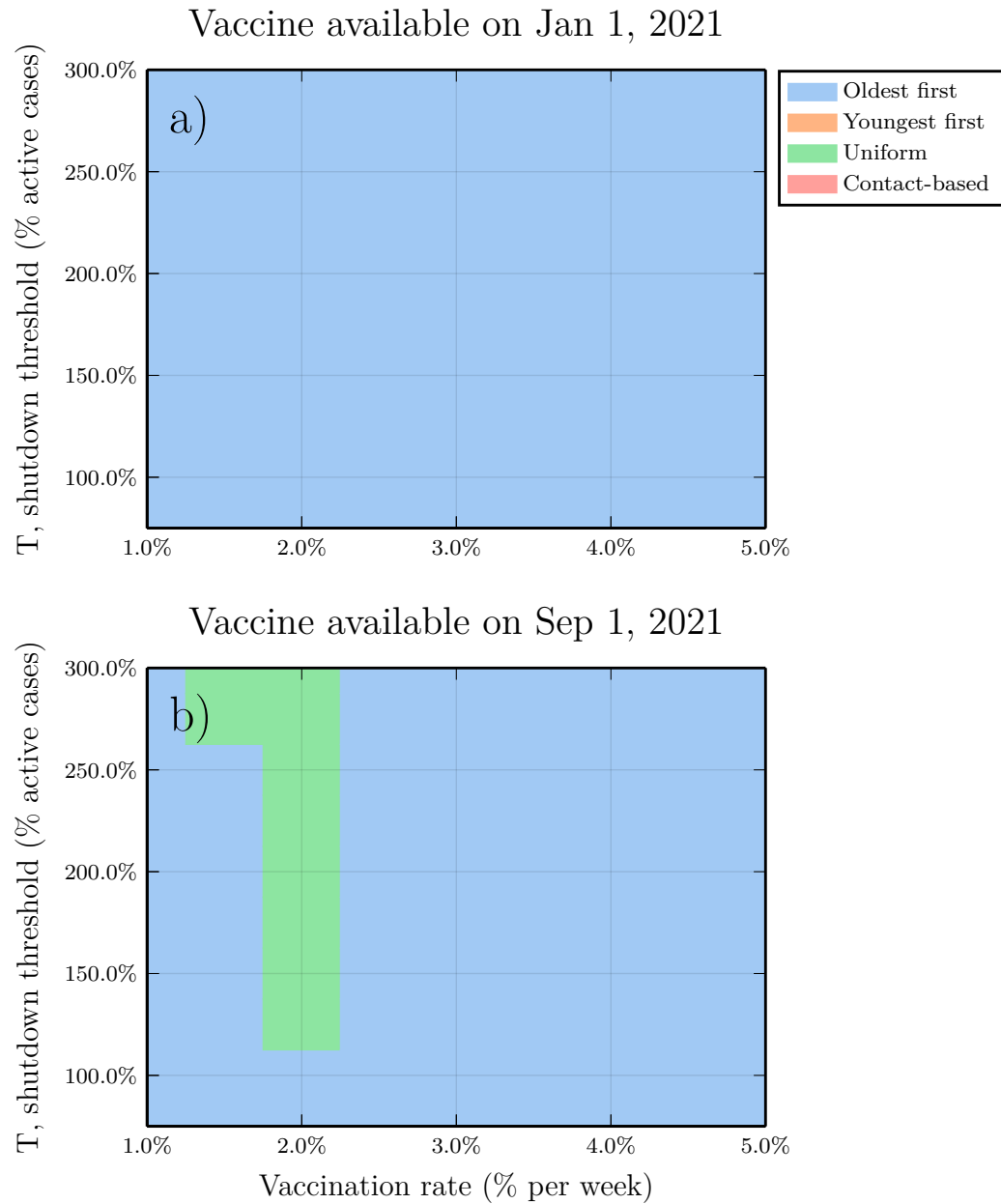


Figure A.18: **Sensitivity analysis for the scenario where $R_0 = 2.5$ for December 2020 onward.** Subpanels are (left) parameter planes for January and September availability showing the vaccination strategy that prevents the most COVID-19 deaths as a function of T and ψ_0 , and (right) percentage reductions in mortality. Other parameter values are as in Table S1.

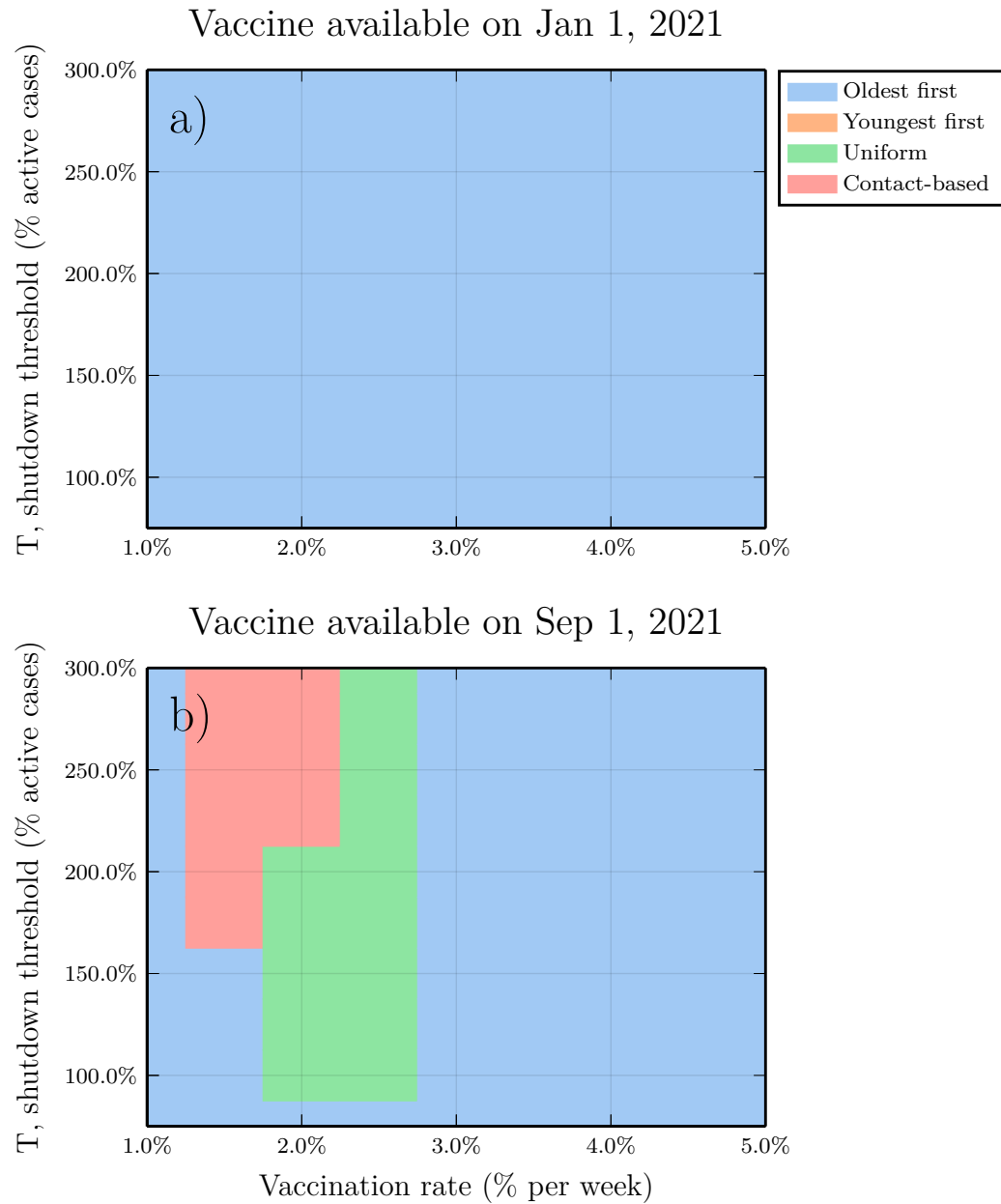


Figure A.19: **Sensitivity analysis for the scenario of 30% heightened ascertainment across all ages from December 2020 onward.** Subpanels are parameter planes for January and September availability showing the vaccination strategy that reduces COVID-19 mortality the most as a function of T and ψ_0 (left) and the corresponding posterior parameter distributions for the refitted parameters (right). Other parameter values as in Table S1.

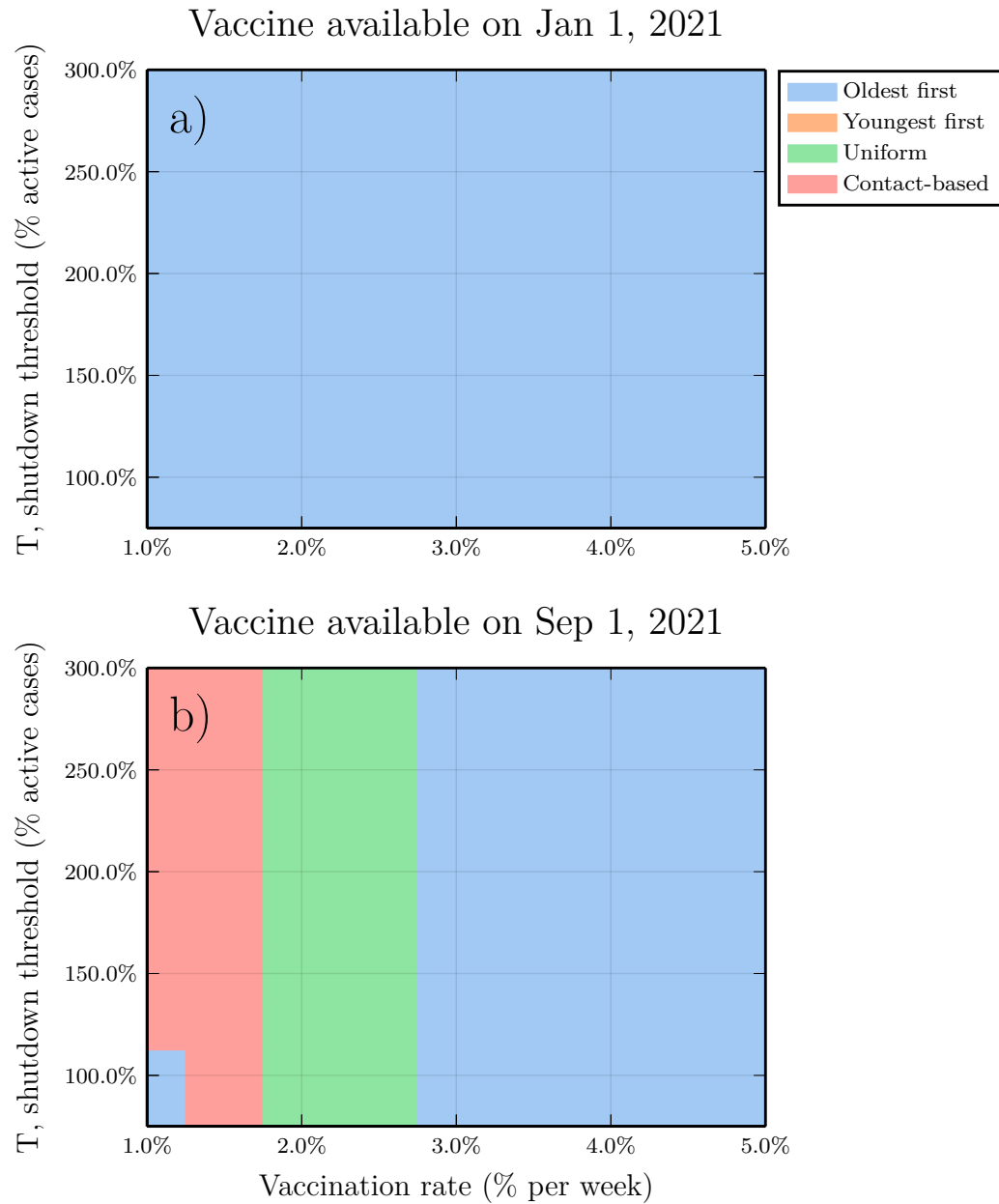


Figure A.20: Sensitivity analysis for the scenario of 30% reduced ascertainment across all ages from December 2020 onward. Subpanels are parameter planes for January and September availability showing the vaccination strategy that reduces COVID-19 mortality the most as a function of T and ψ_0 (left) and the corresponding posterior parameter distributions for the refitted parameters (right). Other parameter values as in Table S1.

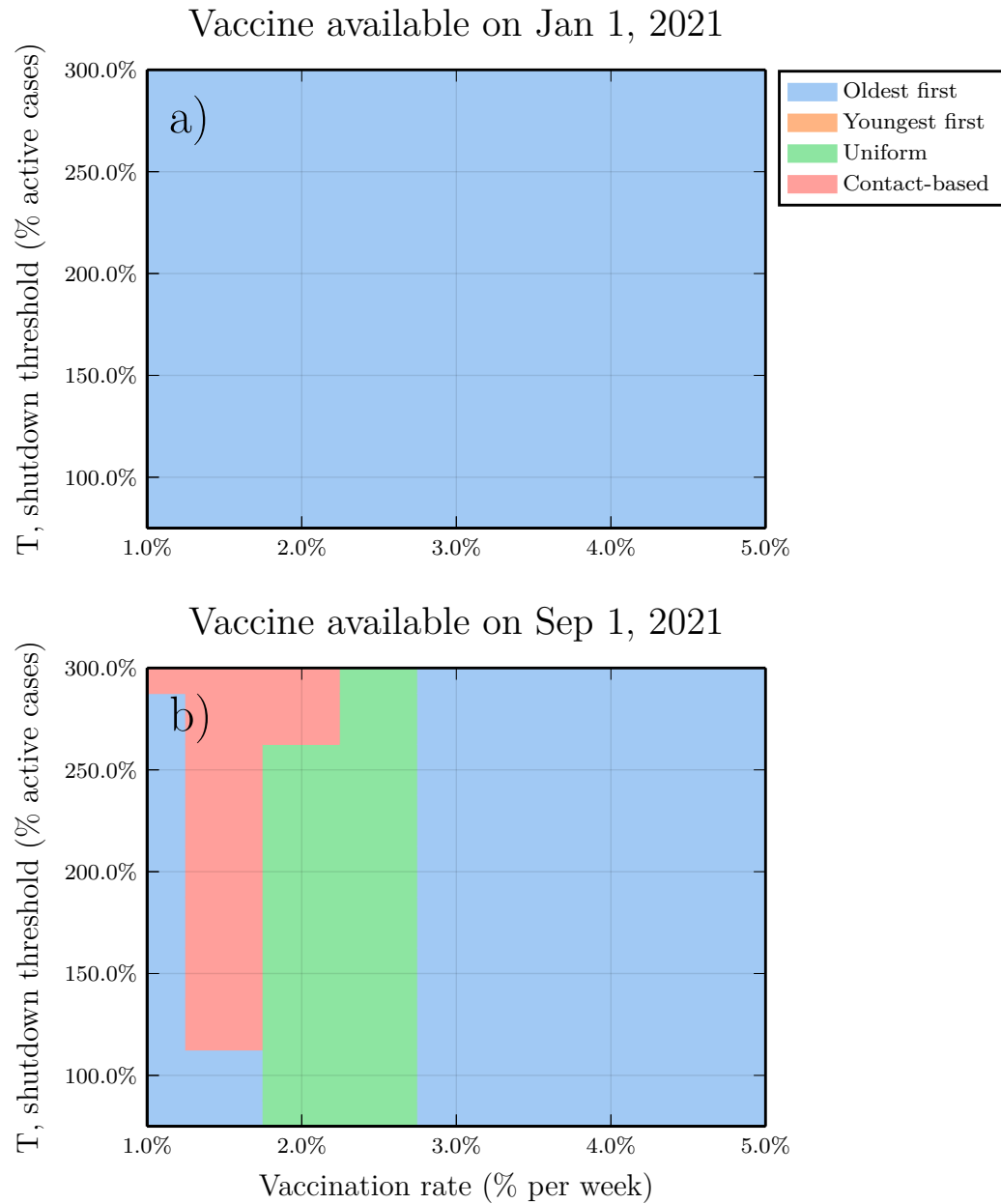


Figure A.21: **Sensitivity analysis for the scenario of four times the baseline social learning rate from December 2020 onward.** Subpanels are parameter planes for January and September availability showing the vaccination strategy that reduces COVID-19 mortality the most as a function of T and ψ_0 (left) and the corresponding posterior parameter distributions for the refitted parameters (right). Other parameter values as in Table S1.

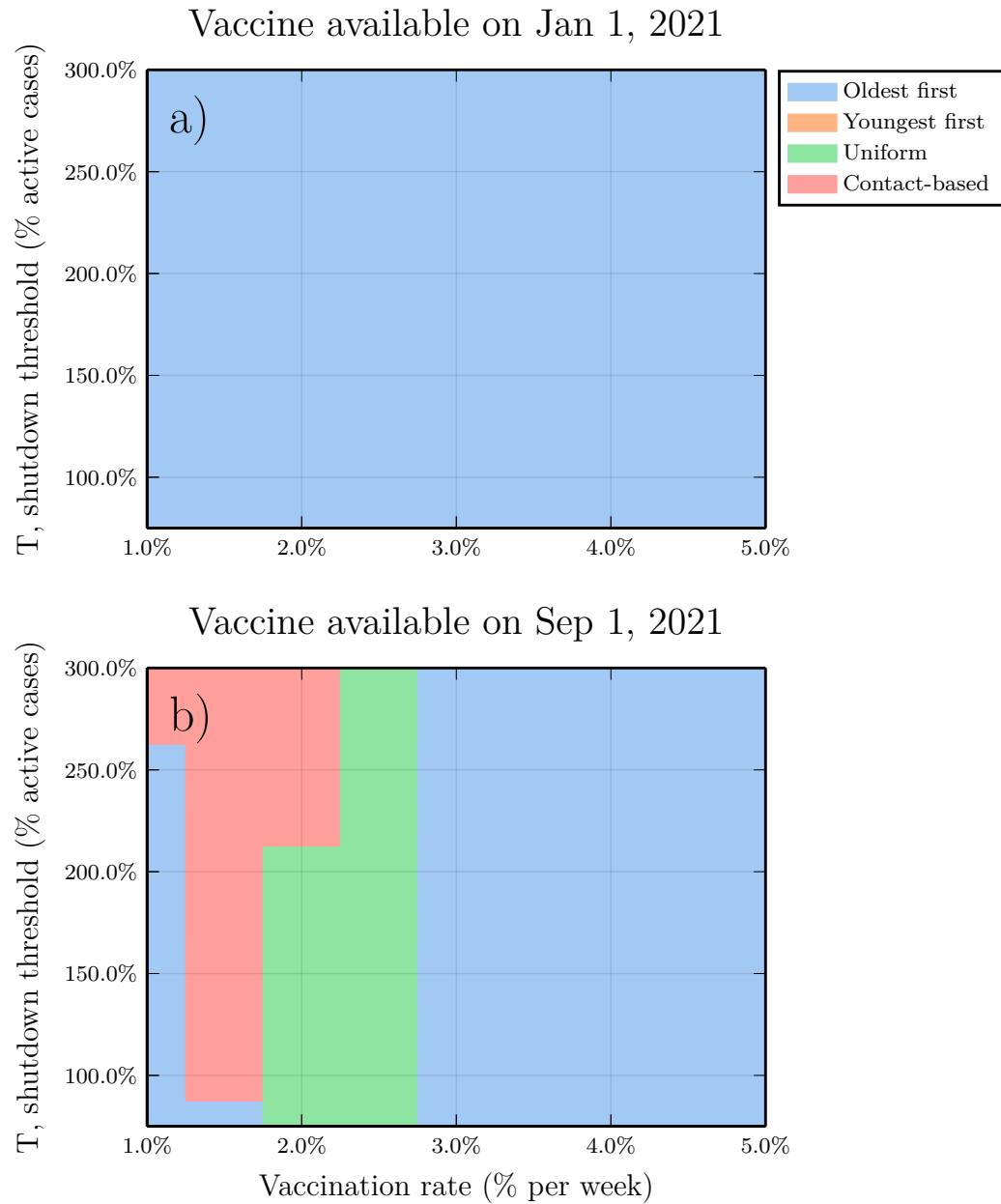
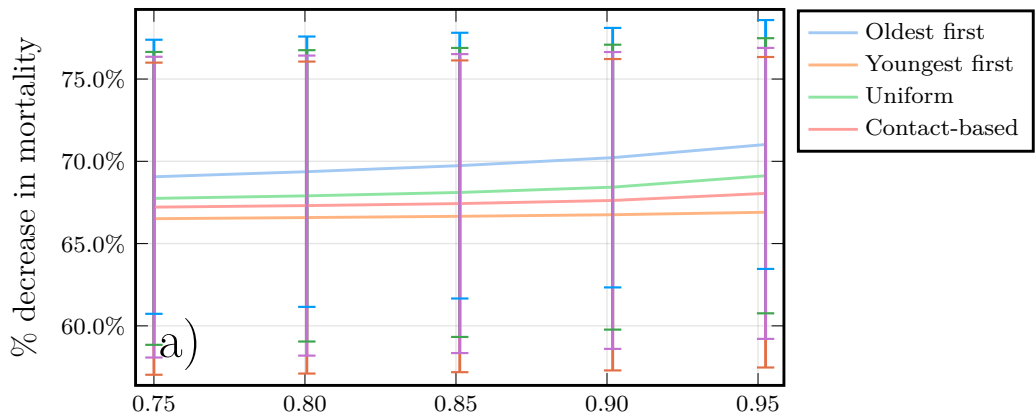


Figure A.22: **Sensitivity analysis for the scenario of one-fourth the baseline social learning rate from December 2020 onward.** Subpanels are parameter planes for January and September availability showing the vaccination strategy that reduces COVID-19 mortality the most as a function of T and ψ_0 . Other parameter values as in Table S1.

Vaccine available: Jan 1, 2021



Vaccine available: Sep 1, 2021

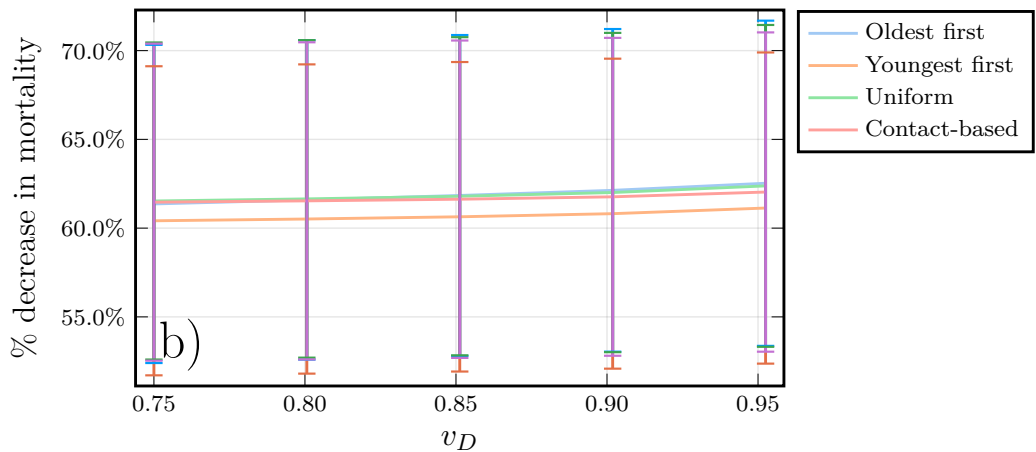


Figure A.23: **Sensitivity analysis for the scenario where efficacy against disease v^D is not the same as efficacy against transmission v^T .** Subpanels show percentage reduction in mortality for the four strategies versus v^D when $v^T = 0.75$ but v^D ranges from 0.75 to 0.95, for January and September availability. Other parameter values as in Table S1. Note that mortality in this plot is computed from March 15, 2020 to March 14, 2025.

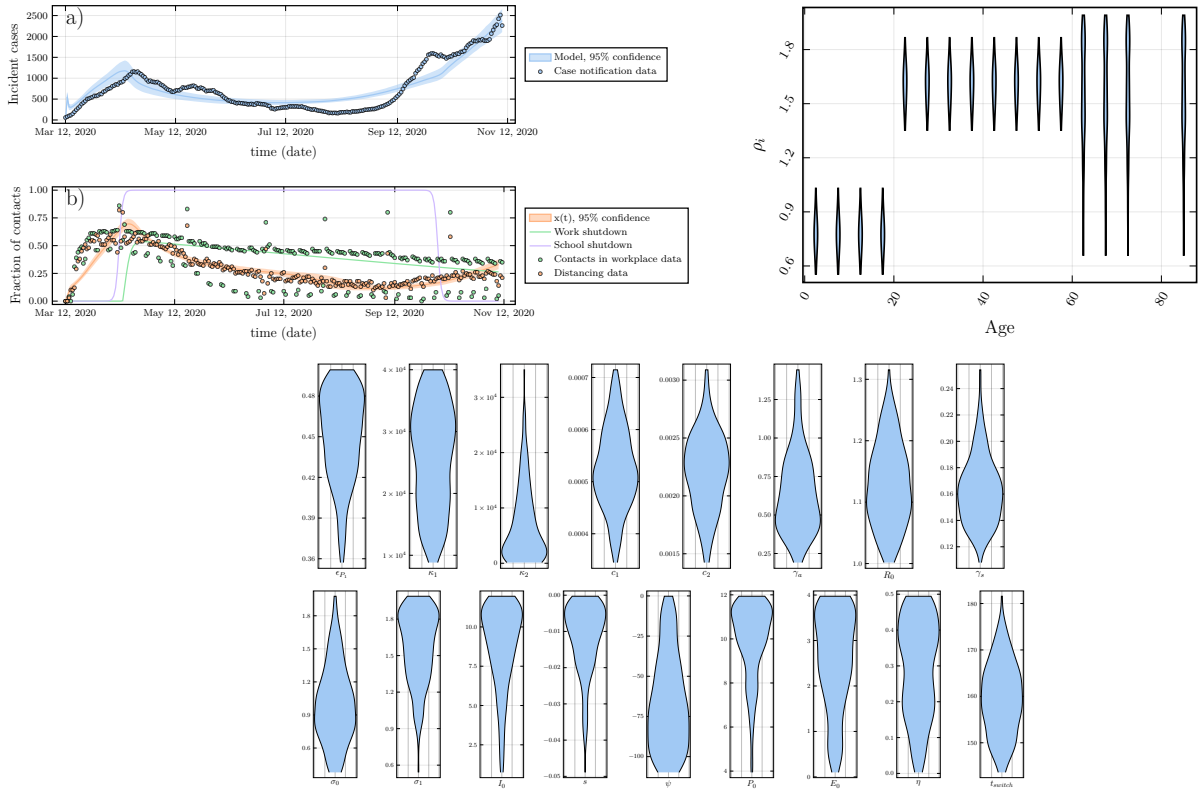


Figure A.24: Posterior parameter distributions and model outputs for more stringent particle filtering criteria under Bayesian particle filtering algorithm. Top left panel shows (a) COVID-19 case incidence by date of report in Ontario, 7-day running average (circles) and ascertainment case incidence from best fitting models (lines). (b) Percentage change from baseline in time spent at retail and recreation destinations (orange circles) and at workplaces (green circles) from Google mobility data, and proportion of the population x adhering to NPIs (orange line) and workplace shutdown curve (green line) from fitted model. Top right panel shows posterior parameter distribution for age-specific susceptibility modifier, ρ_i . Bottom panel shows other posterior parameter distributions. Other parameter values as in Appendix, pp. 1-11.

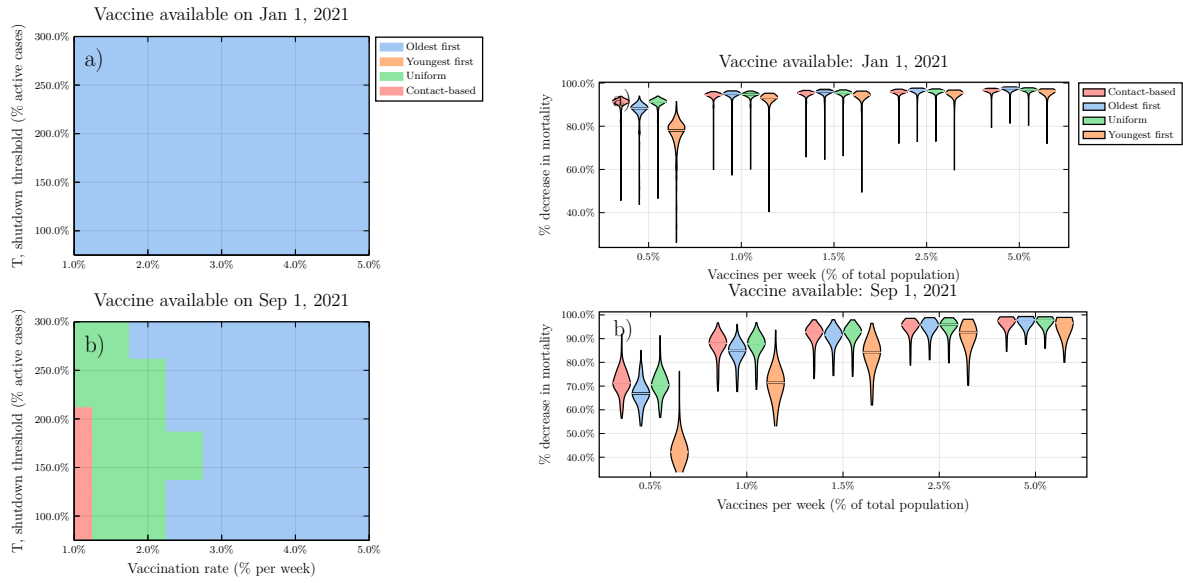


Figure A.25: Sensitivity analysis for more stringent particle filtering criteria under Bayesian particle filtering algorithm. Subpanels are parameter planes for January and September availability showing the vaccination strategy that reduces COVID-19 mortality the most as a function of T and ψ_0 (left) and violin plots showing percentage reduction in mortality (right). Horizontal lines represent median values of posterior model projections. Shutdown threshold $T=200\%$ and other parameter values in Appendix, pp. 1-11. Percentage reductions are relative to no vaccination. Projected number of deaths in the absence of vaccination was 72,000 (95% credible interval: 40,000 to 122,000) from January 1, 2021 to March 14, 2025 for (a) and 60,000 (95% credible interval: 31,000 to 108,000) from September 1, 2021 to March 14, 2025 for (b). Ontario Population size: 14.6 million.

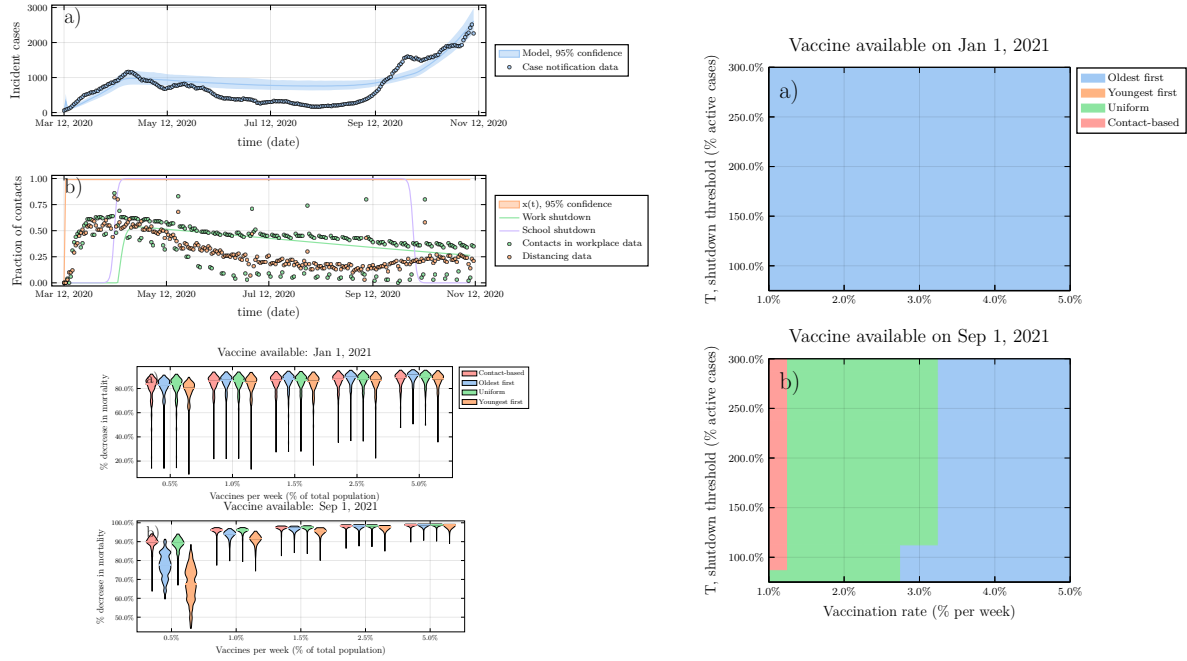


Figure A.26: Model fit to data and baseline projections of mortality reductions under the four vaccine strategies, when behaviour is held constant over time.

Top left: a) COVID-19 case incidence by date of report in Ontario, 7-day running average (circles) and ascertained case incidence from best fitting models (lines). (b) Percentage change from baseline in time spent at retail and recreation destinations (orange circles) and at workplaces (green circles) from Google mobility data, and proportion of the population x adhering to NPIs (orange line) and workplace shutdown curve (green line) from fitted model. Bottom left: Violin plots of the percent reduction in mortality under the four vaccine strategies, relative to no vaccination, as a function of the vaccination rate 0, for (a) January and (b) September 2021 availability. Horizontal lines represent median values of posterior model projections. Shutdown threshold $T=200\%$. Percentage reductions are relative to no vaccination. Projected number of deaths in the absence of vaccination was 72,000 (95% credible interval: 40,000 to 122,000) from January 1, 2021 to March 14, 2025 for (a) and 60,000 (95% credible interval: 31,000 to 108,000) from September 1, 2021 to March 14, 2025 for (b). Ontario Population size: 14.6 million. Right: Each parameter combination on the plane is colour coded according to which of the four strategies prevented the most deaths, on average across all model realizations, for (a) January and (b) September 2021 availability. Other parameter values in Appendix, pp. 1-11.

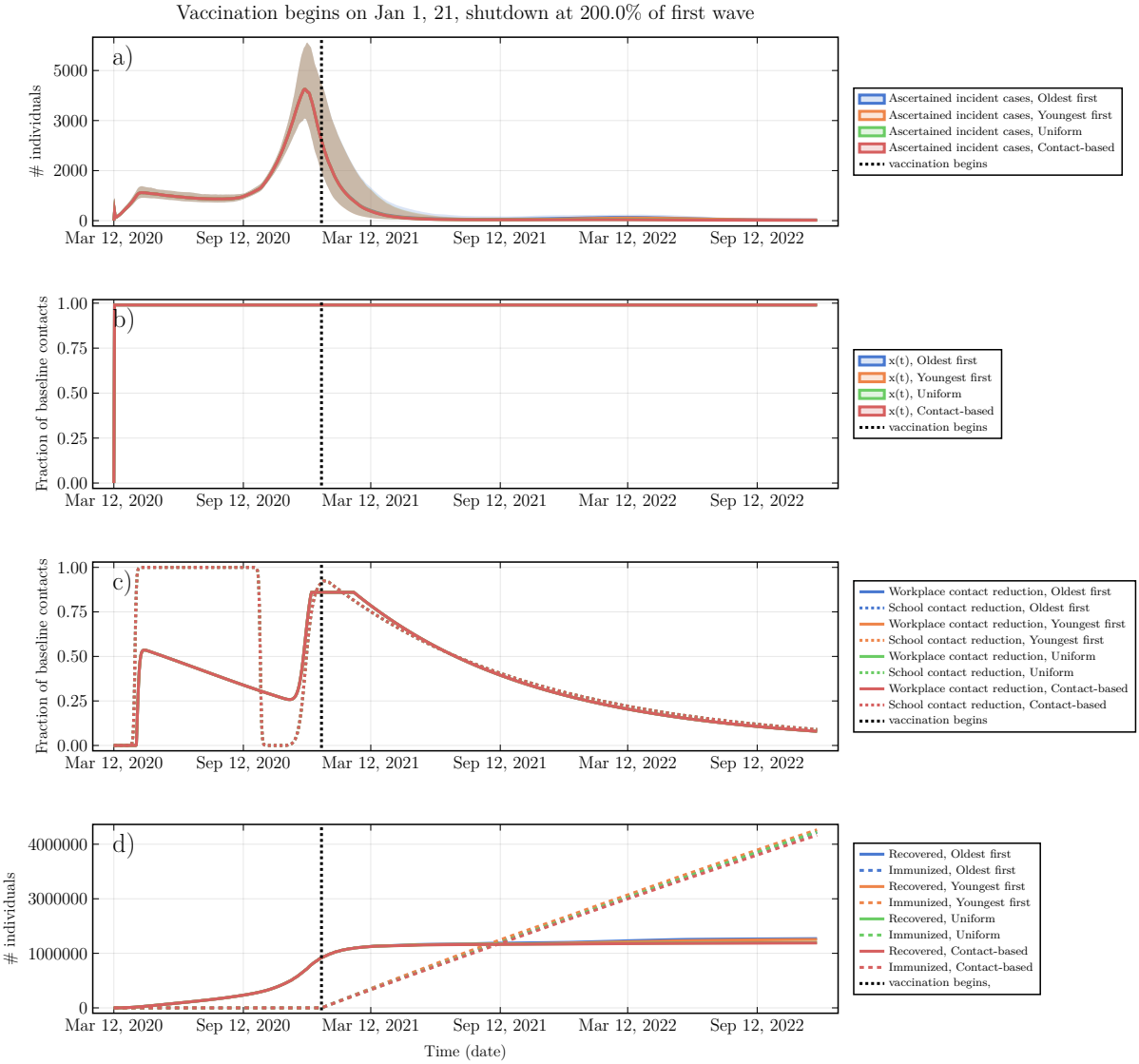


Figure A.27: Epidemic dynamics and social dynamics for both NPI adherence and vaccinating behaviour, when behaviour is held constant over time. (a) Ascertained incident COVID-19 cases, (b) proportion x of the population practicing NPIs, (c) Intensity of school and workplace closure, (d) percentage of population with natural or vaccine-derived immunity versus time. $T = 200\%$, $\psi_0 = 0.5\%$ per week, vaccine available in January 2021. Other parameters are in Table 3.1.

Glossary

This document is incomplete. The external file associated with the glossary ‘main’ (which should be called `thesis.gls`) hasn’t been created.

Check the contents of the file `thesis.glo`. If it’s empty, that means you haven’t indexed any of your entries in this glossary (using commands like `\gls` or `\glsadd`) so this list can’t be generated. If the file isn’t empty, the document build process hasn’t been completed.

You may need to rerun L^AT_EX. If you already have, it may be that T_EX’s shell escape doesn’t allow you to run `makeindex`. Check the transcript file `thesis.log`. If the shell escape is disabled, try one of the following:

- Run the external (Lua) application:

```
makeglossaries-lite "thesis"
```

- Run the external (Perl) application:

```
makeglossaries "thesis"
```

Then rerun L^AT_EX on this document.

This message will be removed once the problem has been fixed.

Abbreviations

This document is incomplete. The external file associated with the glossary ‘abbreviations’ (which should be called `thesis.gls-abr`) hasn’t been created.

Check the contents of the file `thesis.glo-abr`. If it’s empty, that means you haven’t indexed any of your entries in this glossary (using commands like `\gls` or `\glsadd`) so this list can’t be generated. If the file isn’t empty, the document build process hasn’t been completed.

You may need to rerun L^AT_EX. If you already have, it may be that T_EX’s shell escape doesn’t allow you to run `makeindex`. Check the transcript file `thesis.log`. If the shell escape is disabled, try one of the following:

- Run the external (Lua) application:

```
makeglossaries-lite "thesis"
```

- Run the external (Perl) application:

```
makeglossaries "thesis"
```

Then rerun L^AT_EX on this document.

This message will be removed once the problem has been fixed.

Nomenclature

This document is incomplete. The external file associated with the glossary ‘nomenclature’ (which should be called `thesis.nomenclature-gls`) hasn’t been created.

Check the contents of the file `thesis.nomenclature-glo`. If it’s empty, that means you haven’t indexed any of your entries in this glossary (using commands like `\gls` or `\glsadd`) so this list can’t be generated. If the file isn’t empty, the document build process hasn’t been completed.

You may need to rerun L^AT_EX. If you already have, it may be that T_EX’s shell escape doesn’t allow you to run `makeindex`. Check the transcript file `thesis.log`. If the shell escape is disabled, try one of the following:

- Run the external (Lua) application:

```
makeglossaries-lite "thesis"
```

- Run the external (Perl) application:

```
makeglossaries "thesis"
```

Then rerun L^AT_EX on this document.

This message will be removed once the problem has been fixed.

List of Symbols

This document is incomplete. The external file associated with the glossary ‘symbols’ (which should be called `thesis.symbols-gls`) hasn’t been created.

Check the contents of the file `thesis.symbols-glo`. If it’s empty, that means you haven’t indexed any of your entries in this glossary (using commands like `\gls` or `\glsadd`) so this list can’t be generated. If the file isn’t empty, the document build process hasn’t been completed.

You may need to rerun L^AT_EX. If you already have, it may be that T_EX’s shell escape doesn’t allow you to run `makeindex`. Check the transcript file `thesis.log`. If the shell escape is disabled, try one of the following:

- Run the external (Lua) application:

```
makeglossaries-lite "thesis"
```

- Run the external (Perl) application:

```
makeglossaries "thesis"
```

Then rerun L^AT_EX on this document.

This message will be removed once the problem has been fixed.